# STRUCTURAL PERFORMANCE OF 117J TANK CARS AND 117R VARIANTS UNDER DERAILMENT CONDITIONS

## FINAL REPORT

SHARMA & ASSOCIATES, INC.



Submitted To:

TDG, Transport Canada

For Contract #: T8080-200562
TP 15544E

June 2022

For more information, contact:
Transport Canada
330 Sparks Street
Ottawa ON Canada K1A 0N5



Cat. No. T44-3/32-2022E-PDF (Electronic PDF, English)

ISBN 978-0-660-46123-6

TP 15544E

**TABLE OF CONTENTS**

## EXECUTIVE SUMMARY

This report describes the methods used and the results obtained in the analysis of structural performance of TC-117 tank cars in derailments. TC-117J tank cars (compliant with the new specifications) were found to have fewer punctures than several variants of TC-117R tank cars (retrofitted older cars).

The methodology used was an enhanced version of one developed earlier for the US Department of Transportation and Transport Canada. Improvements were made to the modelling of tank cars in derailment scenarios. These included more accurate representation of inter-car connections and modelling of top fittings protection.

A material model was developed to account for the change in properties and failure mode with temperature. The model was calibrated by comparing simulations of Charpy impact tests with laboratory test results and further extended to cover both normalized and non-normalized tank car steels.

Predictions were made at ambient temperatures between 20 and -40 °C, based on assumed material behavior/properties at the simulated temperatures. Tank car punctures are predicted to increase by up to 10% at -40 °C with respect to the ambient temperature at 20 °C.

Comparisons to prior work suggest that any of the TC-117 variants had better performance than the legacy TC-111 cars, with the TC-117J designs offering the best performance. The number of tank cars derailed and tanks punctured increased with increasing speed. TC-117R tank cars with non-normalized steel shells were found to have on average 6% more punctures than cars with normalized steel shells. Among the variants, the TC-117R tank car design where the source car had a 1/2” thick shell made from A516-70 steel was predicted to have the highest number of punctures.

Top fittings failures were found to increase significantly with speed in a similar way to tank punctures.

Comparisons to a limited set of available accident data suggest that the model predictions are consistent with field observations from derailments.

# 1 INTRODUCTION

This report describes the study performed by Sharma & Associates, Inc. (SA) for Transport Canada (TC) on the crashworthiness of various designs of rail tank cars. It describes several improvements to the methodology used in earlier work including the effect of temperature on material properties. The results are presented in terms of the estimated number of tank car punctures and top fittings failures in a range of accident scenarios.

## 1.1 Background

The current standard for rail tank cars carrying flammable liquids in Canada, TC-117, was introduced in 2015. The structural requirements for new cars, TC-117J, are a 9/16-inch-thick tank shell made from normalized TC128-B steel, an 11-gauge jacket, a 1/2 inch thick, full height head shield, and top fittings protection that meets Section 8.2.3.4.1 of TP14877.

The requirements for retrofitting existing cars, TC-117R, cover source cars that are older, legacy TC 111 and newer, CPC 1232 tank cars. While the modifications required by TC-117R are expected to improve crashworthiness performance, the level of improvement will depend on the specifications of the original car.

Prior work conducted by SA for the US Department of Transportation/Federal Railroad Administration (USDOT/FRA) supported the development of the TC-117 standard. Its 2014 report described a methodology for quantifying the probability of puncture for different designs of tank car [1]. The methodology captured several parameters that are relevant to tank car derailment performance including derailment cause, derailment dynamics, impact load distributions, impactor sizes, operating conditions, and tank car design.

SA has conducted detailed analyses and full-scale tests to investigate the damage to top fittings when tank cars roll over [2, 3, 4]. The results demonstrated the benefits of protective structures for top fittings. Top fittings protection is mandatory for TC-117 and CPC 1232 tank cars.

Laboratory tests have shown the steel used to make tank car shells becomes more brittle as its temperature drops [5]. Thus, there is a concern that cold temperatures might reduce the puncture resistance of tank cars during derailments.

## 1.2 Objectives

The overall objective of the work reported here is to predict the crashworthiness performance of TC-117J tank cars and TC-117R variants. The performance metrics are the number of cars punctured and the number of failed top fittings in a range of different accident scenarios. Specific objectives are to:

- Update the earlier methodology to include the effects of top fittings protection and to more accurately model inter-car connections
- Study the effects of cold temperatures on tank car puncture resistance
- Assess the predicted performance through review of engineering expectations and comparisons to historical data

## 1.3 Overview of Methodology

As outlined in prior work, the methodology used for estimating the number of punctures was as follows:

- Characterize the load environment associated with nominal tank car derailments through multiple derailment simulations of trains of tank cars to derive a histogram of 'nominal' impact forces
- Quantify the puncture resistance of given tank car designs for a nominal range of impactor sizes and impact forces, based on prior research
- Combine the load environment histograms, the puncture resistance curves, and nominal impactor size distributions, to evaluate the safety performance or probability of puncture for a set of designs and operating speeds

A similar methodology was also adopted for the estimation of fittings failures, as outlined below:

- Velocities with which fitting protective structures hit the ground during derailments were quantified through derailment simulations of trains of cars to estimate a distribution of such velocities
- The strength of fittings protective structures was characterized through detailed finite element analysis of individual cars' fittings protective structures impacting the ground surface at specified speeds
- The likelihood of fittings failure was estimated by combining the above two elements

### 1.4 Report Structure

Section 2 of this report describes the enhancements made to the methodology for quantifying crashworthiness performance originally developed by SA for the US DOT/FRA and TC.

Section 3 provides details of the derailment simulations that were performed to estimate both histograms of the impact forces between tank cars, as well as the fittings protective structure impact velocities.

Section 4 describes modelling that was performed to determine the effect of temperature on tank car puncture resistance.

Section 5 provides the results derived by combining the histograms derived in section 3, with the puncture resistance of tank cars or the fittings characteristic strengths, with further consideration for the temperature effects identified in section 4.

Section 6 reviews the results of the modelling methodology through comparisons with accident data.

## 2 ENHANCEMENTS TO TANK CAR MODELLING

Several enhancements were made to the modelling of tank cars from the earlier study [1]. These included improvements to the representation of the track and ground height, and the coupler connection, as well as a simplified truck representation to better capture the initial height of the tank as it rolls off.

Dimensions of the tank car are similar to the one presented in prior work for Transport Canada [2, 3]; the difference between the top of the rail and ground surface is assumed to be 12 inches. The model was developed and analyzed using LS-Dyna [5]. The ground surface is modeled as a finite rigid-wall; the truck representation is defined to move along the centerline of the track through a lateral spring connection between the truck representation and the ground, with the spring stiffness representing a measure of the lateral track stiffness; when the displacement of this spring exceeded a nominal 1”, the truck was considered to have derailed and the car was subsequently free to move laterally. Figure 1 presents an overview.

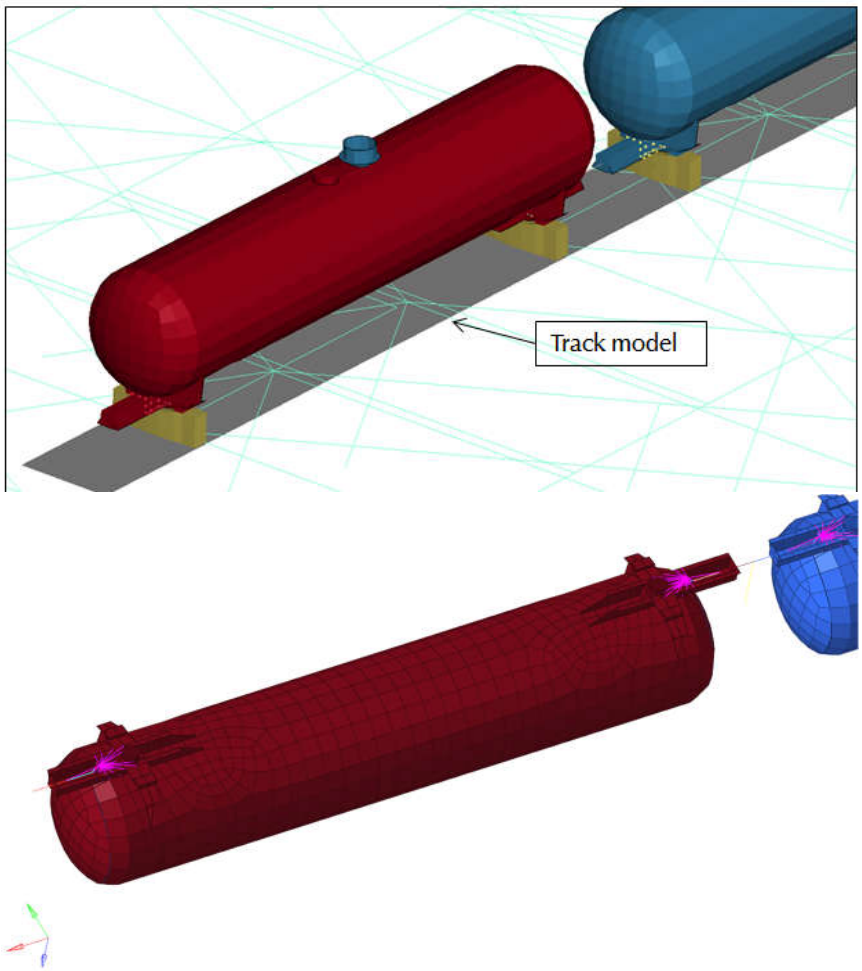


**Figure 1. Track model and Lateral Spring Connection**

Note that the intent of the truck representation is to model an appropriate rollover height for capturing rollover velocities and dynamics; the intent is not to present the truck as a potential impact element or to otherwise model truck performance. The differences between the truck representation presented in the previous report [3] and the one used in this study are shown below. The bottom of the tank car bolster was also modified to allow for proper connection between the truck representations and the tank cars, Figure 2.

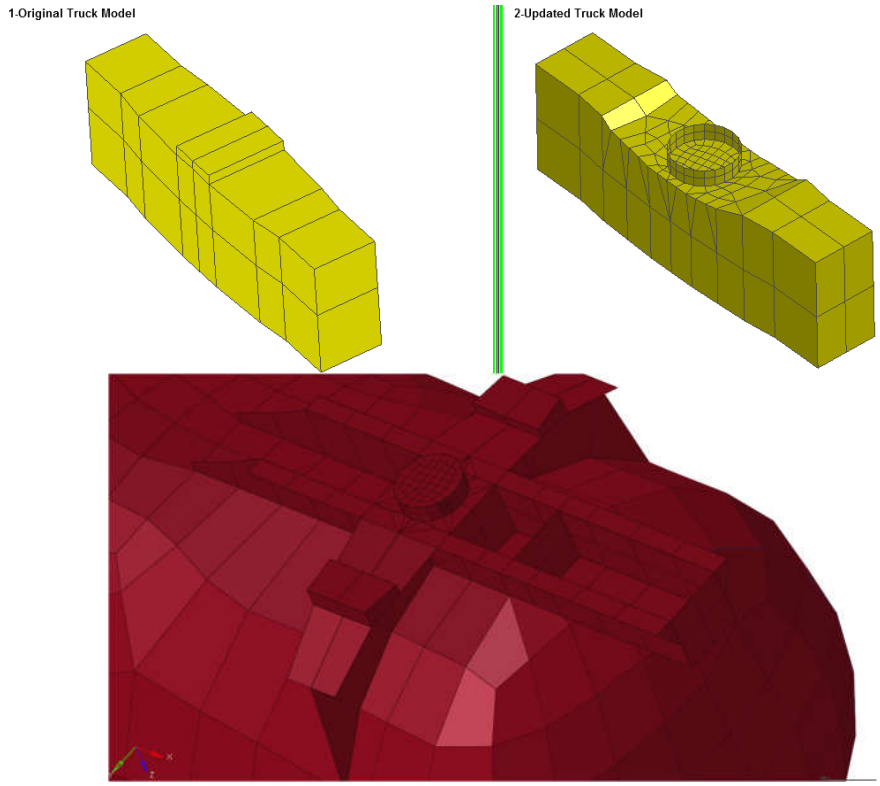


**Figure 2. FE Adjustments**

The updated tank car model also included the top fittings protective structure (described in Section 2.1) and a more accurate representation of the coupler (see Section 2.2). For the derailment model, shell elements with a Belytscko-Tsay formulation were used, with a nominal element length of 12” and finer mesh densities where appropriate.

### 2.1 Fittings and Manway

To investigate the detailed impact behavior between the top fittings protective structures (bonnets) and the ground surface, two different FE models of the fittings protective structure were developed and used (see Figure 3).

- A detailed model was developed to characterize the deformation and strength characteristics of the fittings protective structures on an individual car, under different impact velocities and ground surface conditions. For this effort, the protective structure was consistent with designs used on TC-117 cars, meeting the requirements in Section 8.2.3.4.1 of TP14877. The thickness of the protective structure was 0.5” and diameter of the structure was 36”. Upon impact, a deformation of 4” or higher on the protective structure was considered failure.

- A less detailed version of the fittings protective structure was used in the train derailment model, as the intent of the modelling was primarily to quantify the impact velocities between the fittings structures and the ground for the derailed cars.

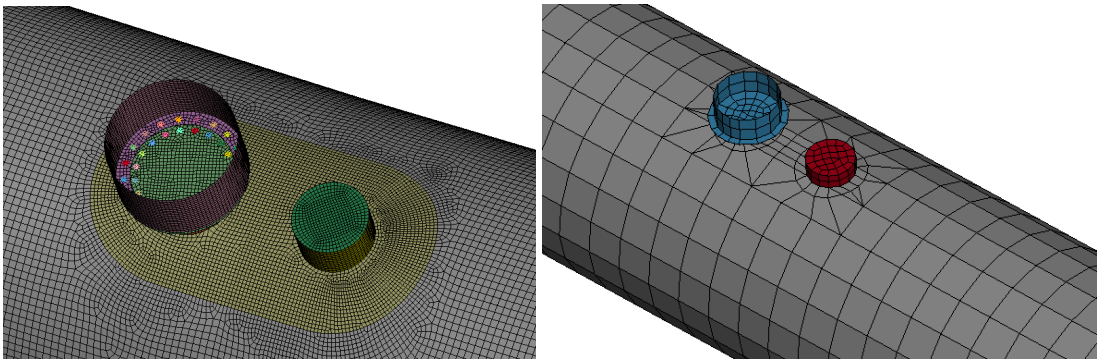

**Figure 3. Car-level (detailed) and Train-level Models for Top Fittings Protection**

In this study, the impact velocities generated using the train derailment model were analyzed in conjunction with the fittings protection strength characterization curves obtained using the detailed model from the previous investigation [2,3], to evaluate the likelihood of fittings failure (Chapter 5).

All fittings components were modeled using A516 Gr 70 steel, common for non-pressure tank car fittings. The key results expected from these models are the distributed forces and velocities at the fittings protective structures.

## 2.2 Coupler Representation

Figure 4 shows the updated inter-car connection, which consists of rigid beams modelling the coupler and nonlinear spring-damper arrangements representing the draft gear.

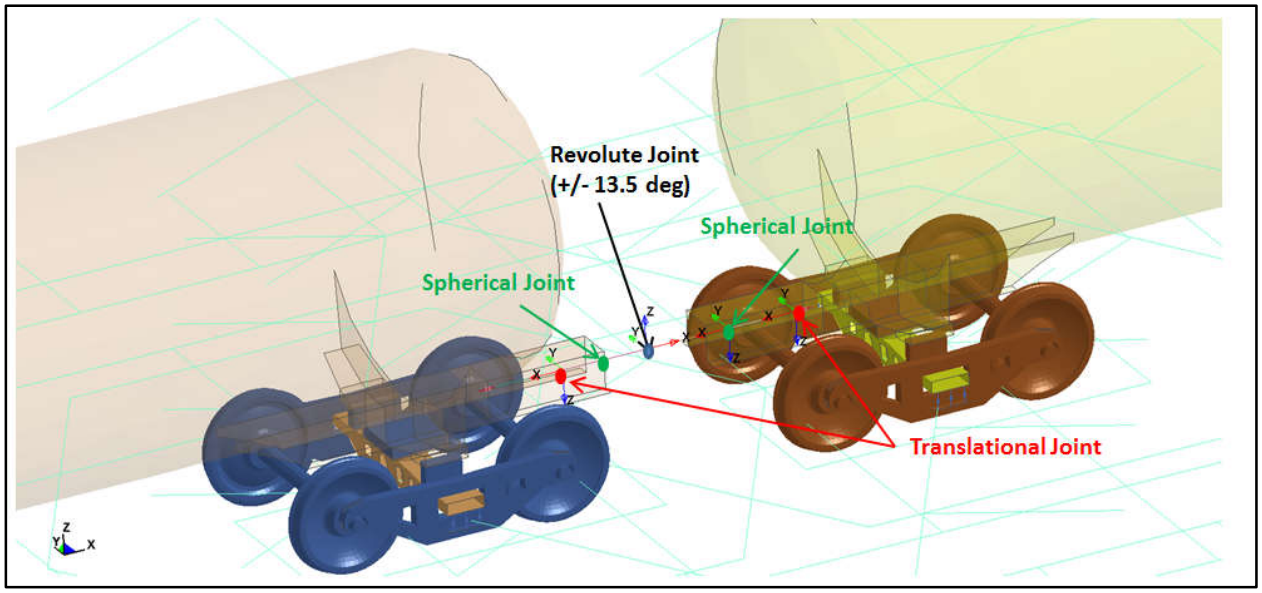


**Figure 4. Updated inter-car connections**

The knuckle is modeled as a revolute joint, with rotation allowed only around the local vertical axis. A nonlinear stiffness is assigned to this joint that allows rotation up to 13.5 degrees[1] in either direction. Beyond the 13.5 degrees, the stiffness increases sharply representing the physical limit of knuckle rotation. All modeled coupler movements and limits are as outlined in the AAR Manual [7]. The wheelsets shown in Figure 4 are only for visualization purposes.

The coupler pin connections are modeled as spherical joints with separate nonlinear stiffness in each of the three rotation directions:

1. Rotational stiffness about the local vertical axis is unrestrained up to 7 degrees in either direction and then becomes very stiff, limiting further rotation [7]
2. Rotational stiffness about the lateral local axis (the car's pitch axis) is unrestrained up to 3.4 degrees in either direction and then becomes very stiff
3. Rotational stiffness about the longitudinal local axis (the car's roll axis) is unrestrained up to 5 degrees in either direction and then becomes very stiff

The draft gear movement is simulated using translational joints. To separate the cars, a SENSOR card in LS-Dyna was used to deactivate the knuckle connections once the maximum rotation angles were reached.

[1] These limiting values are consistent with the expected rotational allowances prescribed in the AAR manual for E-couplers.

# 3 DERAILMENT SIMULATIONS

As in the earlier study, derailments were modeled using LS-Dyna [5]. Outputs from the modelling included car-to-car impact forces and fittings impact velocities. Derailments were modeled at 5, 20, 25, 30, 35, 40, 50, 55, and 60 mph. These are the speeds of the train when the derailment was initiated. This range of speeds is consistent with those expected in revenue service and is as requested by TC. The value of 50 mph is the highest speed at which a key train can travel in Canada [8]. The highest value studied, 60 mph, was added as an upper bound to encompass potential future requests.

Upon initiation of derailment, a retarding force equivalent to an emergency brake application is imparted to all the cars, propagating from the point of the derailment to the rear of the train. The retarding force applied was 13,255 lb. per car, which represents an emergency brake application associated with a 12% Net Braking Ratio [1].

A commonly used parameter to define the likelihood of a rail wheel derailing is the ratio between the lateral force “L” and the vertical force “V” acting on the wheel (L/V ratio). When the lateral force exceeds a certain limit, a derailment becomes likely.

In this study, to initiate the derailment, the leading truck of the first car was subjected to a brief lateral force. Three values of lateral forces were used to initiate derailment: 50, 70, and 90 kips. These values represent a truck-side L/V ratio of 0.76 to 1.06; a value of 0.6 is considered a safety limit for rail rollover (truck-side L/V criterion in Table 1, [9]) and higher values are needed to initiate a derailment, as used here.

Two values of lateral track stiffness were used to represent variations in track quality: 30 and 40 kips/in. The 40 kips/in value gave 1 inch of lateral movement for a truck side L/V ratio of 0.6. The 30 kip/in value represented poorer quality track that was 25% more flexible.

Three values of coefficient of friction between the tank car and the ground were used: 0.27, 0.3, and 0.5. This range is consistent with nominal values for friction between steel and soil, which generally range from 0.2 to 0.4, and is similar to prior work performed by SA for US DOT/TC [2]. The highest value represents a higher degree of friction between the ground and the moving derailed tank car.
Four values of temperature were used: -40, -25, -15, and 20 °C. The lower temperatures represent possible ambient conditions in Canadian winters. The value of -25 °C is based on Transport Canada Ministerial Order MO 20-10 [11].

Table 1 summarizes the derailment scenarios that were considered. It was assumed that the temperature does not affect the derailment dynamics, and that it only affected the tank steel material and therefore the probability of puncture. There are 18 derailment scenarios for each speed as shown in Table 2.

**Table 1: Derailment scenario matrix**

| Train speed (mph) | Coefficient of friction between tank car and ground | Lateral force to initiate derailment (kips) | Track stiffness (kips/in) | Temperature (°C) |
|---|---|---|---|---|
| 5 | 0.27/0.3/0.5 | 50/70/90 | 30/40 | -40 |
| 5 | 0.27/0.3/0.5 | 50/70/90 | 30/40 | -25 |
| 5 | 0.27/0.3/0.5 | 50/70/90 | 30/40 | -15 |
| 5 | 0.27/0.3/0.5 | 50/70/90 | 30/40 | 20 |
| 25 | 0.27/0.3/0.5 | 50/70/90 | 30/40 | -40 |
| 25 | 0.27/0.3/0.5 | 50/70/90 | 30/40 | -25 |
| 25 | 0.27/0.3/0.5 | 50/70/90 | 30/40 | -15 |
| 25 | 0.27/0.3/0.5 | 50/70/90 | 30/40 | 20 |
| 30 | 0.27/0.3/0.5 | 50/70/90 | 30/40 | -40 |
| 30 | 0.27/0.3/0.5 | 50/70/90 | 30/40 | -25 |
| 30 | 0.27/0.3/0.5 | 50/70/90 | 30/40 | -15 |
| 30 | 0.27/0.3/0.5 | 50/70/90 | 30/40 | 20 |
| 35 | 0.27/0.3/0.5 | 50/70/90 | 30/40 | -40 |
| 35 | 0.27/0.3/0.5 | 50/70/90 | 30/40 | -25 |
| 35 | 0.27/0.3/0.5 | 50/70/90 | 30/40 | -15 |
| 35 | 0.27/0.3/0.5 | 50/70/90 | 30/40 | 20 |
| 40 | 0.27/0.3/0.5 | 50/70/90 | 30/40 | -40 |
| 40 | 0.27/0.3/0.5 | 50/70/90 | 30/40 | -25 |
| 40 | 0.27/0.3/0.5 | 50/70/90 | 30/40 | -15 |
| 40 | 0.27/0.3/0.5 | 50/70/90 | 30/40 | 20 |
| 50 | 0.27/0.3/0.5 | 50/70/90 | 30/40 | -40 |
| 50 | 0.27/0.3/0.5 | 50/70/90 | 30/40 | -25 |
| 50 | 0.27/0.3/0.5 | 50/70/90 | 30/40 | -15 |
| 50 | 0.27/0.3/0.5 | 50/70/90 | 30/40 | 20 |
| 55 | 0.27/0.3/0.5 | 50/70/90 | 30/40 | -40 |
| 55 | 0.27/0.3/0.5 | 50/70/90 | 30/40 | -25 |
| 55 | 0.27/0.3/0.5 | 50/70/90 | 30/40 | -15 |
| 55 | 0.27/0.3/0.5 | 50/70/90 | 30/40 | 20 |
| 60 | 0.27/0.3/0.5 | 50/70/90 | 30/40 | -40 |
| 60 | 0.27/0.3/0.5 | 50/70/90 | 30/40 | -25 |
| 60 | 0.27/0.3/0.5 | 50/70/90 | 30/40 | -15 |
| 60 | 0.27/0.3/0.5 | 50/70/90 | 30/40 | 20 |

**Table 2: Derailment scenarios for each speed**

| Run # | Track Stiffness (kips/in) | Friction Coefficient | Initiating Force (kips) |
|---|---|---|---|
| 1 | 30 | 0.27 | 50 |
| 2 | 30 | 0.30 | 50 |
| 3 | 30 | 0.50 | 50 |
| 4 | 30 | 0.27 | 70 |
| 5 | 30 | 0.30 | 70 |
| 6 | 30 | 0.50 | 70 |
| 7 | 30 | 0.27 | 90 |
| 8 | 30 | 0.30 | 90 |
| 9 | 30 | 0.50 | 90 |
| 10 | 40 | 0.27 | 50 |
| 11 | 40 | 0.30 | 50 |
| 12 | 40 | 0.50 | 50 |
| 13 | 40 | 0.27 | 70 |
| 14 | 40 | 0.30 | 70 |
| 15 | 40 | 0.50 | 70 |
| 16 | 40 | 0.27 | 90 |
| 17 | 40 | 0.30 | 90 |
| 18 | 40 | 0.50 | 90 |

### 3.1 Initial Simulations

The correct functioning of the top fittings, truck, and coupler was confirmed with a 2-car model before moving onto multi-car simulations. Then, several 20-car train simulations were performed to ensure that the model behaved as expected and to compare the results with prior work. An example of such a simulation is shown in Figure 5. The following observations were made from the 20-car simulations, confirming that the models were behaving as expected:

- The number of collisions was consistent with the speed of the train, the higher the speed the higher the number of collisions;
- The distance between the point of derailment and the farthest car derailed was also consistent with the speed of the car
- Three different ground friction coefficients were used for this initial effort, 0.27, 0.30, and 0.33. The ground friction coefficient did not make a significant difference to the number of fittings hitting the ground.
- Based on observations about the coupler rotation observed, an additional torsional failure mode was added to the coupler system

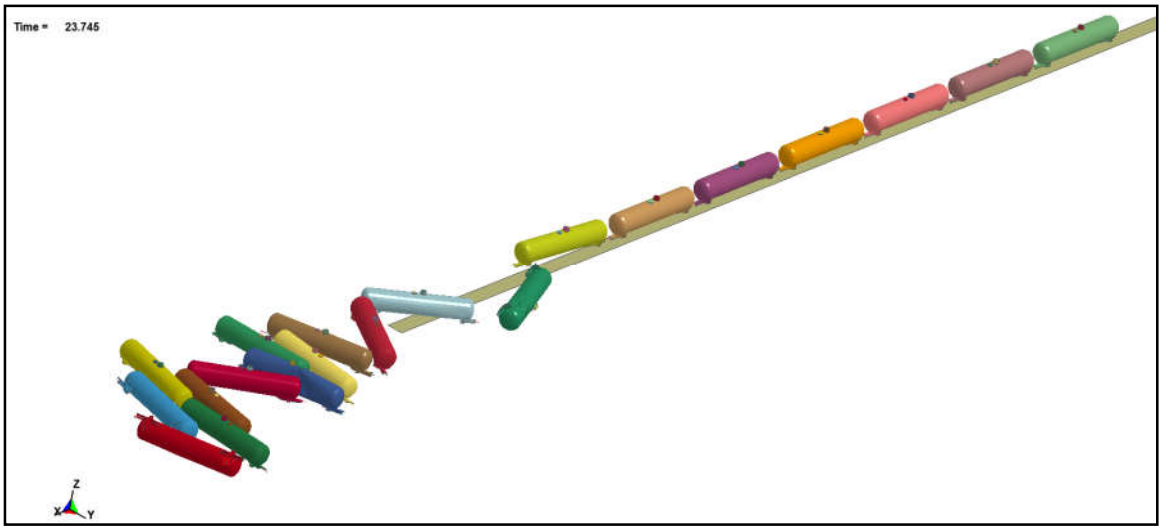


**Figure 5. Example final pile-up – 20-car train at 30mph**

### 3.2 100-car Simulations

Subsequently, the 20-car model was extended to a 100-car model. Figure 6 shows the resulting final pile-up images for each of the 18 runs with a derailment initiation speed of 30 mph. Final pile-up images for each of the speeds used in this study are provided in Appendix A.

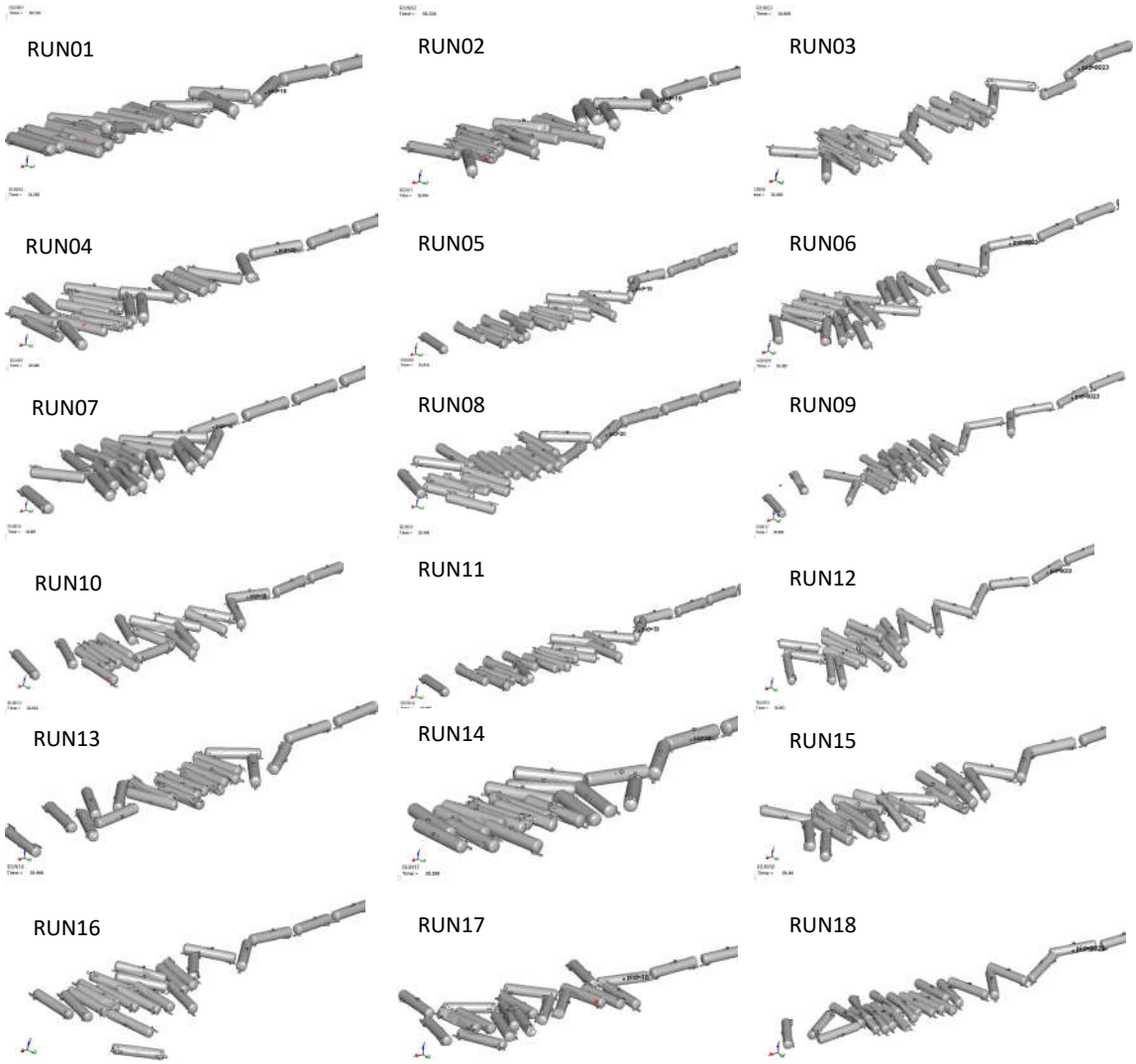


**Figure 6. Final pile-up – 100-car train at 30mph**

Each simulation results in several car-to-car impacts between the involved cars. Table 3 lists the average number of impacts for each speed.

**Table 3: Derailment scenarios for each speed**

| Derailment speed (mph) | Car-to-car Impacts | Number of cars derailed |
|---|---|---|
| 5 | 2 | 4 |
| 20 | 15 | 12 |
| 25 | 27 | 16 |
| 30 | 36 | 20 |
| 35 | 43 | 28 |
| 40 | 54 | 33 |
| 50 | 74 | 46 |
| 55 | 103 | 51 |
| 60 | 122 | 62 |

The forces generated at each impact between any two cars are then analyzed to generate a histogram of forces associated with that derailment scenario. A 30 Hz low-pass filter was used to smooth out the peak forces. Force peaks below 250,000 lbs. were ignored as the potential for puncture associated with such forces is small [19].

The histograms from all simulations were accumulated and then summed over the 18 simulations at a given speed to generate a histogram of impact forces at each speed. Figure 7 shows the results.

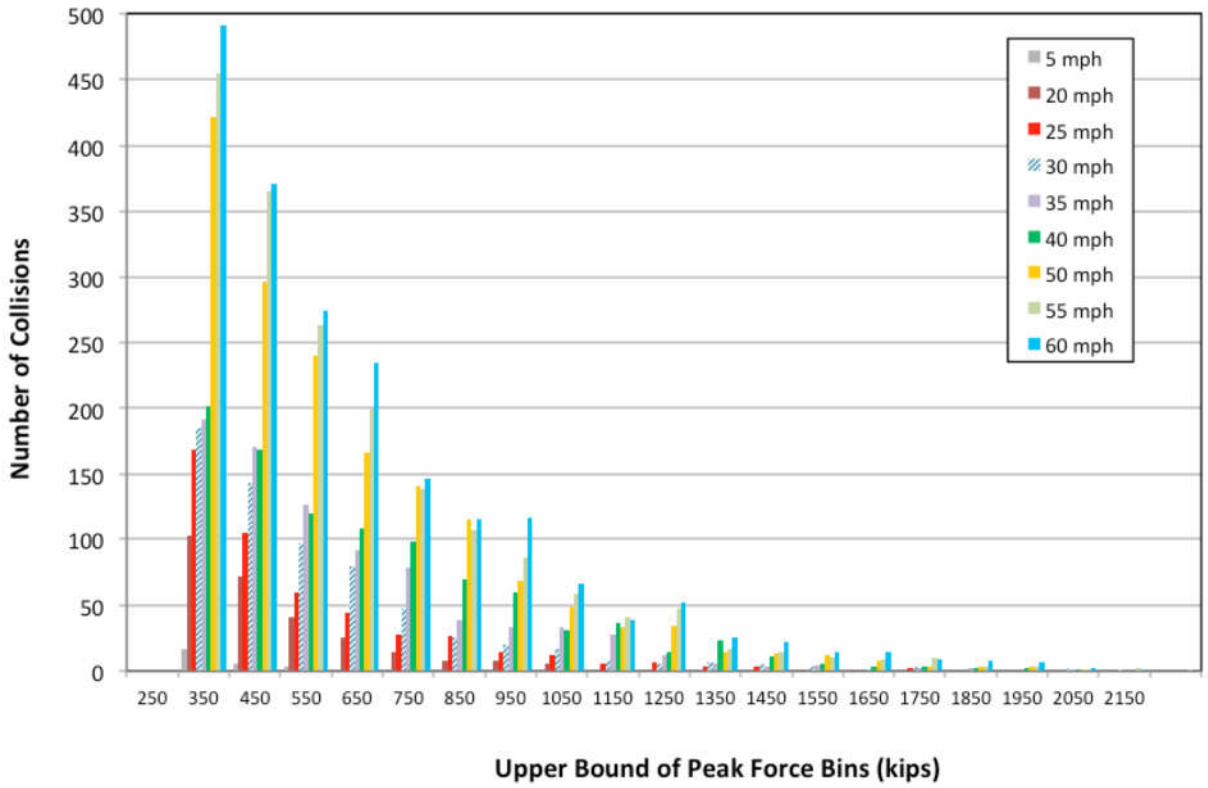


**Figure 7. Cumulative histogram of impact loads resulting from derailments**

The load histogram shown in Figure 7 is independent of the location of the impact – it shows all impacts regardless of location. Based on earlier analysis of head and shell punctures in dangerous goods accidents, it is assumed that the distribution of head to shell impacts is 50:50 [1]. Calculation of the

predicted number of punctures resulting from the impact loads shown in Figure 7 is discussed in Section 5.

Fittings protective structure (bonnet) impact velocities were extracted from the derailment simulation results by examining the vertical displacements of nodes on the upper periphery of each car's fittings protective structure. Whenever one of these bonnet nodes hits the ground, as indicated by its vertical coordinate matching that of the rigid ground plane, the node's velocity just prior to impact is recorded. For this study, only impacts between bonnet and ground were included. While it is recognized that fittings can also be damaged due to collisions with other tanks, such interactions are considered to be of lesser consequence – so these interactions are less likely to cause fittings damage [2]. The impact velocities collated by the above process were analyzed and sorted to generate a histogram of velocities associated with each of the simulated derailments. The histograms from individual derailments are further cumulated and averaged to develop a composite velocity histogram of the impact velocities experienced in a nominal derailment for 100 car trains and different speeds and temperatures, Figure 8. Calculation of the predicted number of fittings failures resulting from the histograms shown in Figure 8 is also discussed in Section 5.

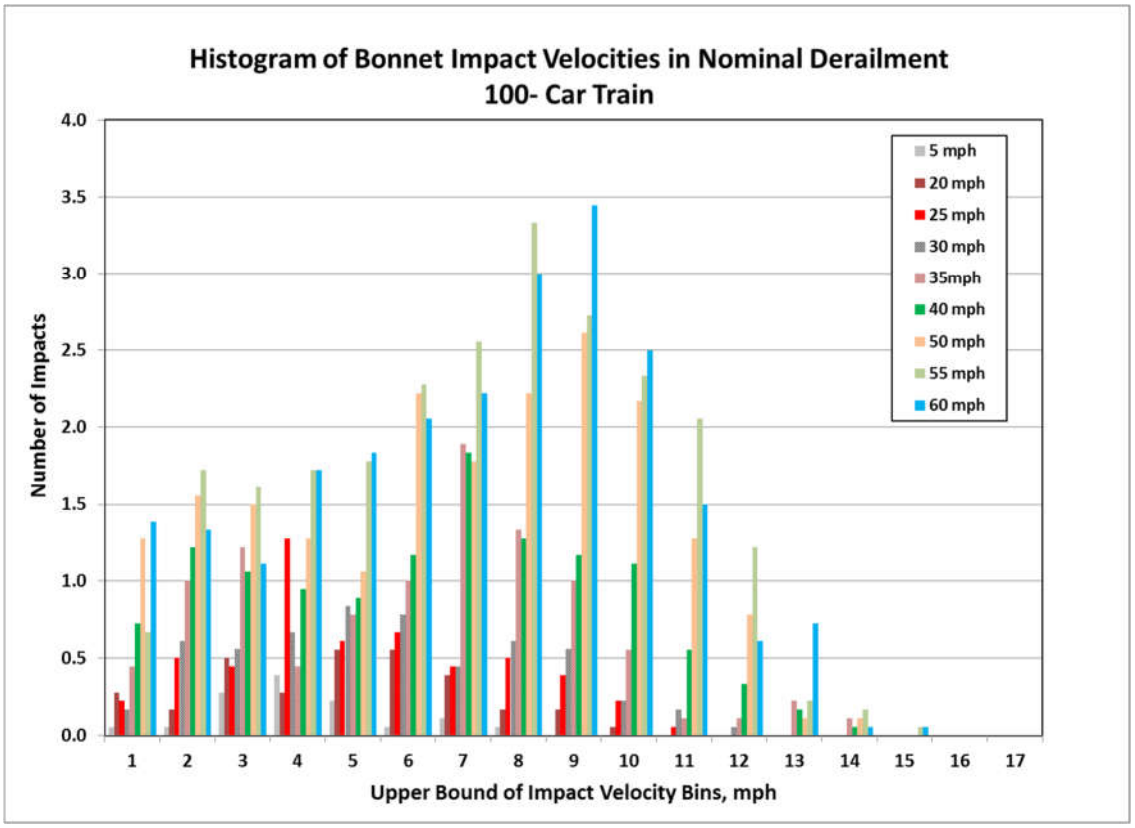


**Figure 8. Histogram of bonnet impact velocities for different speeds**

# 4 EFFECT OF TEMPERATURE ON PUNCTURE RESISTANCE

Since the mechanical properties of steel are affected by temperature, there is a concern that cold temperatures might reduce the puncture resistance of tank cars during train derailments. The effect of temperature on puncture resistance was studied through a two-step process. The first step, described in Section 4.1, was to determine the effect of temperature on material properties. The second step, described in Section 4.2, was to simulate tank car punctures using the material properties derived in Section 4.1.

## 4.1 Effect of Temperature on Material Properties

A report from CanmetMATERIALS details the results of laboratory tests on tank car steels at various temperatures [10]. Figure 9 gives an example from the report showing the effect of temperature on the engineering stress-strain curves for the material TC128B. It shows an initial elastic relationship between stress and strain followed by a plastic region until failure.

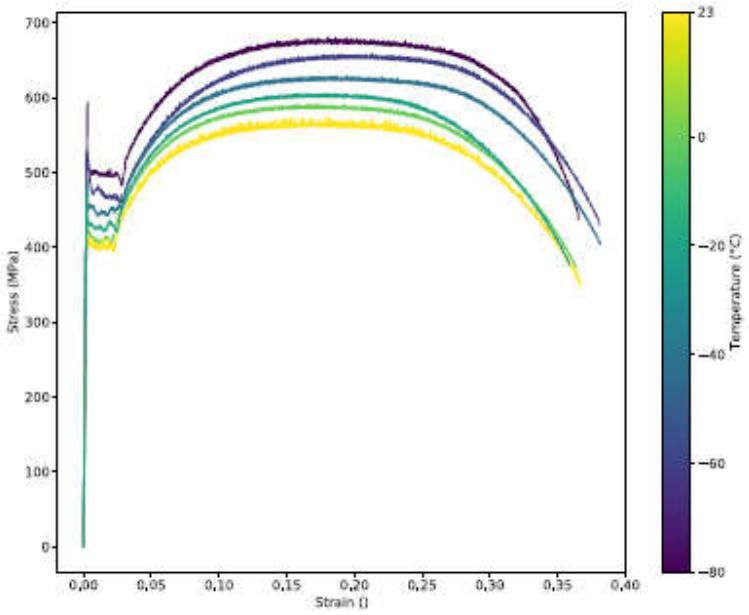


**Figure 9. Effect of temperature on stress-strain curves for TC128B [8]**

Figure 9 shows that the yield and ultimate strengths increase as temperature reduces in the plastic region. In the elastic region the test results at -40 °C had 12% higher yield stress and 9% higher ultimate stress than those at 23 °C. Similar levels of elastic modulus, elongation rate, and area reduction ratio at the failure point were recorded.

Figure 10 gives an example from the CanmetMATERIALS report showing the results of Charpy impact tests on TC128B steel. The Charpy impact test determines the amount of energy absorbed by a material during fracture (expressed as a Charpy V-notch (CVN) value in Joules (J)). It is widely used in industry since the test is easy to prepare for and conduct, and results can be obtained quickly and at low cost.

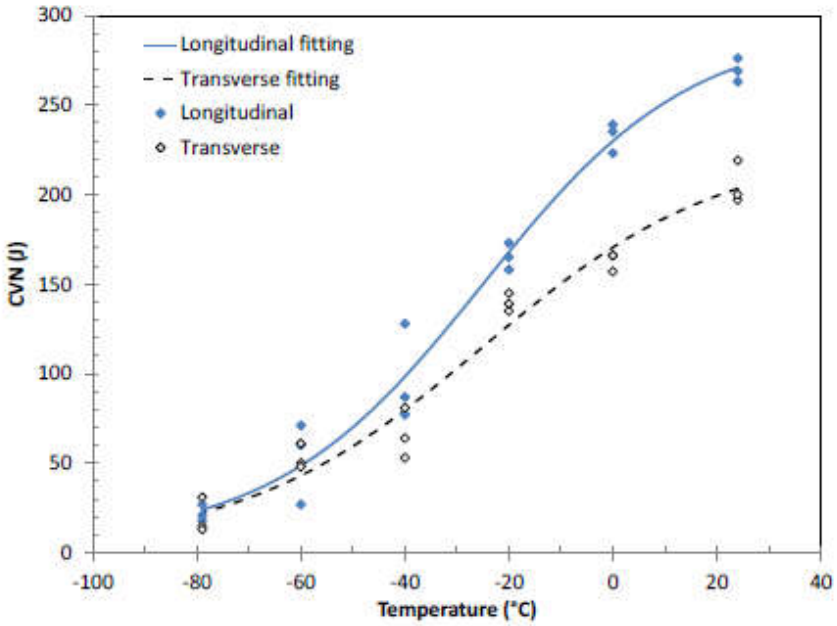


**Figure 10. Charpy impact test results for TC128B [9]**

Figure 10 shows the Charpy impact tests performed at temperatures between -79 and 25 °C. CVN dropped significantly as the temperature was lowered. For example, the CVN value at -40 °C is only 35% of the energy dissipated at room temperature, meaning that the material is locally more prone to fracture at these lower temperatures.

### 4.1.1 Material Model

As an initial literature review of approaches to model this low temperature behavior did not reveal any insights into reasonably characterizing this behavior in any of the standard material models, SA attempted to use a progressive damage material model to characterize the observed behavior of the tank car steel. The model was developed using the ABAQUS finite element modelling tool [12]. Figure 11 shows the stress-strain relationship used by the material model.

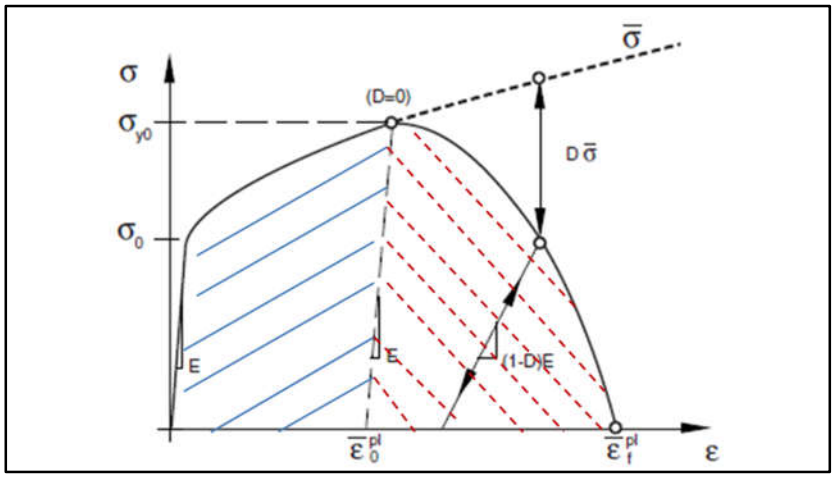


**Figure 11. Stress-strain relationship for the material model [12]**

Figure 11 shows the following four regions:

a) Elastic region (on the left, starting from the origin) – material properties include the elastic modulus (E), Poisson's ratio, and yield stress ($\sigma_0$).
b) Plastic region (shaded in blue) – a rule combining von Mises yield and isotropic hardening was used for the material behavior.
c) Damage initiation point (marked D=0) – the Bao-Wierzbicki criterion [13] was used to define the function between the equivalent plastic strain ($\varepsilon_i^{pl}$) at the initial failure moment and the stress triaxiality ($\eta$). Further details of this approach are given in Appendix B.
d) Damage evolution region (shaded in red) – a damage variable, D, was used to capture the stress softening after the onset of damage. D increases from 0.0 at the initial failure to 1.0 when the plastic strain reaches the final failure value and the element is removed from the simulation.

The plastic strain at failure was computed from the dissipated energy accumulated in the damage process. A linear damage evolution model where the dissipated energy was defined directly through a parameter, $G_{f,}$ which is the fracture energy per unit area, was used.

The following assumptions were made about the effect of temperature in the material model:

- Temperature does not affect the energy dissipated in the elastic-plastic region (blue region in Figure 9). Although the yield stress and ultimate strength increase slightly as temperature reduces, the effect on puncture resistance was not considered significant.
- Post-damage dissipated energy (red region in Figure 11) reduces as temperature reduces. The parameter, $G_f$ is a function of temperature. Conceptually, a small value of $G_f$ is assumed for the brittle damage mode at cold temperatures and a large value is assumed for the ductile damage mode at room temperature.

There is no direct approach or data to generate $G_f$ values for TC128B at a given temperature level. Instead, SA developed a FE model of the Charpy impact test to investigate the relationship between $G_f$ and CVN.

- A group of FE simulations of the standard Charpy impact test with different levels of $G_f$ values of 1, 10, 20, 40, 60 x$10^{-3}$ J/mm$^2$ (0.48, 4.67, 9.35, 18.70, 28.04 ft-lb/in$^2$) was completed. Each FE run gave a unique Charpy dissipated energy (CVN) value.
- Linear interpolation was assumed between the temperature and Charpy CVN value from the lab test data. Another linear interpolation was assumed between the Charpy CVN value and the FE material input, $G_f$ from the FE simulations.
- The temperature and the FE material input, $G_f$, can be linked indirectly through the Charpy CVN value.

### 4.1.2 Charpy Test FE Simulations

Figure 12 shows a schematic of a standard Charpy impact test setup. A hammer is swung on a pendulum from an initial height and impacts the specimen. If failure occurs, the height of the pendulum at the end of its swing is recorded. The delta between the initial and final heights is a measure of the energy absorbed by the specimen. Setup details and specimen dimensions are published in ASTM A370 [14].

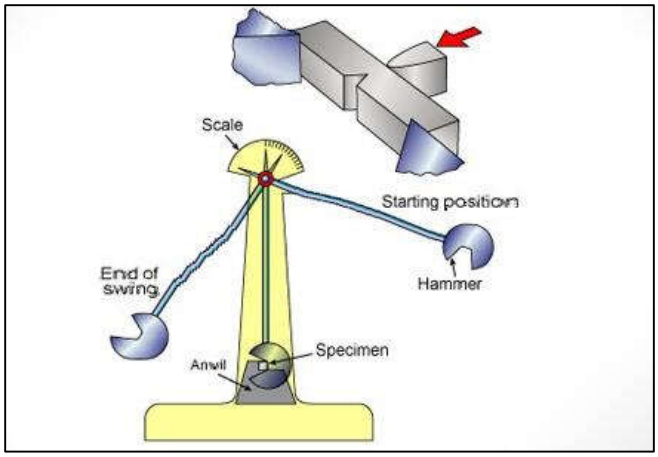


**Figure 12. Standard Charpy impact test setup [15]**

Figure 13 shows the FE model of the Charpy test developed in ABAQUS. The model has three independent parts, the striker (shown in yellow), the V-notch specimen (shown in green), and the supporting fixtures (shown in purple).

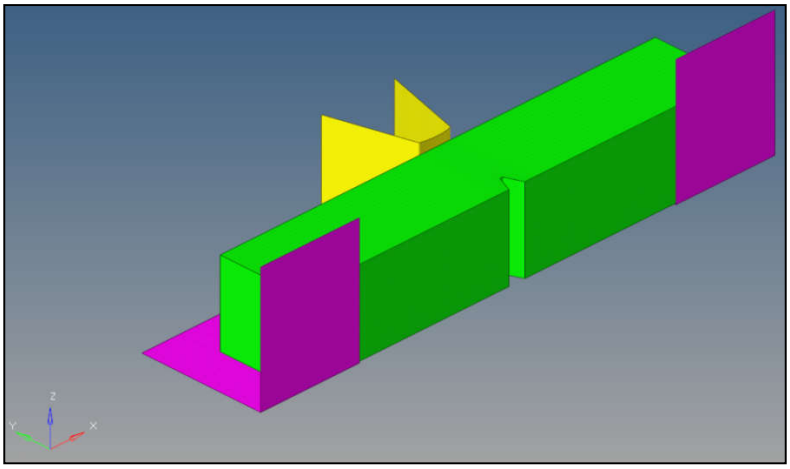

**Figure 13. FE model of Charpy impact test**

The specimen is a full-size 0.4 in x 0.4 in x 2.2 in (10 mm x 10 mm x 55 mm) block with a central V-notch. ASTM A370 [14] was referenced to detail the notch region. The specimen was modeled with three-dimensional (3D) solid elements with reduced integration feature, C3D8R. The overall mesh size was 0.02 in except for the region around the notch where it was refined to 0.001 in. Approximately 500,000 C3D8R elements were created.

A 0.4 in deep striker was included in the model to simulate the contacting surface. ASTM A370 [14] was referenced to detail the front striking face. The striker was modeled with 3D discrete rigid elements, R3D4. The overall mesh size was 0.01 in except for the areas near the corners, which were refined to 0.002 in. In total, 5,280 R3D4 elements were created. A reference point was defined to group all the striker elements as one rigid body.

The supporting fixtures were modeled using 780 R3D4 elements with a mesh size of 0.04 in. Fixed boundary constraints were applied at their reference points.

A point mass element of 55.1 lb. was assigned at the reference point of the striker. An initial velocity of 12.3 mph (mile per hour) in the moving direction and fixed boundary conditions in two other directions were applied at the reference point. The striker had initial kinetic energy of 279 ft-lb.

During the dynamic impact, an explicit surface-to-surface contact algorithm was selected to build the interactions among the three parts. The contact properties were assumed as hard contact in the normal direction and a penalty friction formulation with 0.3 as friction coefficient in the tangential direction.

### 4.1.3 Charpy Test FE Results and Analysis

Figure 14 shows an example result from the FE simulation. It shows how the energy balance changed with time during the test. The value of $G_f$ in this example was 20 x$10^{-3}$J/mm$^2$ (9.35 ft-lb/in$^2$).

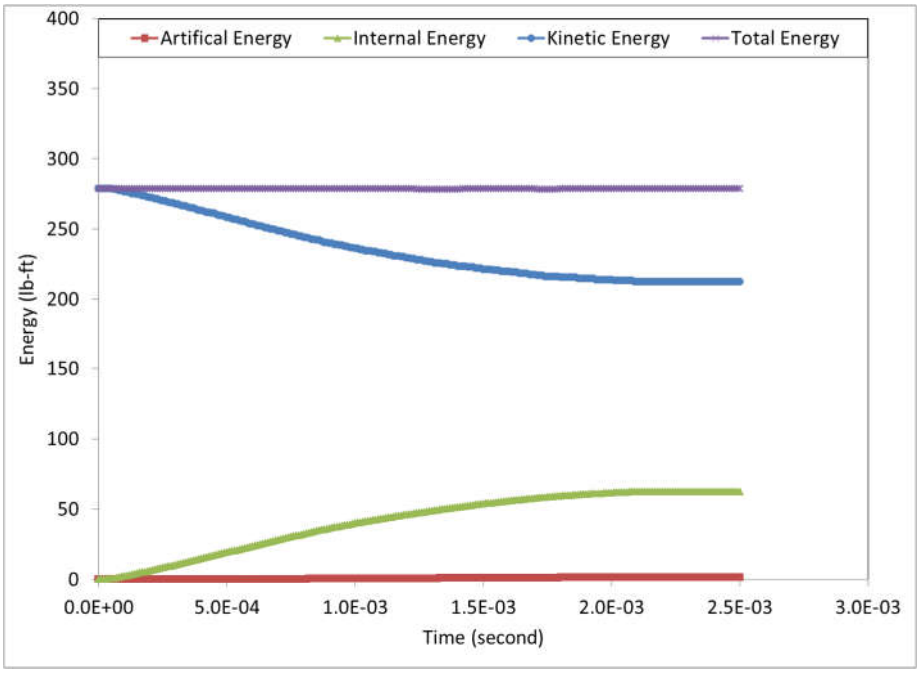


**Figure 14. Energy Balance in the FE Charpy simulation - $G_f$ = 9.35 ft-lb/in$^2$**

Figure 14 shows the initial kinetic energy of 279 ft-lb dropped gradually to 212.8 ft-lb when the specimen finally fractured. The energy difference of 66.2 ft-lb is the CVN value. Internal energy absorbed by the failure of the specimen increased gradually to approximately 66.2 ft-lb. The difference between the drop in kinetic energy and the final internal energy (referred to as the artificial energy) is less than 3.0% of the internal energy. This indicates an acceptable dynamic explicit analysis. Similar results were found for the other values of $G_f$.

Figure 15 shows the relationships between the kinetic energy and the pendulum displacement for the five values of $G_f$ used in the simulations. The absorbed CVN values for each model were computed from these results.

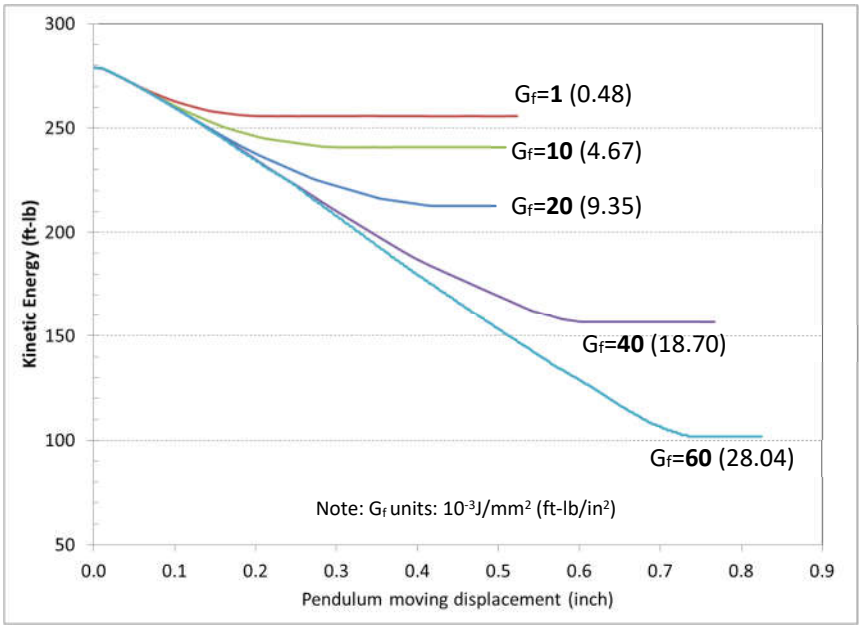


**Figure 15. Kinetic energies in the FE Charpy simulations**

Table 4 shows the CVN values obtained from the five FE simulations.

**Table 4: $G_f$ and CVN results from FE simulations**

| $G_f$ ($10^{-3}$J/mm$^2$) | $G_f$ (ft-lbs/in.$^2$) | Absorbed CVN Values (ft-lb) |
|---|---|---|
| 1 | 0.48 | 23 |
| 10 | 4.67 | 38 |
| 20 | 9.35 | 66 |
| 40 | 18.70 | 122 |
| 60 | 28.04 | 177 |

Table 5 shows key results from the Charpy laboratory tests and the linearly interpolated $G_f$ values needed to match them. The transverse and longitudinal CVN test results were averaged in the table, as the FE simulations use an isotropic material model. The $G_f$ values were found by linear interpolation of the data in Table 4. For example, at room temperature (20°C), the average CVN value from the laboratory tests was 171.9 ft-lb. Linear interpolation between the last two simulation results in Table 4 gives $G_f$ = 27.7 ft-lb/in.$^2$) for an absorbed CVN value of 171.9 ft-lb.

**Table 5: Charpy test and FE simulation results**

| Temp (°C) | Absorbed CVN Values (from test) | | | | Interpolated $G_f$ from FE simulations (ft-lb/in.$^2$) |
|---|---|---|---|---|---|
| | Long. Direction (J) | Trans. Direction (J) | Average | | |
| | | | (J) | (ft-lb) | |
| 20 | 267 | 199 | 233 | 171.9 | 27.7 |
| -15 | 185 | 139 | 162 | 119.5 | 18.6 |
| -25 | 150 | 115 | 133 | 98.1 | 15.0 |
| -40 | 98 | 80 | 89 | 65.6 | 9.3 |

### 4.1.4 Material Behavior Results

The results from the Charpy FE simulations gave insight into how the material behaved at different temperatures. Figure 15 shows the relationships between striker acceleration and displacement at different $G_f$ values.

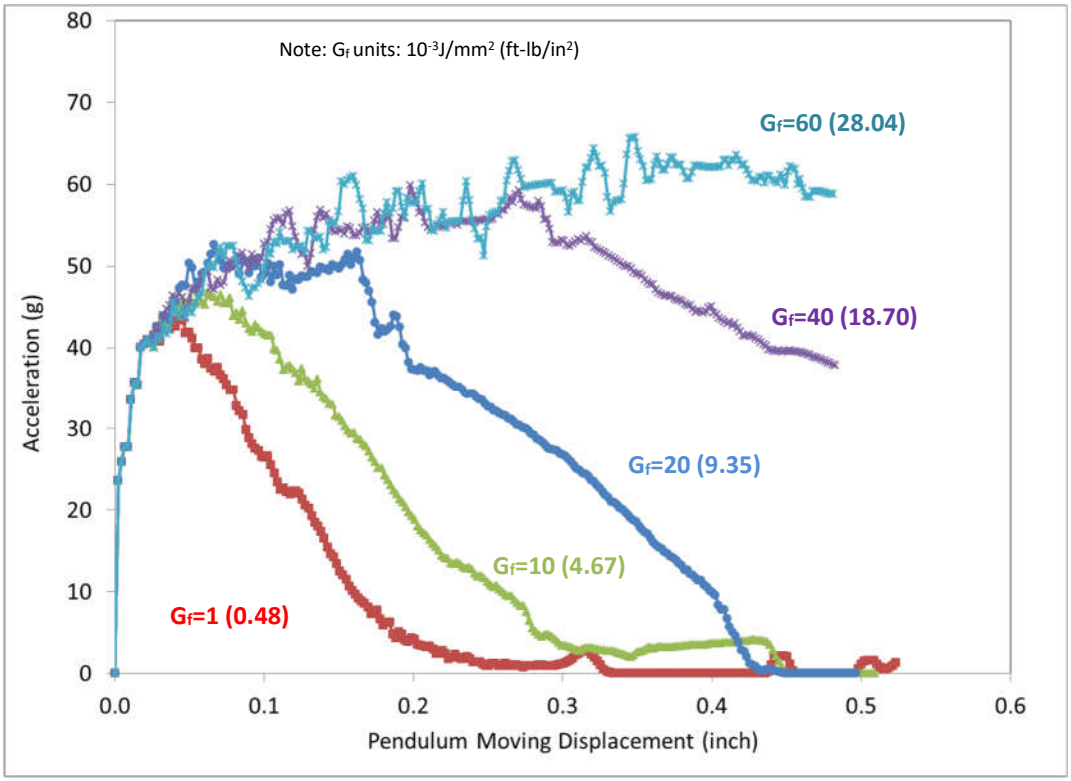


**Figure 15. Acceleration versus displacement at strike reference node**

Figure 15 shows sudden, brittle damage modes for small $G_f$ values and gradual, ductile damage modes for the large $G_f$ values. As shown in Table 5, the small $G_f$ values associated with lower temperatures, confirm that the brittle failure observed with TC128B steel at low temperatures can be modeled with this approach.

Figure 16 and Figure 17 show the equivalent plastic strain in the specimen after failure with $G_f$=0.48 ft-lb/in.$^2$ and $G_f$ = 28.04 ft-lb/in$^2$, respectively. The smooth fracture surfaces and few plastic zones in Figure 16 indicate a brittle damage mode, while the coarse fracture surfaces and numerous plastic zones in Figure 17 indicate a ductile damage mode.

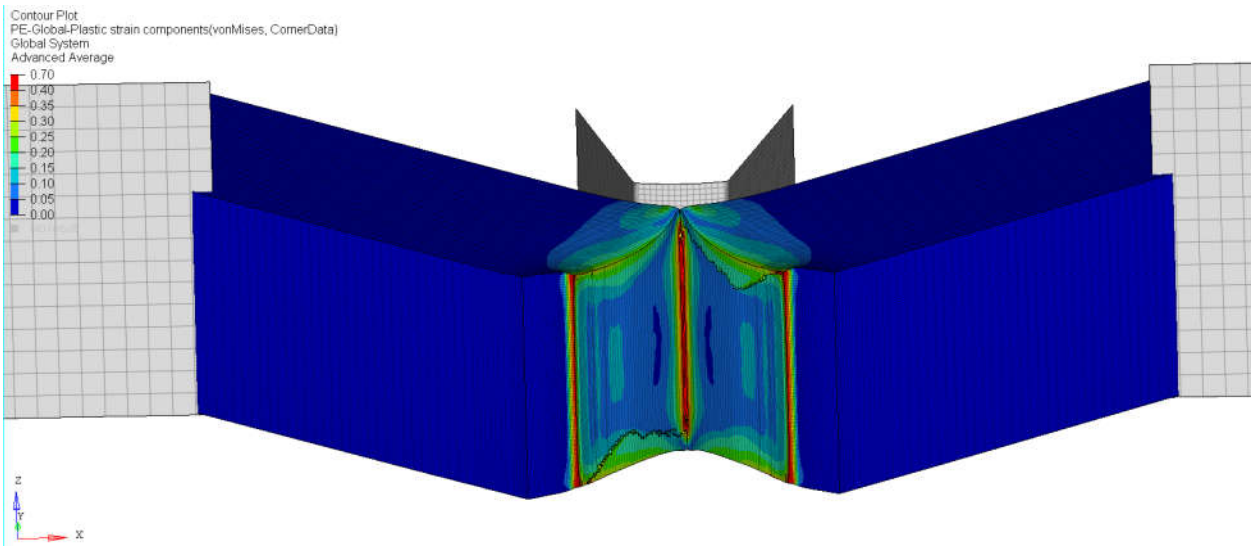


**Figure 16. Brittle damage mode of FE Charpy simulation - $G_f$=0.48 ft-lb/in$^2$**

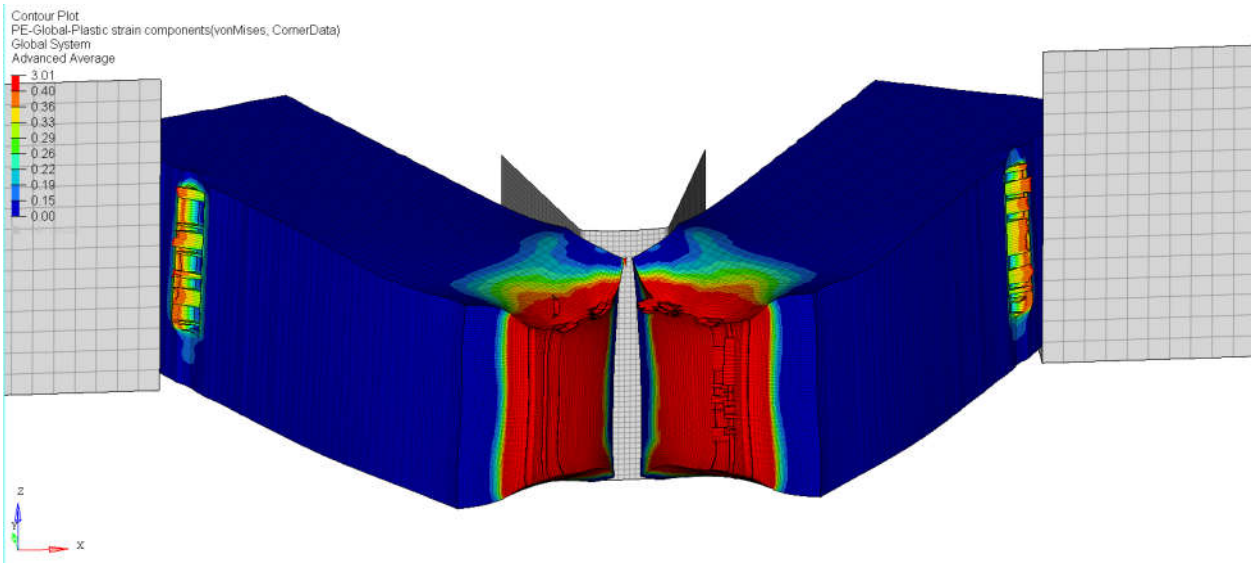


**Figure 17. Ductile damage mode of FE Charpy simulation - $G_f$=28.04 ft-lb/in$^2$),**

## 4.2 Tank Car Side Impact FE Simulations

In order to translate the effect of the $G_f$ values (developed in Section 4.1) on the puncture performance of tank cars under derailment impact conditions, an FE simulation of side impact on a tank car was developed. The effect of steel temperature was studied by adjusting the $G_f$ value of the tank car shell material model.

### 4.2.1 Tank Shell Model

Figure 18 shows the model of the sub-scale tank shell, which was composed of 7/16” thick, TC128B steel. An impactor weighing 50,000 lbs. targeted the center of the shell. The tank shell was fixed at the edges and the impactor was restricted to only move in the normal direction.

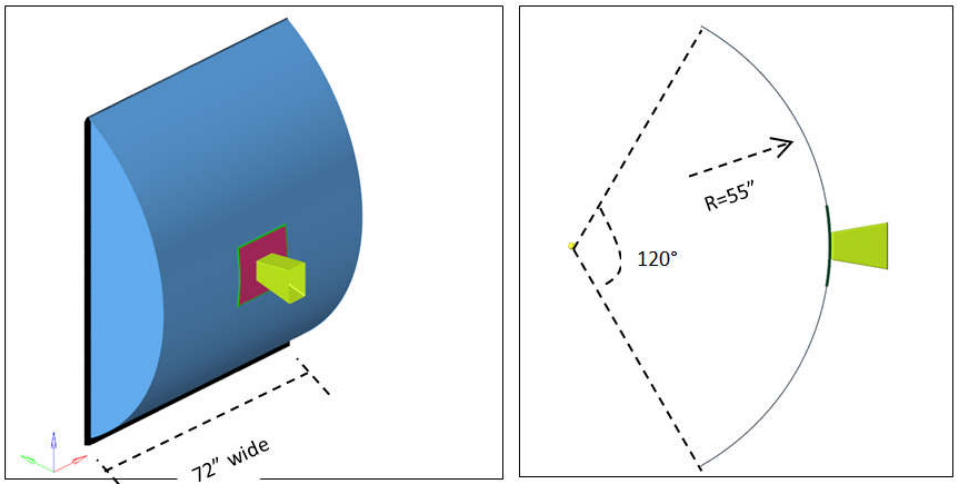


**Figure 18. Tank shell FE model**

The tank shell was meshed with shell elements, S3R and S4R, and solid elements, C3D8R. Figure 19 shows a close-up view near the central zone. The solid elements were sized at 1/16" and the shell elements were sized at 0.5". There were 54,000 shell elements and 216,000 solid elements for the tank shell. A shell-to-solid constraint option available in the ABAQUS software was used to join the shell meshes and the solid meshes.

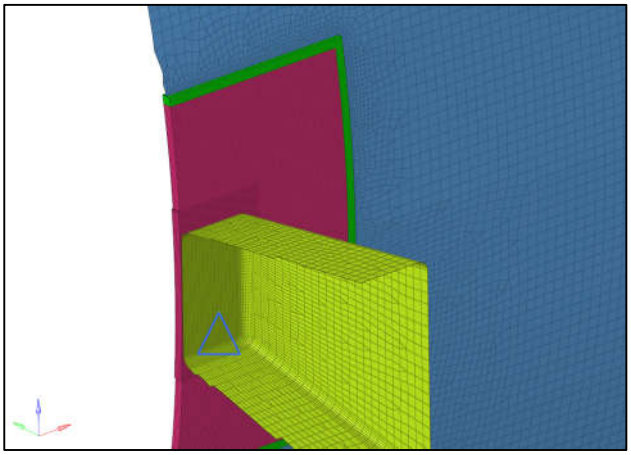

**Figure 19. Close-up FE mesh view at the center of the tank shell**

Three different sized impactors were used: 2"x2", 4"x4", and 6"x6". Figure 20 shows the 6"x6" impactor with a front corner radius of 0.5". The 2"x2" impactor had a front corner radius of 0.25" and the 4"x4" impactor had a front corner radius of 0.375". The same side slope of 10° was used for all impactors.

All the impactors were meshed by 3D rigid shell elements, R3D3 and R3D4. The mesh for the front face was sized at 0.1" and the end edges were meshed at 0.5". A total of 8,000 elements were used for the 6"x6" impactor. A mass element of 50,000 lb. was located at the impactor reference point.

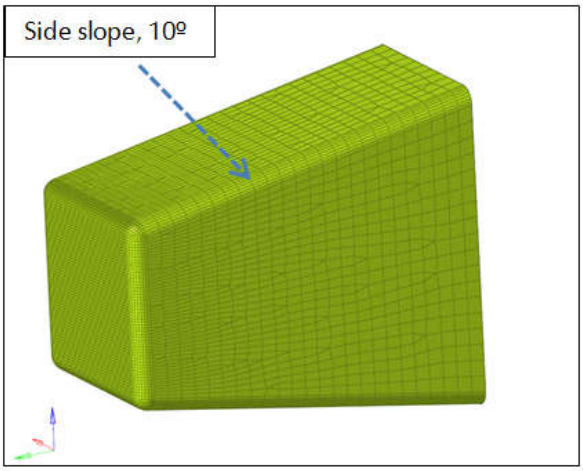


**Figure 20. 6"x6" impactor FE model**

During the impact simulation, an explicit general contact algorithm was selected to generate the interactions between the impactor and tank shell. The hard contact properties were used in the normal direction and the penalty friction formulation with 0.3 as friction coefficient was used in the tangential direction.

Table 6 gives the material properties in terms of the ABAQUS inputs for the model described in Section 4.1.1. Three $G_f$ levels were used to cover a wide range of temperature possibilities.

**Table 6: Material properties used for TC128B with ABAQUS**

| Material properties | ABAQUS Keywords and input with units |
|---|---|
| Density | *density,<br>7.35e-4 (lbm/in.$^3$) |
| Elastic | *elastic, type=isotropic<br>E=29000000 (psi), Poisson Ratio= 0.3 |
| Plastic | *plastic, hardening=isotropic<br>Yield stress ratios in three directions:<br>50086 (psi), 0.0<br>96390 (psi), 0.17<br>121500 (psi), 0.47 |
| Damage Initiation | *damage initiation, criterion = ductile<br>Data of stress triaxiality and equivalent plastic strain are referenced in Appendix B. |
| Damage Evolution | *damage evolution, type=energy<br>1x10$^{-3}$ (J/mm$^2$) (0.48 ft-lb/in$^2$), 0.0, note: $G_f$ value #1<br>35x10$^{-3}$(J/mm$^2$) (16.7 ft-lb/in$^2$), 0.0, note: $G_f$ value #2<br>245x10$^{-3}$ (J/mm$^2$) (116.7 ft-lb/in$^2$), 0.0, note: $G_f$ value #3 |

### 4.2.2 Tank Car FE Results and Analysis

Nine FE scenarios were performed to cover the three sizes of impactor and three $G_f$ values. For each scenario, a series of explicit dynamic runs with increasing initial speed was completed. In this report, this approach is termed 'Incremental Puncture Analysis' (IPA).

Figure 21 shows example results from the simulations with a 2”x2” impactor and a $G_f$ value of 0.48 ft-lb/in.$^2$). As shown in this example, the impactor did not penetrate the shell at 5.5 mph, but at 6.0 mph it did. Simulations were also performed at 5.6 and 5.7 mph.

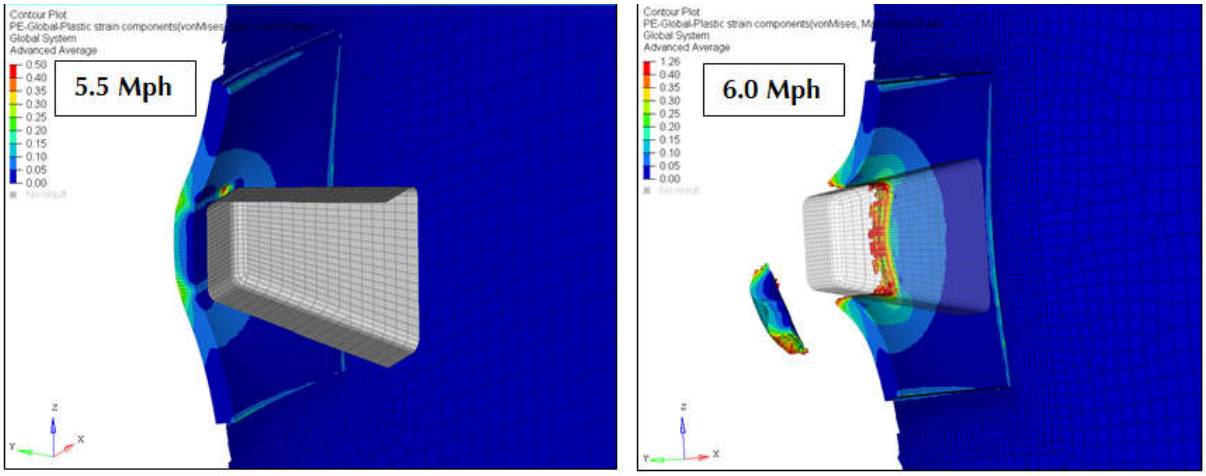


**Figure 21. Deformation modes in the case of $G_f$=0.48 ft-lb/in$^2$ and 2”x2” impactor**

Figure 22 shows the relationships between impactor velocity and displacement for all four simulation speeds with a 2”x2” impactor and a $G_f$ value of 0.48ft-lb/in.$^2$. The lowest initial velocity under which the impactor can penetrate the tank shell is defined as the puncture velocity. In this example the puncture velocity is 5.6 mph.

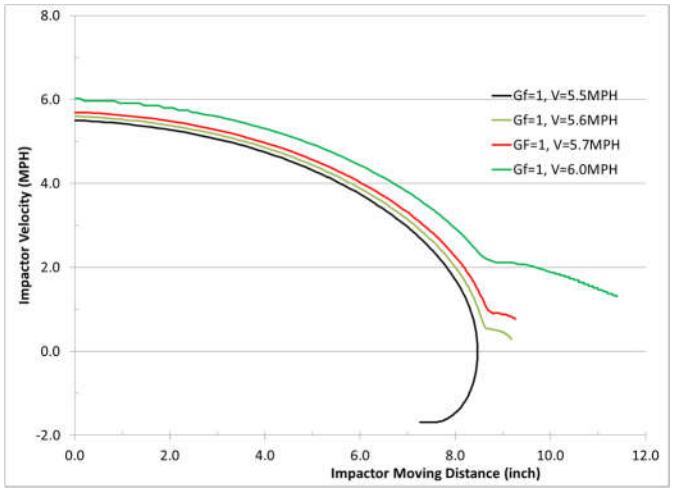


**Figure 22. Velocity vs. displacement – 2”x2” impactor, $G_f$=0.48 ft-lb/in$^2$**

Figure 23 shows the relationships between impactor deceleration and displacement for all four simulation speeds with a 2”x2” impactor and a $G_f$ value of 0.48 ft-lb/in.$^2$. For the simulation at 5.6 mph case, a peak deceleration of 2.53 g was recorded.

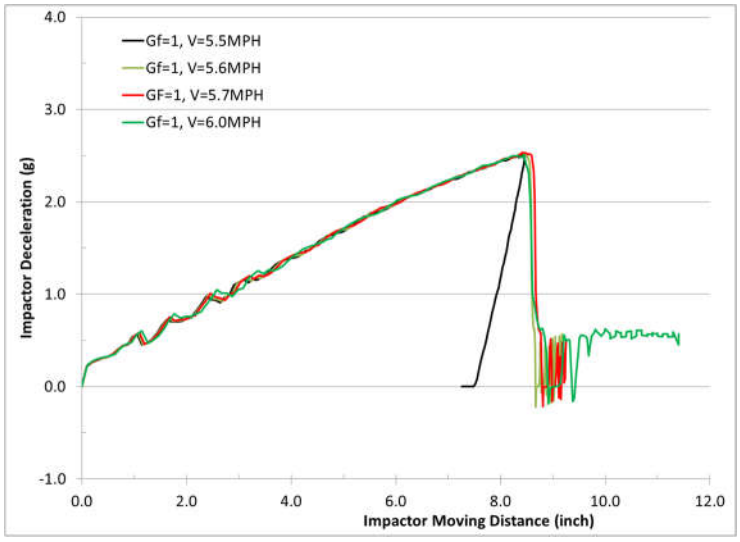


**Figure 23. Deceleration vs. displacement – 2"x2" impactor, $G_f$=0.48 ft-lb/in$^2$**

The same IPA approach was used to determine the puncture velocities and the peak decelerations in the remaining eight scenarios. Table 7 gives the results from the FE simulations.

**Table 7: Results of tank shell puncture simulations**

| $G_f$ (ft-lb/in$^2$) | Simulation Results | | | | | |
|---|---|---|---|---|---|---|
| | Puncture Speed (mph) | | | Impactor deceleration (g) | | |
| | Impactor size (in.×in.) | | | Impactor size (in.×in.) | | |
| | 2x2 | 4x4 | 6x6 | 2x2 | 4x4 | 6x6 |
| 0.48 | 5.6 | 14.2 | 20.5 | 2.53 | 4.55 | 6.50 |
| 16.7 | 5.8 | 14.9 | 21.5 | 2.61 | 4.88 | 6.86 |
| 116.7 | 6.8 | 17.0 | 26.0 | 3.00 | 5.70 | 7.66 |

Table 8 presents the interpolated (linear) puncture speeds and decelerations for the different $G_f$ values (corresponding to the different temperatures), which were estimated from the FE results in Table 7.

**Table 8: Interpolated results from puncture simulations**

| Temp (°C) | $G_f$ (ft-lb/in$^2$) | Simulation Results | | | | | |
|---|---|---|---|---|---|---|---|
| | | Puncture Speed (mph) | | | Impactor deceleration (g) | | |
| | | Impactor size (in.×in.) | | | Impactor size (in.×in.) | | |
| | | 2x2 | 4x4 | 6x6 | 2x2 | 4x4 | 6x6 |
| 20 | 27.7 | 5.91 | 15.13 | 22.00 | 2.65 | 4.97 | 6.95 |
| -15 | 18.6 | 5.82 | 14.94 | 21.59 | 2.62 | 4.90 | 6.88 |
| | % Change from 20°C | -1.54% | -1.26% | -1.86% | -1.34% | **-1.50%** | -1.05% |
| -25 | 15.0 | 5.78 | 14.83 | 21.40 | 2.60 | 4.85 | 6.82 |
| | % Change from 20°C | -2.21% | -2.01% | -2.72% | -1.93% | **-2.51%** | -1.81% |
| -40 | 9.3 | 5.71 | 14.59 | 21.05 | 2.57 | 4.73 | 6.70 |
| | % Change from 20°C | -3.38% | -3.60% | -4.29% | -2.97% | **-4.79%** | -3.59% |

Since the mass of the impactor was constant, puncture force is directly related to puncture deceleration through Newton's second law. To be conservative, the worst-case reductions (shown in bold font in

Table 8) were used to generate adjustments to puncture resistance to account for temperature. Using the relevant percentages from Table 8 (shown in bold), this led to the following estimates:

- At -15 °C the puncture resistance is 98.5% of its value at 20 °C
- At -25 °C the puncture resistance is 97.5% of its value at 20 °C
- At -40 °C the puncture resistance is 95.0% of its value at 20 °C

### 4.2.3 Results for Non-normalized Steel

In the late 1980s, the Association of American Railroads' recommended practices were changed to require all subsequent pressure cars to be fabricated from normalized TC128B steel. Prior to 1989, non-normalized steel was predominantly used, including non-normalized TC128B and A516[16]. Non-normalized steel has a higher transition temperature and potentially lower fracture toughness when compared to normalized steel [16]. Comparing the material properties between normalized and non-normalized steels suggests that the basic stress-strain curves are similar, with the non-normalized steels having slightly higher yield and ultimate strengths and a slightly lower elongation. The CVN values, however, are notably lower for the non-normalized steels. Therefore, it is assumed for this analysis that the potential lower performance for non-normalized steels is largely driven by the lower CVN values, and not by changes to the basic stress-strain characteristics. It was further assumed that the non-normalized, -50°F, case represented a 'baseline' scenario with no 'post-damage' energy[2]; i.e., the FE element fails as soon as it has fractured, corresponding to a $G_f$ value of zero. Post-damage energies for the other cases were calculated based on the baseline from the non-normalized case at -50°F. $G_f$ values were then estimated from the post-damage energies and used to estimate puncture velocities and decelerations, using results from the nine scenarios simulated earlier. Table 9 shows the results.

**Table 9: Estimation for puncture responses for normalized vs. non-normalized steel**

| Steel Type | Temp | Test Energy Values (ft-lb) | | Estimated $G_f$ (ft-lb/in2) | Puncture Speed (mph) | | | Impactor deceleration (g) | | |
|---|---|---|---|---|---|---|---|---|---|---|
| | | CVN | Post damage | | Impactor size (in.×in.) | | | Impactor size (in.×in.) | | |
| | | | | | 2x2 | 4x4 | 6x6 | 2x2 | 4x4 | 6x6 |
| Non-normalized | 50F | 21.3 | 15.7 | 4.6 | 5.65 | 14.38 | 20.76 | 2.55 | 4.64 | 6.59 |
| | 0 | 10.8 | 5.2 | 1.5 | 5.61 | 14.25 | 20.57 | 2.54 | 4.57 | 6.52 |
| | -50F | 5.6 | 0.0 | 0.0 | 5.60 | 14.18 | 20.48 | 2.53 | 4.54 | 6.49 |
| Normalized | 50F | 77.3 | 71.7 | 13.9 | 5.77 | 14.78 | 21.33 | 2.60 | 4.82 | 6.80 |
| | 0 | 52.2 | 46.6 | 9.7 | 5.71 | 14.60 | 21.07 | 2.58 | 4.74 | 6.70 |
| | -50F | 26.4 | 20.8 | 5.5 | 5.66 | 14.42 | 20.81 | 2.55 | 4.65 | 6.61 |
| Difference with normalized | 50F | | | | -2.0% | -2.8% | -2.7% | -1.8% | **-4.0%** | -3.1% |
| | 0 | | | | -1.8% | -2.5% | -2.4% | -1.6% | -3.6% | -2.8% |
| | -50F | | | | -1.2% | -1.6% | -1.6% | -1.1% | -2.4% | -1.8% |

Table 9 further shows the percentage reductions in puncture velocity and deceleration for non-normalized compared to normalized tank shell steels. To be conservative, based on the maximum difference of 4 %, it was estimated that the puncture resistance of non-normalized steel is 96% of that of normalized steel. This reduction of 4% was applied in addition to the difference in temperatures computed earlier.

[2] The area under the red dashed lines in Figure 11 is assumed to be zero.

# 5 RESULTS

## 5.1 Tank Puncture Calculations

The impact force histograms derived from the derailment simulations outlined in Section 3 were combined with the tank car resistance data and an assumed impactor distribution to predict the number of punctures for a TC-117J tank car and nine variations of TC-117R tank cars. The results described in Section 4 were used to account for the effect of temperature on puncture resistance.

Table 10 lists the characteristics of the cars that were evaluated.

**Table 10: Characteristics of evaluated tank cars**

| Model Code | Tank car type | Source Tank Car | Steel Type | Shell Thickness | Top fittings protection specification |
|---|---|---|---|---|---|
| TC-A | TC-117J | N/A | TC128B normalized | 9/16” | Section 8.2.3.4.1 of TP14877 |
| TC-B | TC-117R | Unjacketed CPC 1232 | TC128B, normalized | 1/2” | Section 8.2.3.4.1 of TP14877 |
| TC-C | TC-117R | Jacketed CPC 1232 | TC128B normalized | 7/16” | Section 8.2.3.4.1 of TP14877 |
| TC-D | TC-117R | Jacketed CPC 1232 | TC128B normalized | 7/16” | Section 8.2.3.4.2, ½” protective housing |
| TC-E | TC-117R | Legacy TC 111 | TC128B non-normalized | 7/16” | Section 8.2.3.4.1 of TP14877 |
| TC-F | TC-117R | Legacy TC 111 | TC128B non-normalized | 7/16” | Section 8.2.3.4.2, ½” protective housing |
| TC-G | TC-117R | Legacy TC 111 | TC128B normalized | 7/16” | Section 8.2.3.4.1 of TP14877 |
| TC-H | TC-117R | Legacy TC 111 | TC128B normalized | 7/16” | Section 8.2.3.4.2, ½” protective housing |
| TC-J | TC-117R | | A516-70, normalized | 9/16” | Section 8.2.3.4.1 of TP14877 |
| TC-K | TC-117R | | A516-70, normalized | 1/2” | Section 8.2.3.4.1 of TP14877 |

The minimum values for tank car steels that meet the current specification (Appendix M of M-1002 - AAR Tank Car Manual 2014 Edition) were used to represent the worst-case scenario.

In all cases the tank car was fitted with a jacket. The jacket thickness and type was 11 gauge, ASTM-A1011. Although the source car for case TC-B did not have a jacket, one was included to comply with the TC-117R retrofit requirements. The same mechanical properties were considered for the jacket in all cases. In all cases the ends of the tank cars had 1/2” thick, full height head shields. The material for the headshields was normalized steel with a tensile strength of 379 MPa, and the same properties were used for all headshields.

Figure 24 shows the impactor distribution used in the analysis. This distribution was also used in prior work for FRA and TC [1]. It assumes that a large majority of impactors (about 71%) are in the range from

3”x3” to 13”x13”, with a small fraction of impactors (3%) being smaller and the rest being larger. Other researchers have also followed this approach for impactor distributions, though the format of representation may be a little different [20].

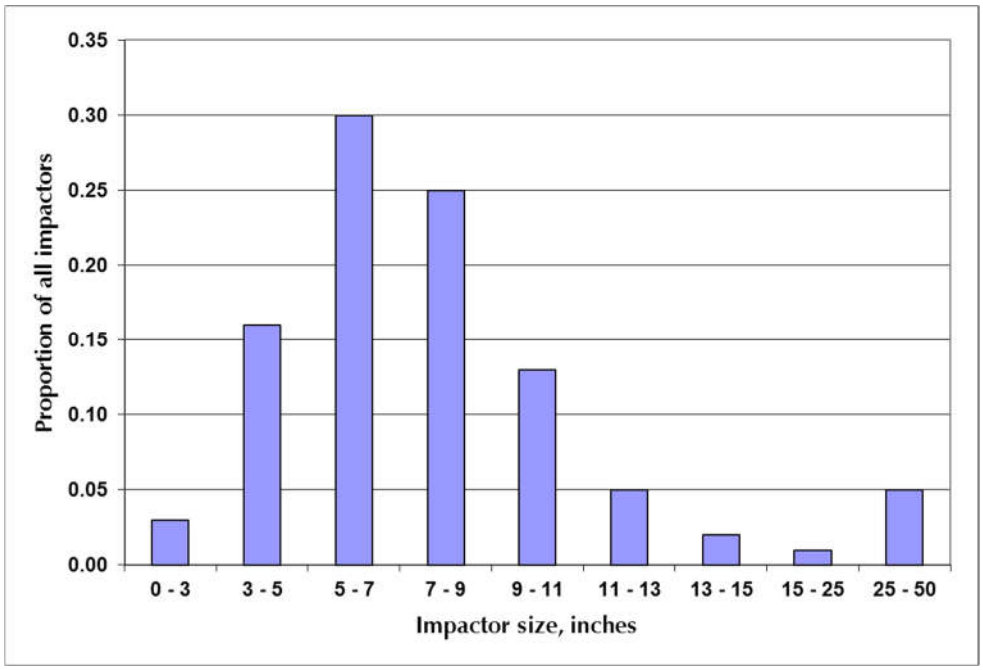


**Figure 24. Assumed impactor distribution**

The number of punctures following a derailment was calculated based on previously established methods [1]. In summary, the process for each car design is as follows:

1. Select the appropriate head and shell puncture resistance curves for the car design being analyzed from previous published data [17].
2. Adjust the puncture resistance curve to account for temperature and steel normalization condition (as discussed in Sections 4.2.2 and 4.2.3)
3. For each load magnitude (bin) in the load histogram:
   3.1. Determine the largest impactor size that will result in car puncture for the head and shell.
   3.2. Calculate the proportion of impactors that fall below that size threshold using the distribution of impactors (Figure 24). This gives the probability that a load of that magnitude will result in a car puncture.
4. Weigh the probabilities by the corresponding prevalence of the impact type (head or shell) and multiply by the number of collisions in the load magnitude bin.
5. Sum this probability over all the load bins in the histogram to estimate the probability that an individual car will be punctured.

Tables 11 through 14 give the results of this analysis for temperatures of 20, -15, -25, and -40 °C respectively. Each table shows the predicted number of punctures in a 100-car train for derailment speeds of 5, 20, 25, 30, 35, 40, 50, 55, and 60 mph.

## Table 11. Puncture Performance of TC-117 Variants at 20 °C

| Model Code | Tank car type | Source Tank Car | Steel Type | Shell Thickness | Jacket type and thickness | Top fittings protection description | Head shield | Number of punctures (20 degrees C) | | | | | | | | |
|---|---|---|---|---|---|---|---|---|---|---|---|---|---|---|---|---|
| | | | | | | | | 5 mph | 20 mph | 25mph | 30 mph | 35 mph | 40 mph | 50 mph | 55 mph | 60mph |
| TC-A | **TC-117J** | N/A | TC128B normalized | 9/16" | 11 gauge, ASTM A1011 steel | Meet the requirements in Section 8.2.3.4.1 of TP14877 | ½" thick, full height, normalized steel (minimum tensile strength equal to or greater than 379 MPa) | 0.036 | 1.0 | 2.2 | 3.3 | 5.0 | 6.9 | 10.0 | 11.5 | 13.5 |
| TC-B | **TC-117R** | Unjacketed CPC 1232 | TC128B normalized | ½" | 11 gauge, ASTM A1011 | Meet the requirements in Section 8.2.3.4.1 of TP14877 | ½" thick, full height, normalized steel | 0.046 | 1.2 | 2.5 | 3.8 | 5.6 | 7.7 | 11.2 | 12.8 | 15.0 |
| TC-C | **TC-117R** | Jacketed CPC 1232 | TC128B normalized | 7/16" | 11 gauge, ASTM A1011 | Meet the requirements in Section 8.2.3.4.1 of TP14877 | ½" thick, full height, normalized steel | 0.056 | 1.4 | 2.9 | 4.3 | 6.3 | 8.6 | 12.6 | 14.4 | 16.7 |
| TC-D | **TC-117R** | Jacketed CPC 1232 | TC128B normalized | 7/16" | 11 gauge, ASTM A1011 | Section 8.2.3.4.2, ½" protective housing | ½" thick, full height, normalized steel | 0.056 | 1.4 | 2.9 | 4.3 | 6.3 | 8.6 | 12.6 | 14.4 | 16.7 |
| TC-E | **TC-117R** | Legacy TC 111 | TC128B non-normalized | 7/16" | 11 gauge, ASTM A1011 | Meet the requirements in Section 8.2.3.4.1 of TP14877 | ½" thick, full height, normalized steel | 0.064 | 1.5 | 3.1 | 4.6 | 6.7 | 9.2 | 13.4 | 15.3 | 17.8 |
| TC-F | **TC-117R** | Legacy TC 111 | TC128B non-normalized | 7/16" | 11 gauge, ASTM A1011 | Section 8.2.3.4.2, ½" protective housing | ½" thick, full height, normalized steel | 0.064 | 1.5 | 3.1 | 4.6 | 6.7 | 9.2 | 13.4 | 15.3 | 17.8 |
| TC-G | **TC-117R** | Legacy TC 111 | TC128B normalized | 7/16" | 11 gauge, ASTM A1011 | Meet the requirements in Section 8.2.3.4.1 of TP14877 | ½" thick, full height, normalized steel | 0.056 | 1.4 | 2.9 | 4.3 | 6.3 | 8.6 | 12.6 | 14.4 | 16.7 |
| TC-H | **TC-117R** | Legacy TC 111 | TC128B normalized | 7/16" | 11 gauge, ASTM A1011 | Section 8.2.3.4.2, ½" protective housing | ½" thick, full height, normalized steel | 0.056 | 1.4 | 2.9 | 4.3 | 6.3 | 8.6 | 12.6 | 14.4 | 16.7 |
| TC-J | **TC- 117R** | | A516-70, normalized | 9/16" | 11 gauge, ASTM A1011 | Meet the requirements in Section 8.2.3.4.1 of TP14877 | ½" thick, full height, normalized steel | 0.058 | 1.4 | 2.9 | 4.3 | 6.3 | 8.6 | 12.6 | 14.4 | 16.7 |
| TC-K | **TC- 117R** | | A516-70, normalized | 1/2" | 11 gauge, ASTM A1011 | Meet the requirements in Section 8.2.3.4.1 of TP14877 | ½" thick, full height, normalized steel | 0.070 | 1.6 | 3.2 | 4.8 | 7.0 | 9.4 | 13.9 | 15.8 | 18.3 |

## Table 12. Puncture Performance of TC-117 Variants at -15 °C

| Model Code | Tank car type | Source Tank Car | Steel Type | Shell Thickness | Jacket type and thickness | Top fittings protection description | Head shield | Number of punctures (-15 degrees C) | | | | | | | | |
|---|---|---|---|---|---|---|---|---|---|---|---|---|---|---|---|---|
| | | | | | | | | 5 mph | 20 mph | 25mph | 30 mph | 35 mph | 40 mph | 50 mph | 55 mph | 60 mph |
| TC-A | **TC-117J** | N/A | TC128B normalized | 9/16" | 11 gauge, ASTM A1011 steel | Meet the requirements in Section 8.2.3.4.1 of TP14877 | ½" thick, full height, normalized steel (minimum tensile strength equal to or greater than 379 MPa) | 0.0 | 1.0 | 2.3 | 3.4 | 5.1 | 7.1 | 10.2 | 11.8 | 13.8 |
| TC-B | **TC-117R** | Unjacketed CPC 1232 | TC128B normalized | ½" | 11 gauge, ASTM A1011 | Meet the requirements in Section 8.2.3.4.1 of TP14877 | ½" thick, full height, normalized steel | 0.0 | 1.2 | 2.6 | 3.9 | 5.8 | 7.9 | 11.5 | 13.2 | 15.4 |
| TC-C | **TC-117R** | Jacketed CPC 1232 | TC128B normalized | 7/16" | 11 gauge, ASTM A1011 | Meet the requirements in Section 8.2.3.4.1 of TP14877 | ½" thick, full height, normalized steel | 0.1 | 1.4 | 3.0 | 4.4 | 6.5 | 8.8 | 12.9 | 14.70 | 17.1 |
| TC-D | **TC-117R** | Jacketed CPC 1232 | TC128B normalized | 7/16" | 11 gauge, ASTM A1011 | Section 8.2.3.4.2, ½" protective housing | ½" thick, full height, normalized steel | 0.1 | 1.4 | 3.0 | 4.4 | 6.5 | 8.8 | 12.9 | 14.7 | 17.1 |
| TC-E | **TC-117R** | Legacy TC 111 | TC128B non-normalized | 7/16" | 11 gauge, ASTM A1011 | Meet the requirements in Section 8.2.3.4.1 of TP14877 | ½" thick, full height, normalized steel | 0.1 | 1.5 | 3.2 | 4.7 | 6.9 | 9.4 | 13.8 | 15.7 | 18.2 |
| TC-F | **TC-117R** | Legacy TC 111 | TC128B non-normalized | 7/16" | 11 gauge, ASTM A1011 | Section 8.2.3.4.2, ½" protective housing | ½" thick, full height, normalized steel | 0.1 | 1.5 | 3.2 | 4.7 | 6.9 | 9.4 | 13.8 | 15.7 | 18.2 |
| TC-G | **TC-117R** | Legacy TC 111 | TC128B normalized | 7/16" | 11 gauge, ASTM A1011 | Meet the requirements in Section 8.2.3.4.1 of TP14877 | ½" thick, full height, normalized steel | 0.1 | 1.4 | 3.0 | 4.4 | 6.5 | 8.8 | 12.9 | 14.7 | 17.1 |
| TC-H | **TC-117R** | Legacy TC 111 | TC128B normalized | 7/16" | 11 gauge, ASTM A1011 | Section 8.2.3.4.2, ½" protective housing | ½" thick, full height, normalized steel | 0.1 | 1.4 | 3.0 | 4.4 | 6.5 | 8.8 | 12.9 | 14.7 | 17.1 |
| TC-J | **TC- 117R** | | A516-70, normalized | 9/16" | 11 gauge, ASTM A1011 | Meet the requirements in Section 8.2.3.4.1 of TP14877 | ½" thick, full height, normalized steel | 0.1 | 1.4 | 3.0 | 4.4 | 6.5 | 8.8 | 12.9 | 14.7 | 17.1 |
| TC-K | **TC- 117R** | | A516-70, normalized | 1/2" | 11 gauge, ASTM A1011 | Meet the requirements in Section 8.2.3.4.1 of TP14877 | ½" thick, full height, normalized steel | 0.1 | 1.6 | 3.3 | 4.9 | 7.1 | 9.6 | 14.2 | 16.1 | 18.7 |

## Table 13. Puncture Performance of TC-117 Variants at -25 °C

| Model Code | Tank car type | Source Tank Car | Steel Type | Shell Thickness | Jacket type and thickness | Top fittings protection description | Head shield | Number of punctures (-25 degrees C) | | | | | | | | |
|---|---|---|---|---|---|---|---|---|---|---|---|---|---|---|---|---|
| | | | | | | | | 5 mph | 20 mph | 25 mph | 30 mph | 35 mph | 40 mph | 50 mph | 55 mph | 60 mph |
| TC-A | **TC-117J** | N/A | TC128B normalized | 9/16" | 11 gauge, ASTM A1011 steel | Meet the requirements in Section 8.2.3.4.1 of TP14877 | ½" thick, full height, normalized steel (minimum tensile strength equal to or greater than 379 MPa) | 0.0 | 1.1 | 2.3 | 3.5 | 5.2 | 7.2 | 10.4 | 12.0 | 14.0 |
| TC-B | **TC-117R** | Unjacketed CPC 1232 | TC128B normalized | ½" | 11 gauge, ASTM A1011 | Meet the requirements in Section 8.2.3.4.1 of TP14877 | ½" thick, full height, normalized steel | 0.1 | 1.3 | 2.7 | 4.0 | 5.9 | 8.1 | 11.7 | 13.4 | 15.7 |
| TC-C | **TC-117R** | Jacketed CPC 1232 | TC128B normalized | 7/16" | 11 gauge, ASTM A1011 | Meet the requirements in Section 8.2.3.4.1 of TP14877 | ½" thick, full height, normalized steel | 0.1 | 1.4 | 3.0 | 4.5 | 6.6 | 8.9 | 13.2 | 15.0 | 17.4 |
| TC-D | **TC-117R** | Jacketed CPC 1232 | TC128B normalized | 7/16" | 11 gauge, ASTM A1011 | Section 8.2.3.4.2, ½" protective housing | ½" thick, full height, normalized steel | 0.1 | 1.4 | 3.0 | 4.5 | 6.6 | 8.9 | 13.2 | 15.0 | 17.4 |
| TC-E | **TC-117R** | Legacy TC 111 | TC128B non-normalized | 7/16" | 11 gauge, ASTM A1011 | Meet the requirements in Section 8.2.3.4.1 of TP14877 | ½" thick, full height, normalized steel | 0.1 | 1.6 | 3.3 | 4.8 | 7.1 | 9.6 | 14.0 | 16.4 | 18.4 |
| TC-F | **TC-117R** | Legacy TC 111 | TC128B non-normalized | 7/16" | 11 gauge, ASTM A1011 | Section 8.2.3.4.2, ½" protective housing | ½" thick, full height, normalized steel | 0.1 | 1.6 | 3.3 | 4.8 | 7.1 | 9.6 | 14.0 | 16.4 | 18.4 |
| TC-G | **TC-117R** | Legacy TC 111 | TC128B normalized | 7/16" | 11 gauge, ASTM A1011 | Meet the requirements in Section 8.2.3.4.1 of TP14877 | ½" thick, full height, normalized steel | 0.1 | 1.4 | 3.0 | 4.5 | 6.6 | 8.9 | 13.2 | 15.0 | 17.4 |
| TC-H | **TC-117R** | Legacy TC 111 | TC128B normalized | 7/16" | 11 gauge, ASTM A1011 | Section 8.2.3.4.2, ½" protective housing | ½" thick, full height, normalized steel | 0.1 | 1.4 | 3.0 | 4.5 | 6.6 | 8.9 | 13.2 | 15.0 | 17.4 |
| TC-J | **TC- 117R** | | A516-70, normalized | 9/16" | 11 gauge, ASTM A1011 | Meet the requirements in Section 8.2.3.4.1 of TP14877 | ½" thick, full height, normalized steel | 0.1 | 1.5 | 3.0 | 4.5 | 6.6 | 8.9 | 13.1 | 14.9 | 17.3 |
| TC-K | **TC- 117R** | | A516-70, normalized | 1/2" | 11 gauge, ASTM A1011 | Meet the requirements in Section 8.2.3.4.1 of TP14877 | ½" thick, full height, normalized steel | 0.1 | 1.6 | 3.4 | 5.0 | 7.2 | 9.7 | 14.4 | 16.4 | 19.0 |

## Table 14. Puncture Performance of TC-117 Variants at -40 °C

| Model Code | Tank car type | Source Tank Car | Steel Type | Shell Thickness | Jacket type and thickness | Top fittings protection description | Head shield | Number of punctures (-40 degrees C) | | | | | | | | |
|---|---|---|---|---|---|---|---|---|---|---|---|---|---|---|---|---|
| | | | | | | | | 5 mph | 20 mph | 25 mph | 30 mph | 35 mph | 40 mph | 50 mph | 55 mph | 60 mph |
| TC-A | **TC-117J** | N/A | TC128B normalized | 9/16" | 11 gauge, ASTM A1011 steel | Meet the requirements in Section 8.2.3.4.1 of TP14877 | ½" thick, full height, normalized steel (minimum tensile strength equal to or greater than 379 MPa) | 0.0 | 1.1 | 2.5 | 3.7 | 5.4 | 7.6 | 10.9 | 12.5 | 14.7 |
| TC-B | **TC-117R** | Unjacketed CPC 1232 | TC128B normalized | ½" | 11 gauge, ASTM A1011 | Meet the requirements in Section 8.2.3.4.1 of TP14877 | ½" thick, full height, normalized steel | 0.1 | 1.3 | 2.8 | 4.2 | 6.1 | 8.4 | 12.3 | 14.0 | 16.3 |
| TC-C | **TC-117R** | Jacketed CPC 1232 | TC128B normalized | 7/16" | 11 gauge, ASTM A1011 | Meet the requirements in Section 8.2.3.4.1 of TP14877 | ½" thick, full height, normalized steel | 0.1 | 1.5 | 3.2 | 4.7 | 6.9 | 9.3 | 13.7 | 15.6 | 18.0 |
| TC-D | **TC-117R** | Jacketed CPC 1232 | TC128B normalized | 7/16" | 11 gauge, ASTM A1011 | Section 8.2.3.4.2, ½" protective housing | ½" thick, full height, normalized steel | 0.1 | 1.5 | 3.2 | 4.7 | 6.9 | 9.3 | 13.7 | 15.6 | 18.0 |
| TC-E | **TC-117R** | Legacy TC 111 | TC128B non-normalized | 7/16" | 11 gauge, ASTM A1011 | Meet the requirements in Section 8.2.3.4.1 of TP14877 | ½" thick, full height, normalized steel | 0.1 | 1.7 | 3.4 | 5.0 | 7.3 | 9.8 | 14.5 | 16.5 | 19.1 |
| TC-F | **TC-117R** | Legacy TC 111 | TC128B non-normalized | 7/16" | 11 gauge, ASTM A1011 | Section 8.2.3.4.2, ½" protective housing | ½" thick, full height, normalized steel | 0.1 | 1.7 | 3.4 | 5.0 | 7.3 | 9.8 | 14.5 | 16.5 | 19.1 |
| TC-G | **TC-117R** | Legacy TC 111 | TC128B normalized | 7/16" | 11 gauge, ASTM A1011 | Meet the requirements in Section 8.2.3.4.1 of TP14877 | ½" thick, full height, normalized steel | 0.1 | 1.5 | 3.2 | 4.7 | 6.9 | 9.3 | 13.7 | 15.6 | 18.0 |
| TC-H | **TC-117R** | Legacy TC 111 | TC128B normalized | 7/16" | 11 gauge, ASTM A1011 | Section 8.2.3.4.2, ½" protective housing | ½" thick, full height, normalized steel | 0.1 | 1.5 | 3.2 | 4.7 | 6.9 | 9.3 | 13.7 | 15.6 | 18.0 |
| TC-J | **TC- 117R** | | A516-70, normalized | 9/16" | 11 gauge, ASTM A1011 | Meet the requirements in Section 8.2.3.4.1 of TP14877 | ½" thick, full height, normalized steel | 0.1 | 1.5 | 3.2 | 4.7 | 6.8 | 9.3 | 13.7 | 15.6 | 18.0 |
| TC-K | **TC- 117R** | | A516-70, normalized | 1/2" | 11 gauge, ASTM A1011 | Meet the requirements in Section 8.2.3.4.1 of TP14877 | ½" thick, full height, normalized steel | 0.1 | 1.7 | 3.5 | 5.2 | 7.6 | 10.1 | 15.0 | 17.1 | 19.7 |

These results allow comparisons to be made across car designs, speeds, and temperature. As expected, the number of punctures increases significantly with speed.

Table 15 shows the effect of temperature on the number of punctures for a 100-car train of TC-117J cars at 20 and 50 mph.

**Table 15. Effect of temperature on punctures at 20 and 50 mph – TC-117J cars**

| Temperature (°C) | Punctures at 20 mph | Punctures at 50 mph |
|---|---|---|
| 20 | 1.0 | 10.0 |
| -15 | 1.0 | 10.2 |
| -25 | 1.1 | 10.4 |
| -40 | 1.1 | 10.9 |

The example results in Table 15 show the number of punctures increases slightly as temperature lowers. Similar effects of temperature were found for the TC-117R variants. These results assume that the primary effect of the lower temperatures is the degradation in puncture resistance of the tank material; changes in derailment dynamics either due to track changes under cold weather or lading performance under cold weather were not analyzed, as they were considered secondary.

The results show that at all temperatures and speeds the TC-117J cars had the fewest punctures. The differences in punctures for the TC-117R variants were relatively small. As expected, the two variants with non-normalized steel shells had slightly more punctures than the variants with normalized steel shells. The variant with the 1/2”, A516-70 steel shell had the highest number of punctures.

Figure 25 shows the number of punctures versus different speeds for 4 types of cars at $20^0$C, while Figure 26 shows the number of punctures versus different temperatures for 4 types of cars at 60mph. The inflection point at 20 mph is primarily the result of the number of collisions at 5 mph being near zero; i.e., the train (and derailed cars) come(s) to a stop before there are any notable impacts.

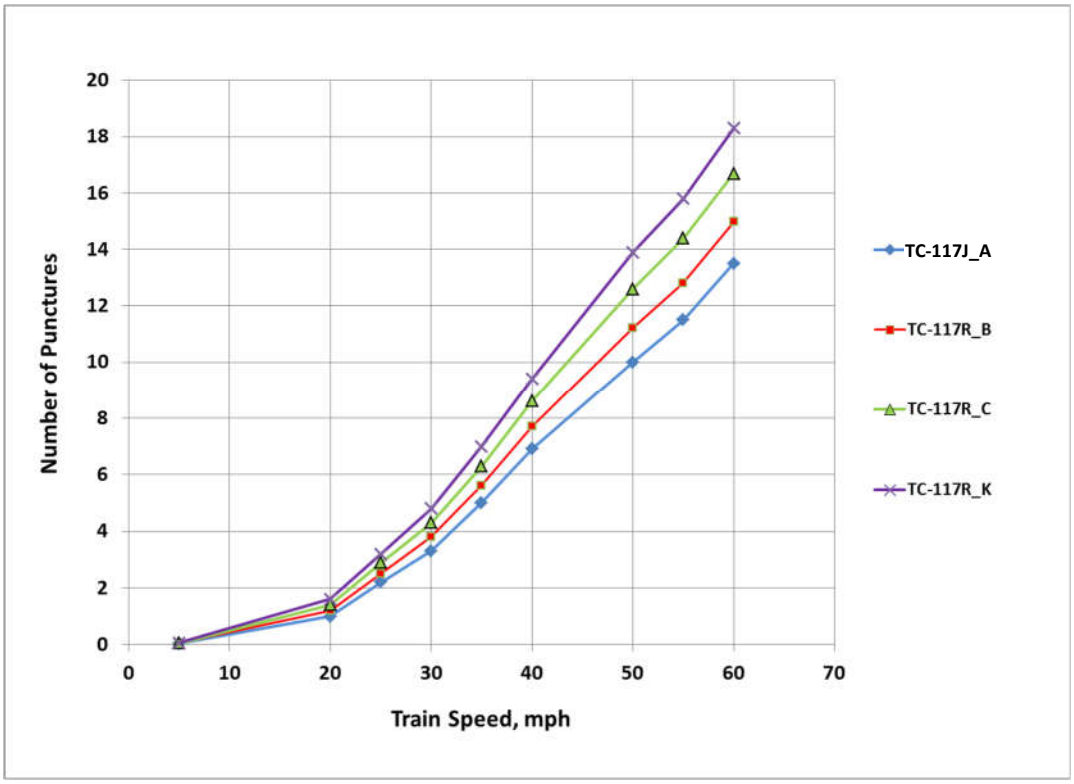


**Figure 25. Number of punctures vs. different speeds for 4 types of cars at 20$^0$C**

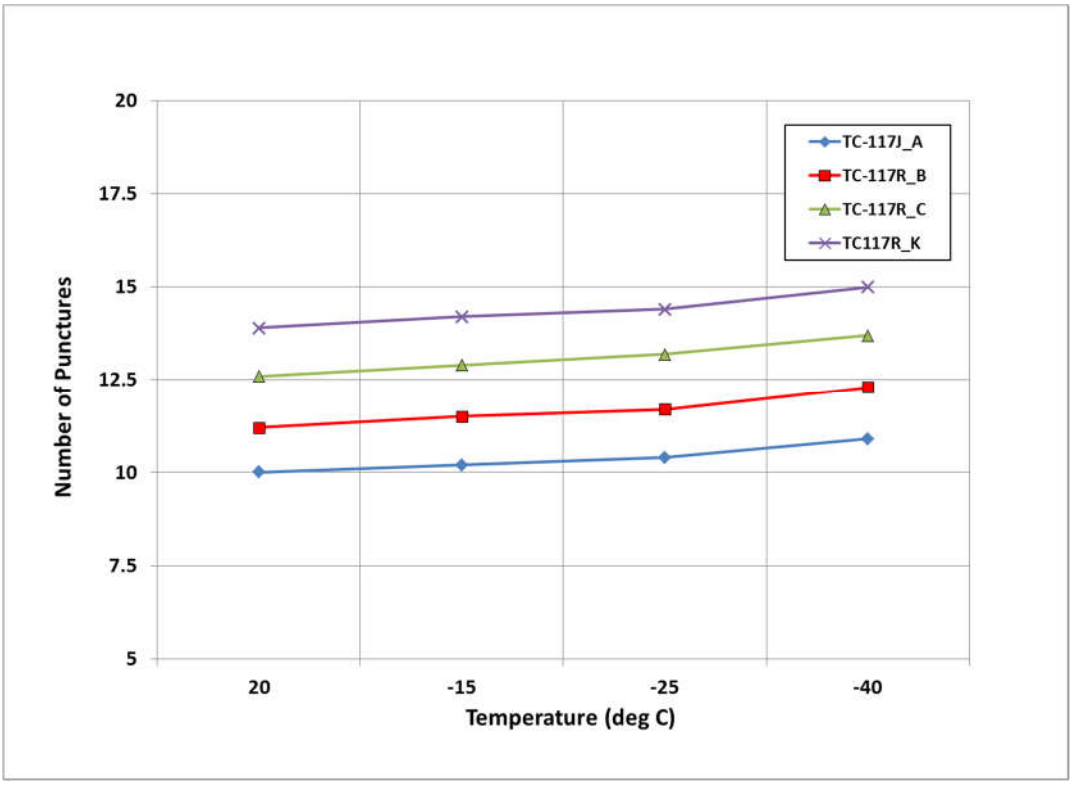


**Figure 26. Number of punctures vs. temperature for 4 types of cars at 50mph**

### 5.2 Top Fitting Failure Calculations

As noted earlier, the histogram of fittings protective structure impact velocities was reviewed against the capacity/resistance of the fittings protective structures to estimate the likelihood of fittings failure.

The methodology for characterizing the capacity of the fittings protective structures was developed during the prior study and is described in detail in reference [2]. A detailed finite element model of a tank car and fittings protective structure (see Figure 27) was developed, and the model was given an initial rotational velocity so that the fittings protective structure impacted the ground; the nominal mass of the tank was assumed to the supported by the ground.

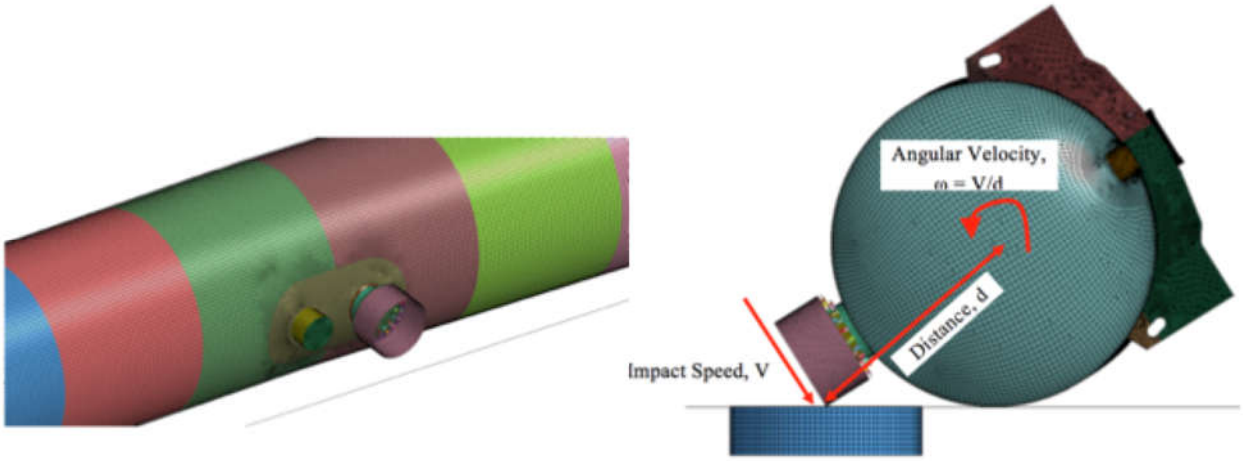


**Figure 27. Model used to characterize strengths of fittings protective structures**

The simulations were run for 4 different impact speeds (3, 6, 9 and 12 mph). In addition, the models were run with 4 different ground stiffness values representing different soil types (soft, medium, concrete and rigid), as the structural behavior of the fittings protective structure can vary significantly based on the rigidity of the surface that is impacted. See reference [2] for additional details on the modelling. A threshold deformation level of the bonnet of 4" was defined as the nominal failure criteria. Deformation curves were obtained for each of the bonnet design as a function of the impact speed. From these curves, the minimum impact speed resulting in fittings failure is determined by interpolating or, in the case of soft and medium soil, extrapolating from the plotted data. Based on these simulations, the failure speeds (4" bonnet deformation) for a bonnet design that meets Section 8.2.3.4.1 of TP14877 (effectively, a 0.5" thick bonnet) are:

- 3.3 mph for rigid surface
- 3.4 mph for concrete surface
- 4.6 mph for medium soil
- 7.7 mph for soft soil

By comparing the data points from the histogram of fittings impact velocities (Figure 8) with the failure speeds noted above, the likelihood of a fittings failure can be calculated. Given that the results between a rigid surface and a concrete surface are very similar and given that a theoretical 'rigid' surface is unlikely to be experienced by a fittings protective structure during an actual derailment, the number of fittings failure for average soil is calculated by averaging the number of fail fittings for concrete, medium and soft soils. Table 16 shows the results averaged over these three ground conditions.

**Table 16. Predicted fittings failures**

| Derailment Speed (mph) | Top Fittings Failures |
|---|---|
| 5 | 0.4 |
| 20 | 1.3 |
| 25 | 2.4 |
| 30 | 2.7 |
| 35 | 5.7 |
| 40 | 7.0 |
| 50 | 12.3 |
| 55 | 15.9 |
| 60 | 22.7 |

As seen in Table 16, the likelihood of failure of the top fittings protective structures increases significantly with derailment speed. The trend of the top fittings failure is shown in Figure 28. Ignoring the data point at 5 mph, one can observe that a second order polynomial with both square and linear terms fits the data well. This suggests that both kinetic energy (the square term) and the velocity (the linear term) have a role to play. This can be explored further in future work.

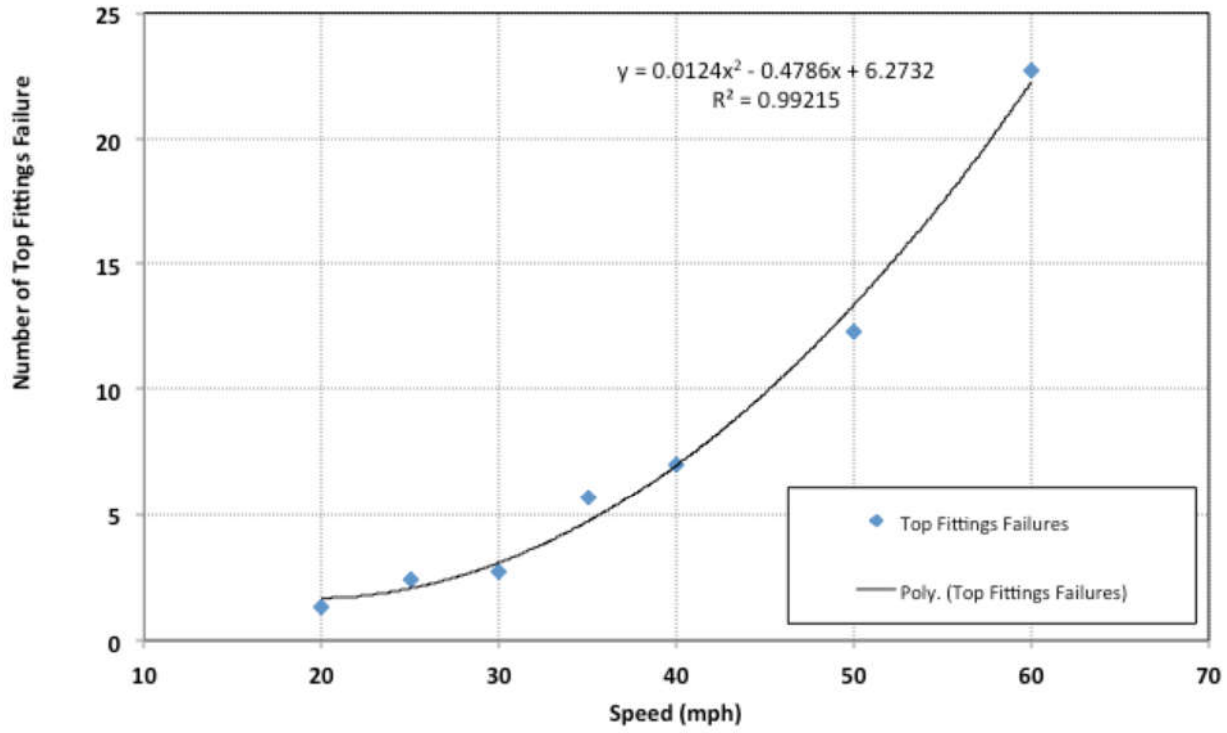


**Figure 28. Top fittings failure as a function of speed**

# 6 COMPARING MODEL ESTIMATES WITH ACCIDENT DATA

There are multiple prior reports and papers that document the effectiveness of the prior methodology in simulating the gross dynamics of derailment performance as well as predicting the number of punctures observed from similar accidents/derailments [1, 19, 21, 22, 23]. These prior efforts have focused on comparing the estimates from the model to relevant data from derailments of trains with a significant proportion of tank cars in their consist. Most of this data represents older, 'legacy' cars that would usually be considered a TC-111/DOT-111 design (with corresponding levels of structural performance), largely because such cars constituted a preponderance of the tank car fleet when the prior work was done.

The intent of this chapter is to compare the results from the current effort to more recent accidents (potentially with updated tank car designs), and to check if the model estimates are in reasonable conformity with data from derailments. Note that neither the prior effort(s) nor the current effort sought to evaluate the results of any specific derailment; the intent was always to estimate relative risk resulting from variations to tank car designs or operating conditions.

For this effort, the team used data from multiple sources including:

- Data from recent derailments that are included in the TSB Rail Safety Advisory Letter issued to Transport Canada in March 2020: Rail Safety Advisory Letter 617-02/20 - Transportation Safety Board of Canada (tsb.gc.ca).
- Data gathered by the FRA or NTSB as part of their investigations into recent accidents
- Data provided by RSI-AAR Tank Car project through a search into their database on tank car accidents
- Other available media sources, including news reports

To provide useful comparisons to model conditions, the derailment must be of reasonable pertinence to model conditions, such as:

- the derailed train having a reasonable number of TC-117 variants in the consist
- the derailed train being a unit train of tank cars or have a substantial number of tank cars in the consist

When the collected data is filtered by the above constraints, the number of available data sets for comparison is a little more limited. Table 17 summarizes the relevant available derailment data.

**Table 17. Puncture data from derailments**

| Date | Location | Speed (mph) | Derailed cars | Cars punctured | Temperature (°C) | Car Type |
|---|---|---|---|---|---|---|
| 2018-06 | Doon, IA | 48 | 35 | 9 | 15 | DOT-117R |
| 2019-02 | St Lazare, MB | 49 | 37 | 13 | -27 | DOT-117R |
| 2019-04 | Fort Worth, TX | 26 | 26 | 3 | 16 | DOT-111+ DOT-117R |
| 2019-05 | Barwick, ON | 24 | 8 | 0 | 10 | DOT-117J |
| 2019-12 | Near Guernsey, SK | 45 | 34 | 21 | -19 | DOT-117R+CPC-1232 |
| 2020-02 | Guernsey, SK | 42 | 32 | 8 | -18 | DOT-117J |
| 2020-02 | Emo, ON | 44 | 33 | 4 | -31 | DOT-117R+CPC-1232 |
| 2020-12 | Custer, Washington | 21 | 10 | 3 | 1 | DOT-117R |
| 2022-01 | Oklaunion, TX | 50 | 31 | 7 | 15 | DOT-117J |

As one can tell from the above data, many of the derailed trains had a mix of variants and were not exclusively one type. Further, it was difficult to get data on which TC-117R variant was involved in a

given accident. Given these constraints, Figure 29 presents the data from derailments where TC-117R variants were involved, along with the modelling results. Figure 29 also notes distinctions about some of the derailments. For example, the derailment in Emo, ON was initiated at car 52; i.e., the energy/mass of cars behind the derailed car was lower than the 100-cars assumed in the simulations, and hence it stands to reason that it had fewer punctures. For the accident at Lanigan, SK, a significant proportion of the cars were of CPC-1232 specification (not as strong as any of the TC-117R variants) and hence one would expect a larger number of punctures.

Overall, Figure 29 suggests that the data from derailments is consistent with expectations from the model, though the model did not explicitly simulate any of these specific incidents. Note that the simulation data shown in Figure 29 is for a temperature of 20°C.

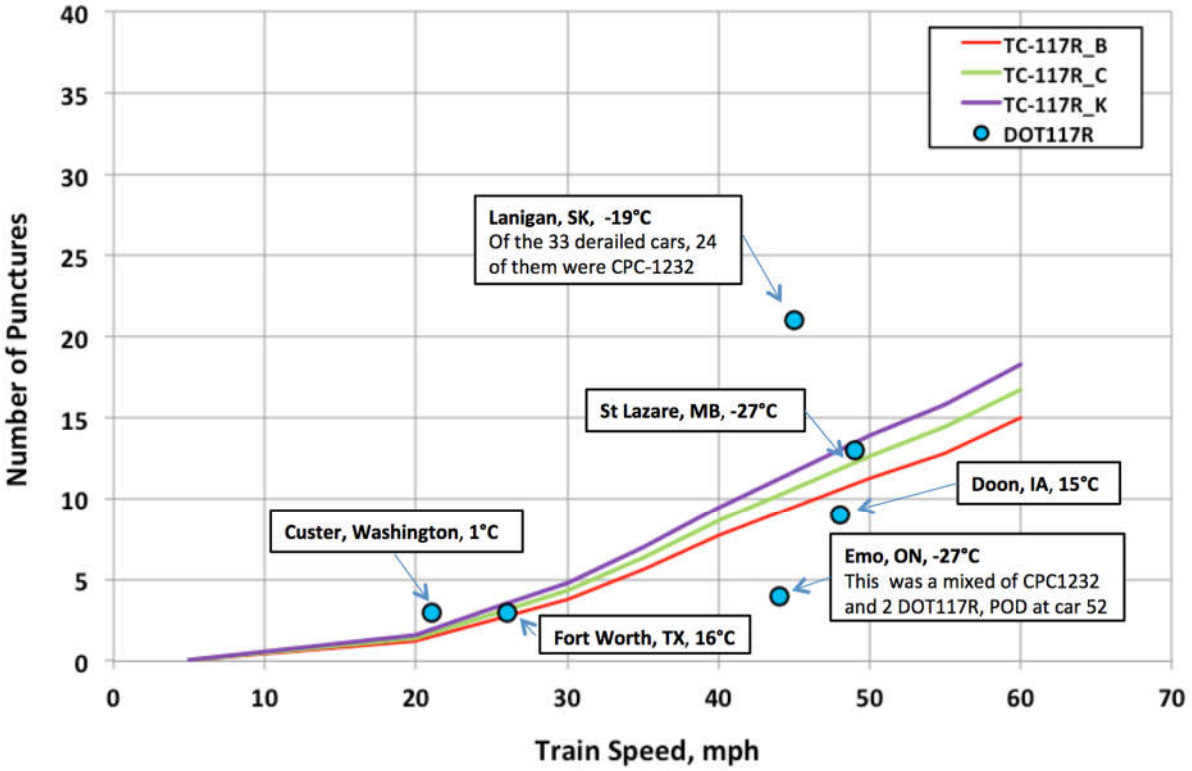


**Figure 29. Number of punctures – TC-117R: Simulation vs. Derailment Data**

The data on TC-117J variants is even more limited. Of the three data points seen on Figure 30:

- The incident at Barwick, ON has very few derailed cars; only 8 cars derailed and it is unclear where along the trains they were.
- The incident in Guernsey, SK seems to have had slightly more cars punctured than the model prediction, but happened at -18°C.
- The incident in Oklaunion, TX has fewer punctures than predicted by the model and the incident occurred at 15°C.

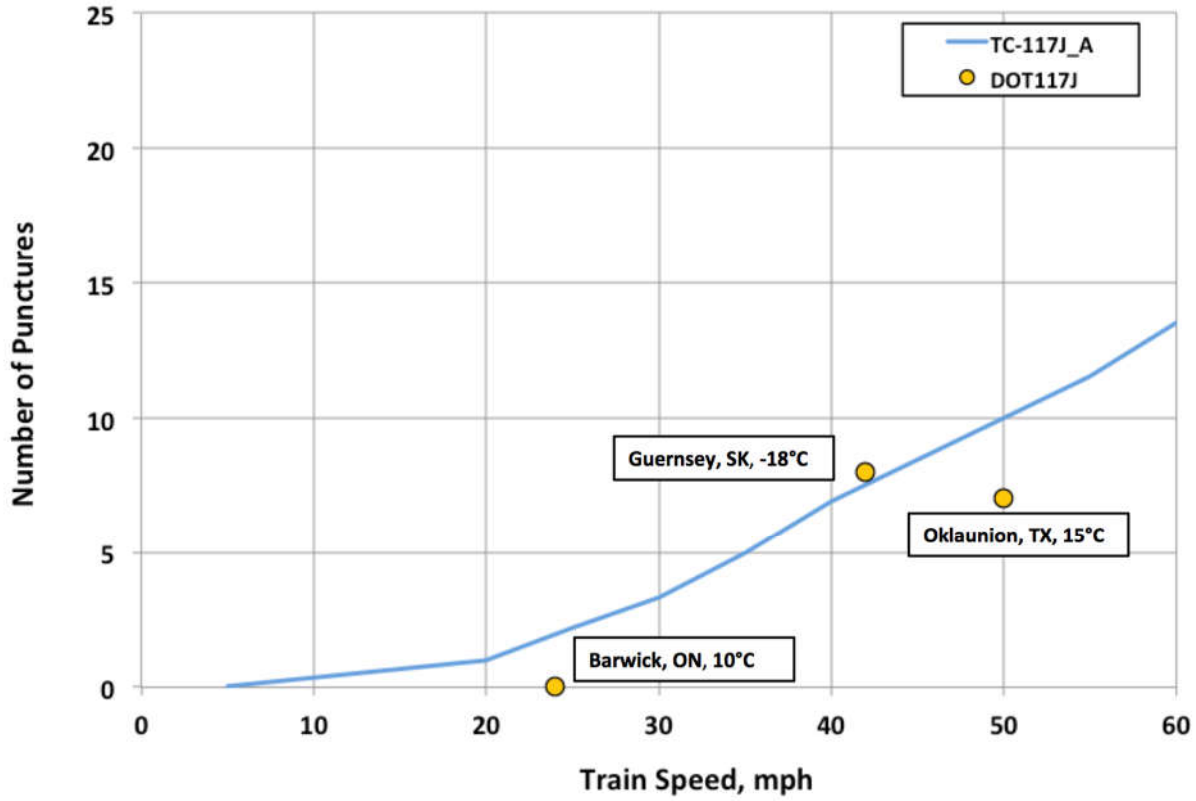


**Figure 30. Number of punctures – TC-117J: Simulation vs. Derailment Data**

Note that the model data in Figure 30 represents 20°C results.

Based on the results and data presented in Figure 29 and Figure 30, one can reasonably conclude that the model predictions are consistent with the number of punctures that can be expected in a nominal derailment. Further, based on the fact that the model data is reasonable for both the TC-117R variants and the TC-117J design, the data suggests that the relative performance between the various TC-117 variants is represented well by the model.

There isn't enough derailment data to clearly sort out the effects of temperature. Figure 29 and Figure 30 show that there is not a significant difference in the number of punctures based on the outside temperature at time of the derailment, with the exception of maybe the difference between the incidents at Guernsey, SK and Oklaunion, TX. Again, there are enough differences between the circumstances surrounding the various incidents that it is difficult to glean out the effects of temperature from this limited dataset.

Just like in the puncture data from the derailments, the fittings protection failure data from the derailments is also fairly limited. Tables 18 and 19 present fittings failure data from two different datasets:

- One set of data was used as part of prior work on fittings failure analysis (see [2]) and represented derailments on TC-111 style cars from 2006-2014. Note that these cars did not have a consistent set of fittings protective structure designs, though one could surmise that many had capacities lower than those required by Section 8.2.3.4.1 of TP14877.

- The other dataset was from tank cars involved in recent derailments and these cars likely had fittings structures that met the requirements of Section 8.2.3.4.1 of TP14877.

**Table 18. Fittings failure data from derailments – 2014 and earlier**

| Date | Incident | Speed at Derailment (mph) | Tank Cars Derailed | Unit Train (Y/N) | Top fittings damaged |
|---|---|---|---|---|---|
| Oct 2006 | New Brighton, PA | 37 | 20 | Y | 14 |
| Oct 2007 | Painesville, OH | 48 | 8 | N | 1 |
| Aug 2008 | Luther, OK | 19 | 8 | N | 4 |
| June 2009 | Cherry Valley, IL | 36 | 19 | N | 2 |
| Feb 2011 | Arcadia, OH | 46 | 31 | Y | 16 |
| Oct 2011 | Tiskilwa, IL | 37 | 10 | N | 3 |
| July 2012 | Columbus, OH | 23 | 3 | N | 0 |
| Aug 2012 | Plevna, MT | 23 | 17 | N | 0 |
| July 2013 | Lac Megantic, QC | 65 | 63 | Y | 20 |
| Nov 2013 | Aliceville, AL | 38 | 32 | Y | 18 |
| Dec 2013 | Casselton, ND | 42 | 20 | Y | 10 |
| Jan 2014 | Plaster Rock, NB | 47 | 9 | N | 0 |
| Jan 2014 | New Augusta, MS | 45 | 21 | N | 0 |
| Feb 2014 | Vandergrift, PA | 31 | 21 | Y | 2 |
| May 2014 | Lynchburg, VA | 23 | 17 | Y | 1 |
| May 2014 | LaSalle, CO | 10 | 6 | Y | 1 |

**Table 19. Fittings failure data from derailments – 2015 and later**

| | | | | | |
|---|---|---|---|---|---|
| Feb 2015 | Gladwick, ON | 38 | 29 | Y | 2 |
| Mar 2015 | Gogama, ON | 43 | 39 | Y | 4 |
| Feb 2019 | St. Lazare, MB | 49 | 37 | Y | 1 |
| May 2019 | Barwick, ON | 24 | 8 | Y | 0 |
| Dec 2019 | Near Guernsey, SK | 45 | 34 | Y | 0 |
| Feb 2020 | Guernsey, SK | 42 | 32 | Y | 0 |
| Feb 2020 | Emo, ON | 44 | 31 | Y | 0 |

The data from the derailments is shown along with the model results in Figure 31. To better understand the performance of the top fittings structures, in addition to the model data from the average ground condition, we also added the model curve from the soft ground simulations. A review of the Figure 31 suggests that while some of the data from the older cars fall on either side of the average simulation curve, the recent data generally falls below the 'soft' curve. This suggests that modern designs perform better than predicted by the derailment model; however, one should be cautious about making that conclusion from the limited data available.

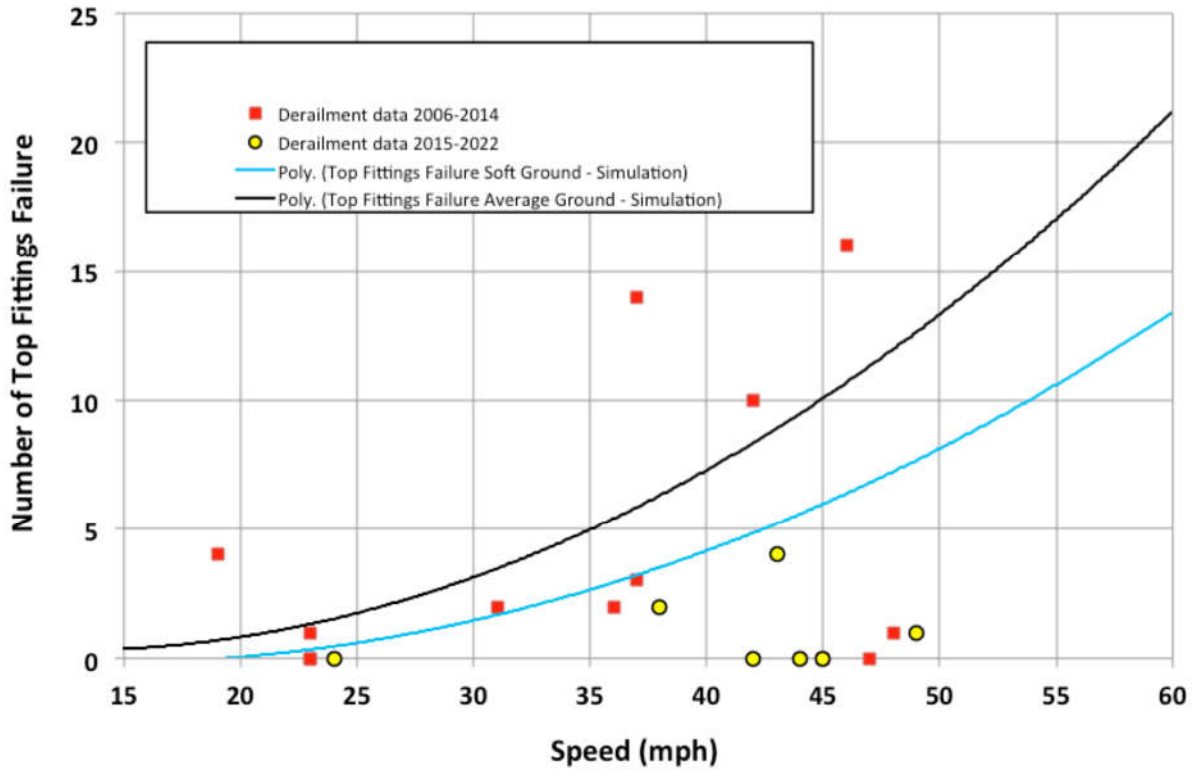


**Figure 31. Number of fittings failures: Simulation vs. Derailment Data**

# 7 CONCLUSIONS

The crashworthiness performance of TC-117 variants from both puncture resistance and fittings protection perspectives was evaluated using through an updated modeling approach. Enhancements to the modeling approach have included more accurate representation of inter-car connections and modelling of top fittings.

The updated model has been used in LS-Dyna simulations of 100-car trains at a range of speeds from 5 to 60 mph. Eighteen simulations were performed at each speed to account for variations in derailment cause, track conditions, and ground conditions. This resulted in a histogram of predicted impact forces at each speed. Outputs from the simulations also gave predicted impact velocities for top fittings in the derailments.

A material model was developed to account for the change in properties and failure mode with temperature. The model was calibrated by comparing simulations of Charpy impact tests with laboratory test results, and further extended to cover both normalized and non-normalized tank car steels.

Predicted impact forces and velocities were used to calculate the number of punctures and top fitting failures for TC-117J tank cars and nine variants of TC-117R tank cars. These predictions were made at ambient temperatures between 20 and -40 °C.

Results showed that structural damage in derailments increases significantly with speed. The increase is consistent with data from derailments in revenue service. For example, at 20 °C, a 30-mph derailment shows 20 derailed cars on average, while a 50-mph derailment shows 46 derailed cars on average, a 130% increase. However, for the same speeds, say for the TC-C variant, the number of punctures would rise from 4.3 to 12.6, which is a 193% increase, on average, based on the data in Table 11.

Temperature has a slight effect on the number of punctures. In general, there is a 10% increase in the predicted number of punctures when temperature drops from 20 to -40 °C.

The TC-117J tank car has fewer punctures than any of the TC-117R variants. The difference in punctures between the TC-117R variants is relatively small. As expected, the two variants with non-normalized steel shells have slightly more punctures than the variants with normalized steel shells. Among the variants, the TC-117R tank car design where the source car had a 1/2” thick shell made from A516-70 steel was predicted to have the highest number of punctures.

Top fittings failures were found to increase significantly with speed in a similar way to tank punctures.

Comparisons to a limited set of available accident data suggest that the model predictions are consistent with field observations from derailments. Comparisons to prior work suggest that any of the TC-117 variants had better performance than the legacy TC-111 cars, with the TC-117J designs offering the best performance.

# 8 REFERENCES


1. Sharma & Associates, Inc., Letter Report to the USDOT/FRA titled, "*Objective Evaluation of Risk Reduction from Tank Car Designs & Operations Improvements*", July 2014
2. Sharma & Associates, Inc., Report to Transport Canada titled, "*Risk Evaluation of Tank Car Breach*", June 2016
3. Di Bacco, B., Kirney, C., Prabhakaran, A., Booth, G., Gantoi, F., Wen, R., "*Tank Car Top Fittings Protection – Evaluation of Derailment Failure Risks – A Conceptual Study*", ASME JRC2016-5821, April 2016.
4. Robert S. Trent, Anand Prabhakaran, Francisco González, III, Dr. Vinaya Sharma and Srinivas Chitti, "*Full Scale Tank Car Rollover Test – Survivability of Top Fittings and Top Fittings Protective Structures*", Proceedings of the 2011 IEEE/ASME Joint Rail Conference JRC2011, March 16-18, 2011, Pueblo, Colorado, USA.
5. "*LS-DYNA Keyword User's Manual*," Livermore Software Technology Corporation, Version 971, May 2007.
6. AAR Manual of Standards and Recommended Practices, Section C Part III – Specifications for Tank Cars (M1002).
7. AAR Manual of Standards and Recommended Practices, Section C Part II – *Design, Fabrication, and Construction of Freight Cars*.
8. Transport Canada Rules Respecting Key Trains (OT-55), accessed at *https://tc.canada.ca/sites/default/files/migrated/rules_respecting_key_trains_and_key_routes.pdf*
9. US Department of Transportation, FRA, "*49 CFR Parts 213 and 238 – Vehicle/Track Interaction Safety Standards; High-Speed and High Cant Deficiency Operations; Proposed Rule*," Federal Register May 10, 2010
10. McKinley, J., Xu, S., Gesing, M., Williams, B., 2019: "*Strength, Creep, and Toughness of Two Tank Car Steels*", TC128B and A516-70".
11. Transport Canada Ministerial Order MO 20-10, accessed at *https://tc.canada.ca/en/rail-transportation/enforcement-action-measures-mitigate-threats-rail-safety/ministerial-orders-emergency-directives/transport-canada-order-pursuant-section-3201-railway-safety-act-mo-20-10*
12. ABAQUS Inc., 2014: ABAQUS 6.14, Analysis User's Manual.
13. Bao, Y., Wierzbicki, T., 2004: "*On Fracture Locus in the Equivalent Strain and Stress Triaxiality Space*", International Journal of Mechanical Sciences 46, 81-98.
14. American Society for Testing and Materials, "*Standard Test Methods and Definitions for Mechanical Testing of Steel Products*", ASTM A370-21, 2021
15. Charpy Impact Steel Testing accessed at: https://www.totalmateria.com/page.aspx?ID=CheckArticle&site=kts&NM=534
16. McKeighan, P.C., Jeong, D.Y., Cardinal, J.W., 2009: "*Mechanical Properties of Tank Car Steels Retired from the Fleet*", ASME JRC2009-63060, March 2009.
17. Kirkpatrick, S.W., "*Detailed Puncture Analyses of Tank Cars: Analysis of Different Impactor Threats and Impact Conditions*", US Department of Transportation, DOT/FRA/ORD-13/17, March 2013.
18. Jeong, D.Y., Yu, H., Gordon, J.E., Tang, Y.H., 2008: "*Finite Element Analysis of Unnotched Charpy Impact Tests*", John A. Volpe National Transportation Systems Center (U.S.).
19. Gonzalez, F., Prabhakaran, A., Booth, G., Gantoi, F., Vithani, A., "*Mitigating Strategies for Hazardous Material Trains: Evaluating the Risk Reduction*", ASME JRC2015-5752, March 2015.

20. Advanced Tank Car Collaborative Research Program, Technical Report for Project TWP-11, Phase 1, “Development of the Relationships between Conditional Probability of Release/Expected Quantity of Release and Modeling and Test Results”, May 2019
21. Gonzalez, F., Prabhakaran, A., et. al., “Validation Of Methodology To Evaluate Risk Reduction In Tank Car Derailments”, VVS2018-9331, Published in the Proceedings of the ASME 2018 Verification and Validation Symposium, May 2018, Minneapolis, MN.
22. Prabhakaran, A., Gonzalez, F., et al, “Evaluation Of Risk Reduction From Tank Car Design And Operations Improvements – An Extended Study”, JRC2016-5832, Presented at the 2016 Joint Rail Conference, April 2016, Columbia, SC.
23. USDOT Report ‘DOT/FRA/ORD-18/36’, “Objective Evaluation of Risk Reduction from Tank Car Design and Operations Improvements – Extended Study”, October 2018.

## APPENDIX A - FINAL PILE-UP RESULTS

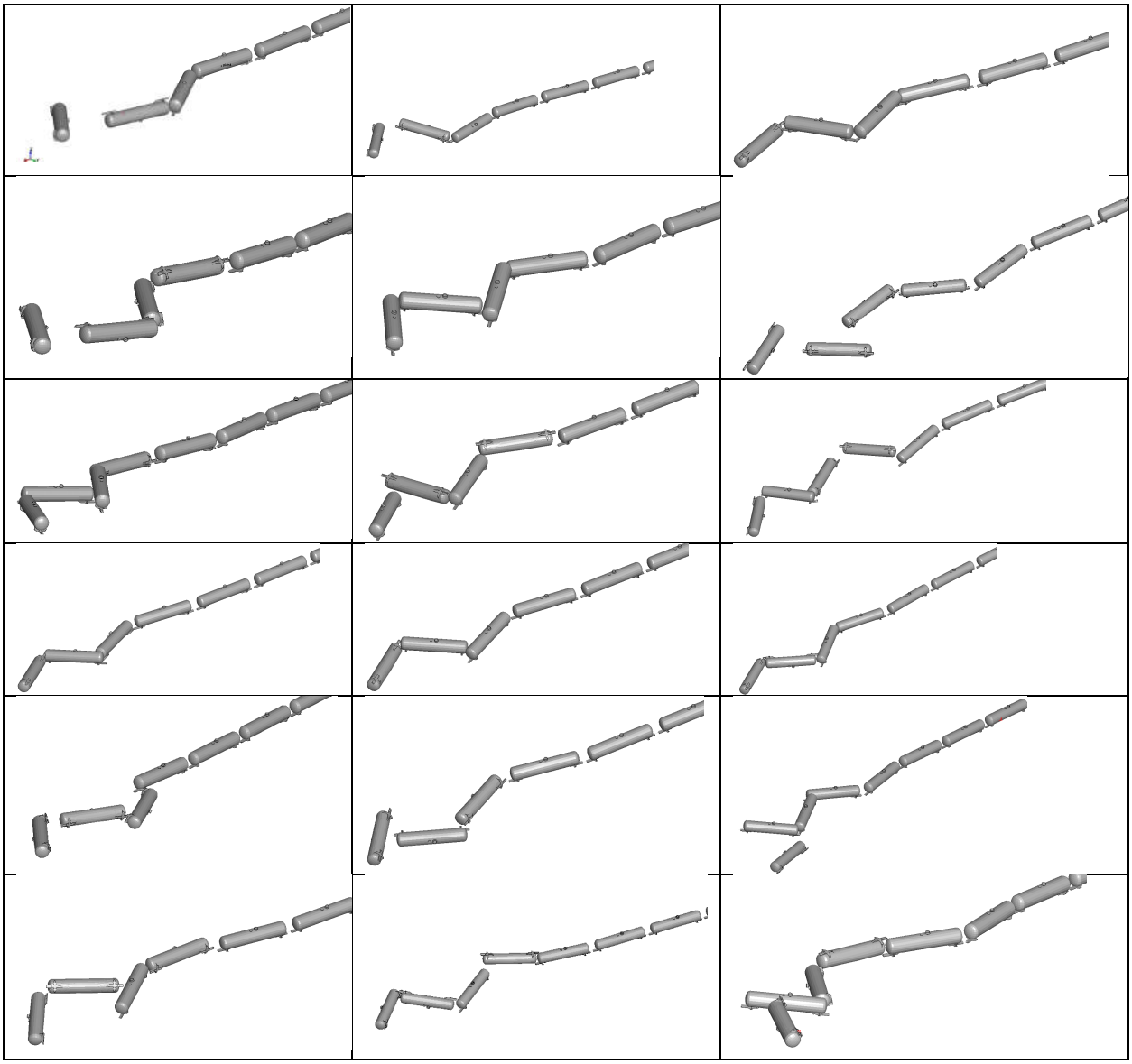

**Figure A1. Final pile-up, simulated derailment of 100-car train, 5mph**

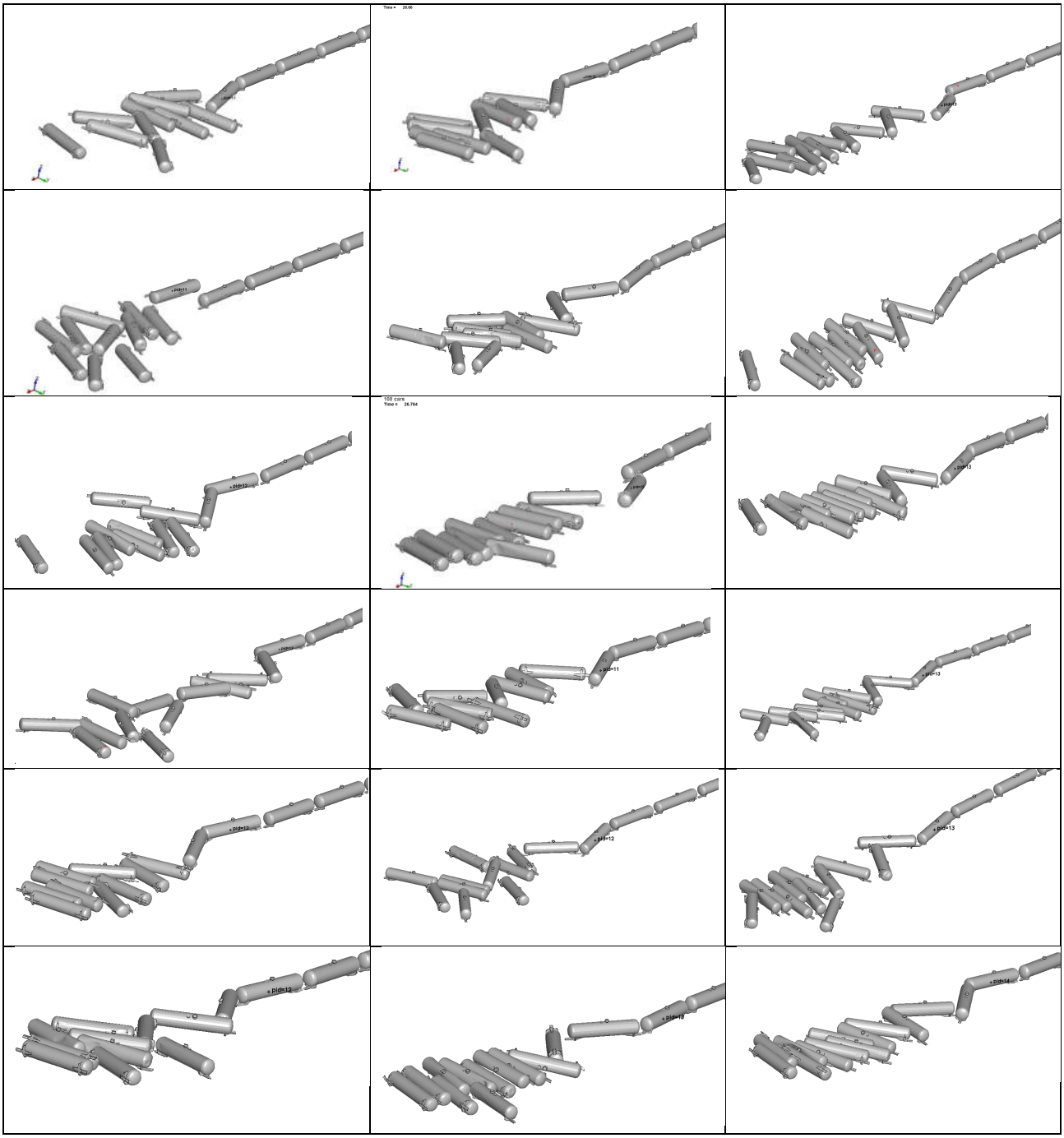

**Figure A2. Final pile-up, simulated derailment of 100-car train, 20mph**

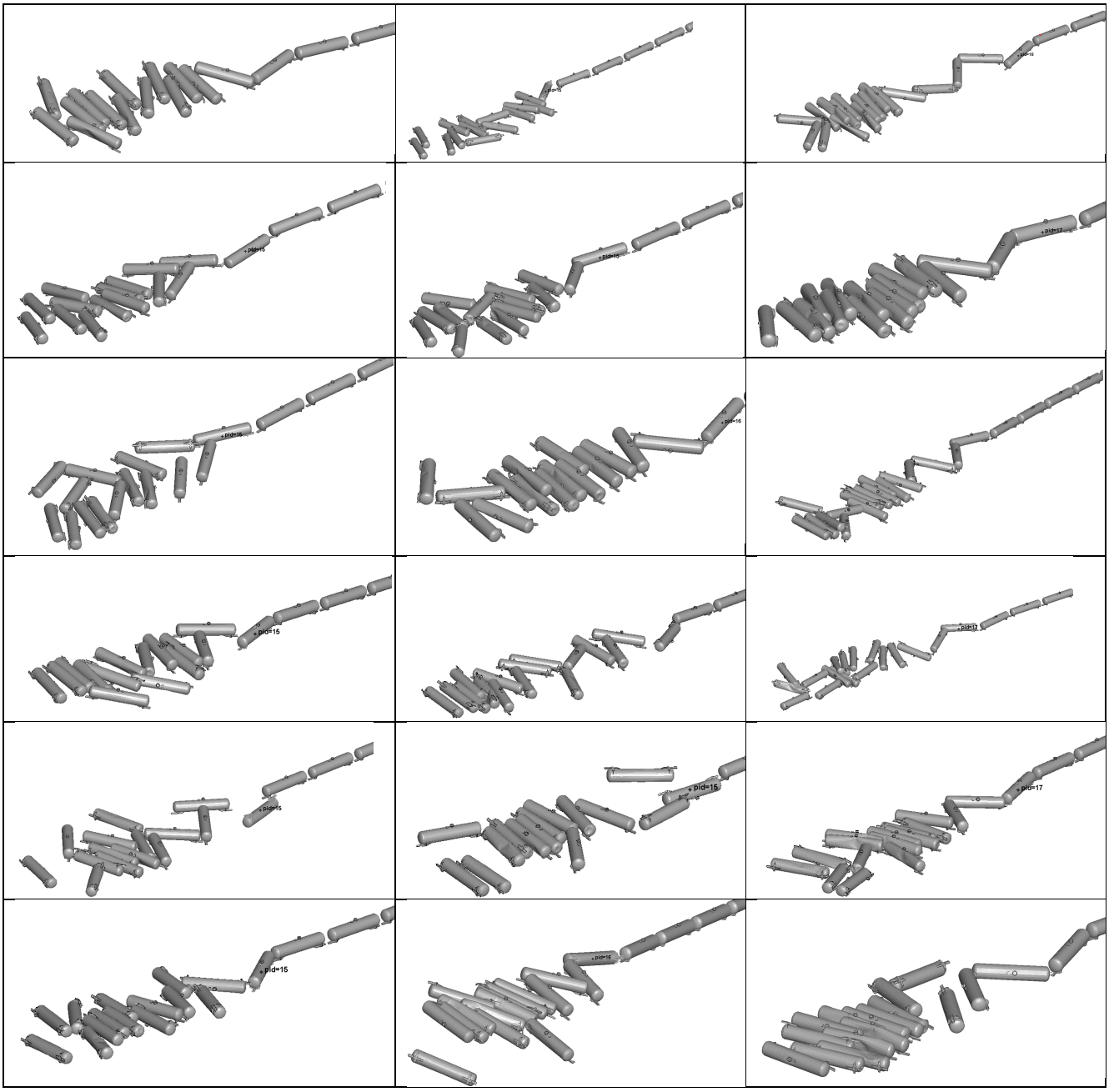

**Figure A3. Final pile-up, simulated derailment of 100-car train, 25mph**

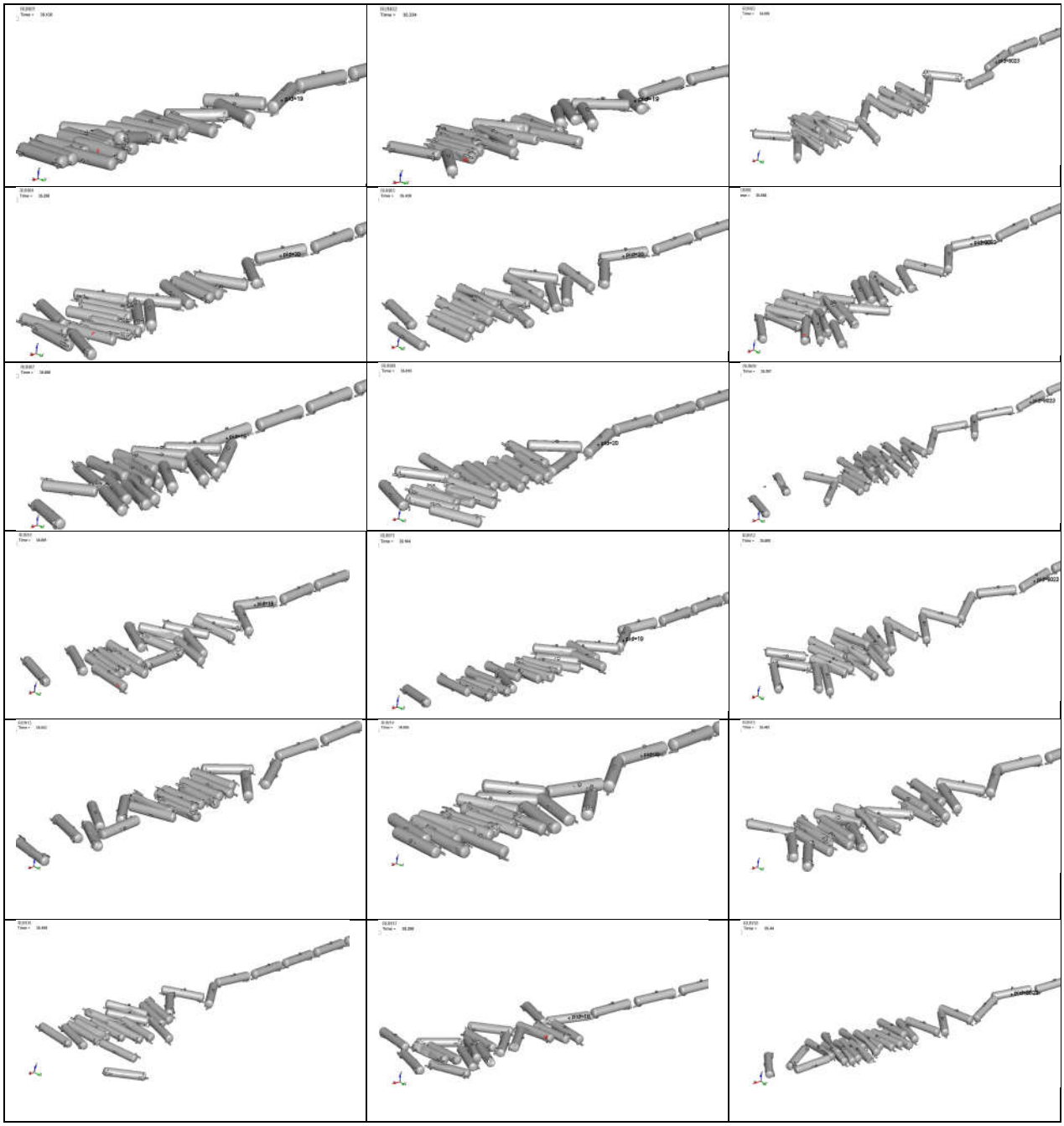

**Figure A4. Final pile-up, simulated derailment of 100-car train, 30mph**

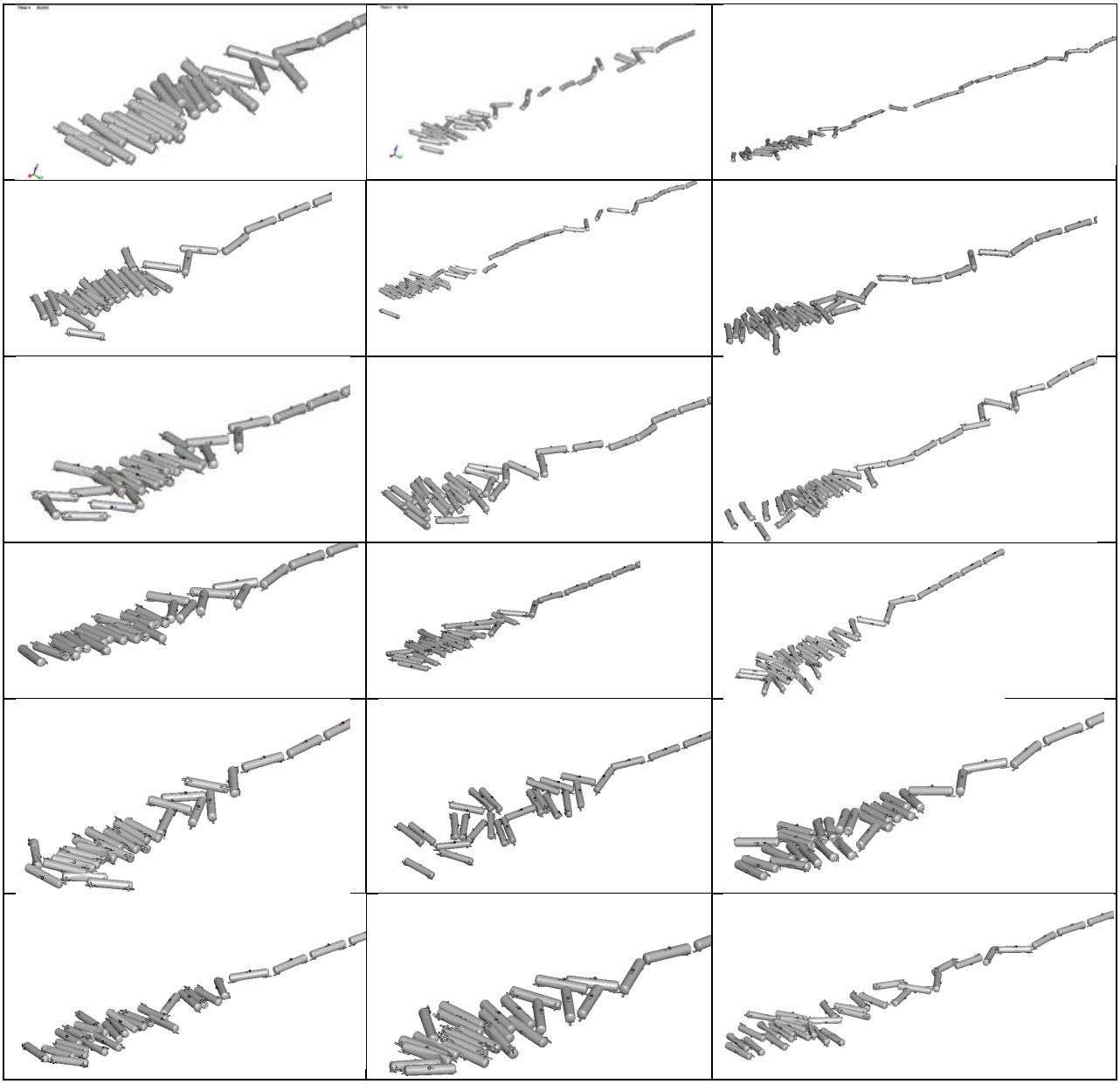

**Figure A5. Final pile-up, simulated derailment of 100-car train, 35mph**

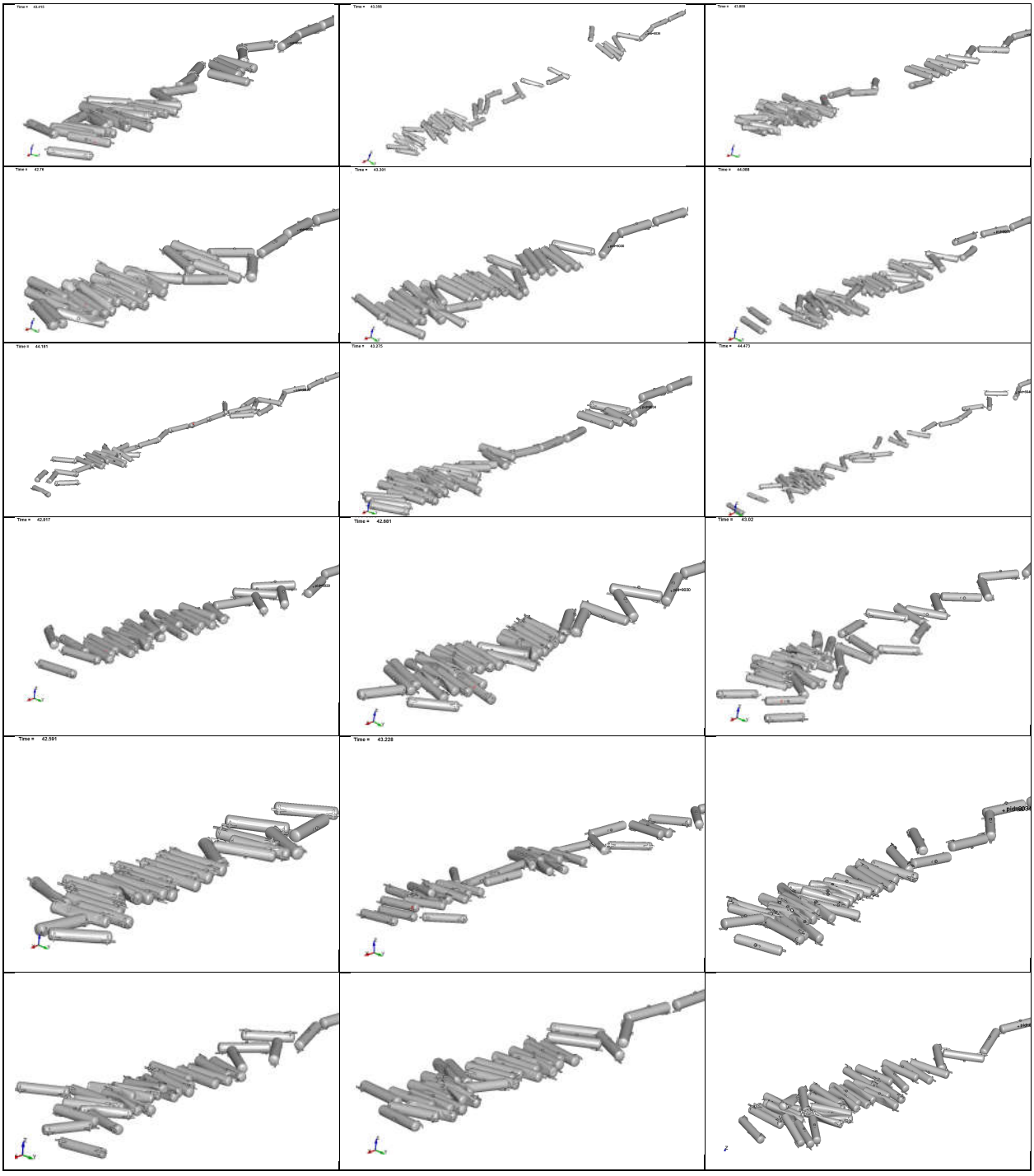

**Figure A6. Final pile-up, simulated derailment of 100-car train, 40mph**

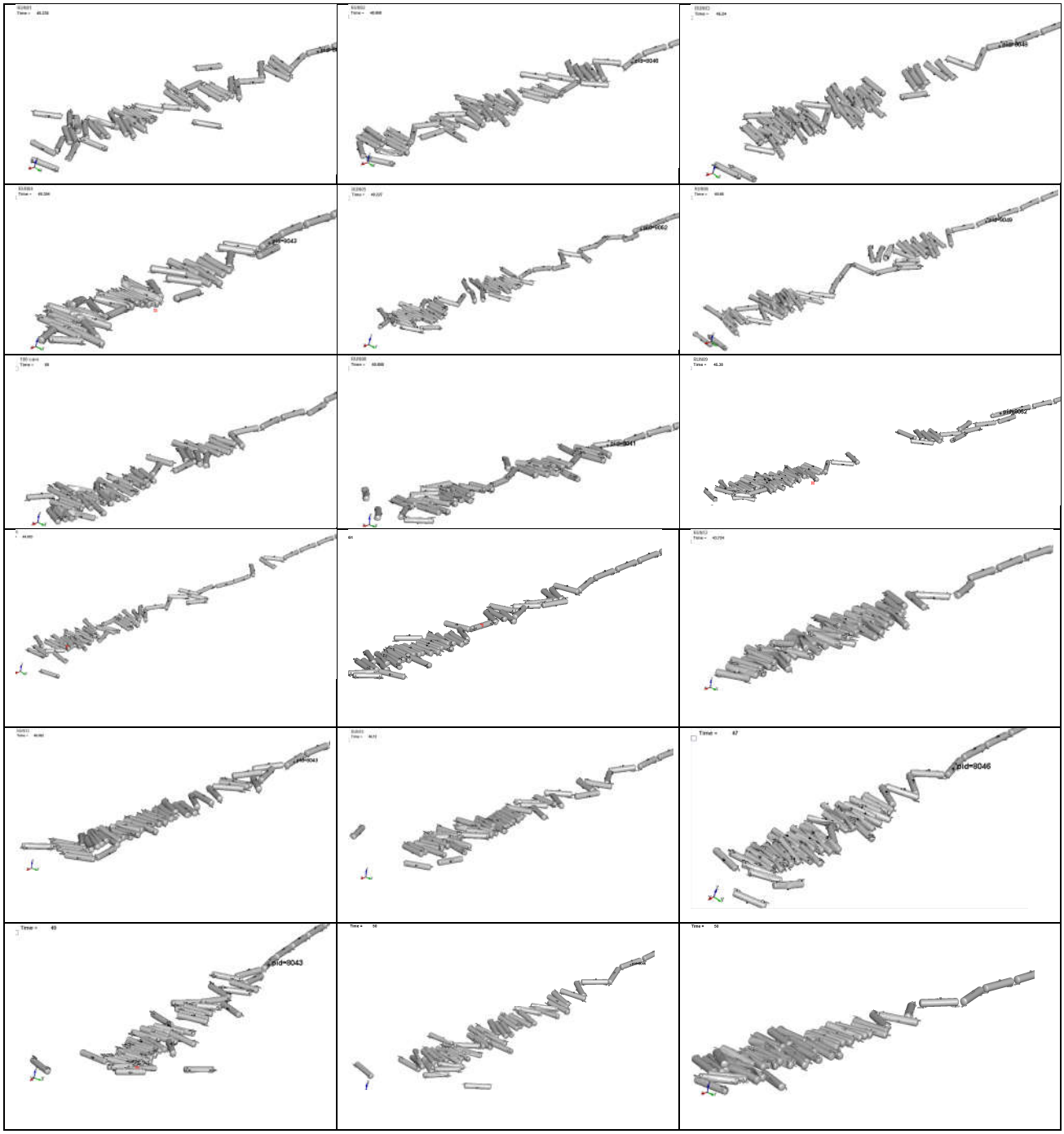

**Figure A7. Final pile-up, simulated derailment of 100-car train, 50mph**

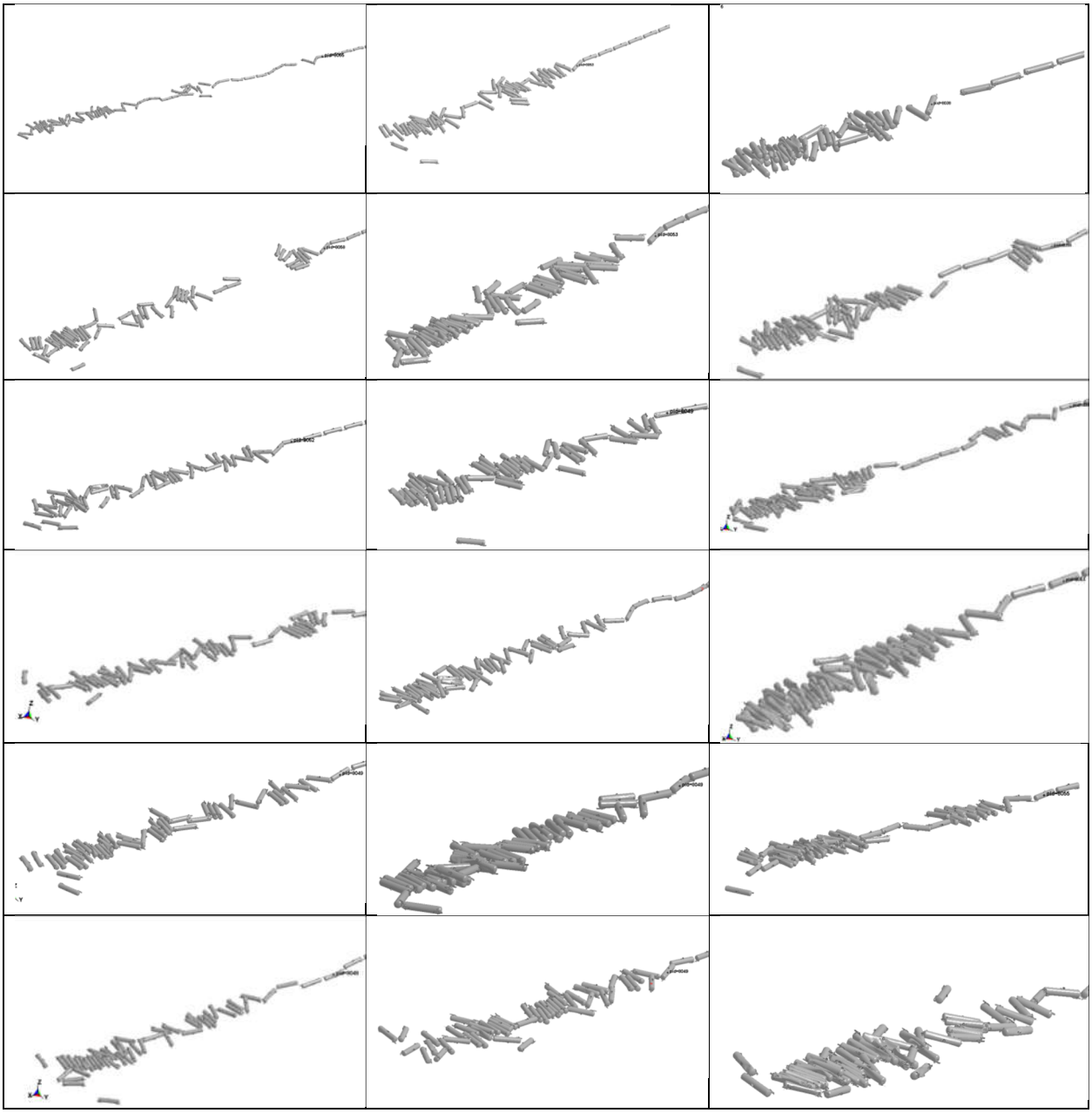

**Figure A8. Final pile-up, simulated derailment of 100-car train, 55mph**

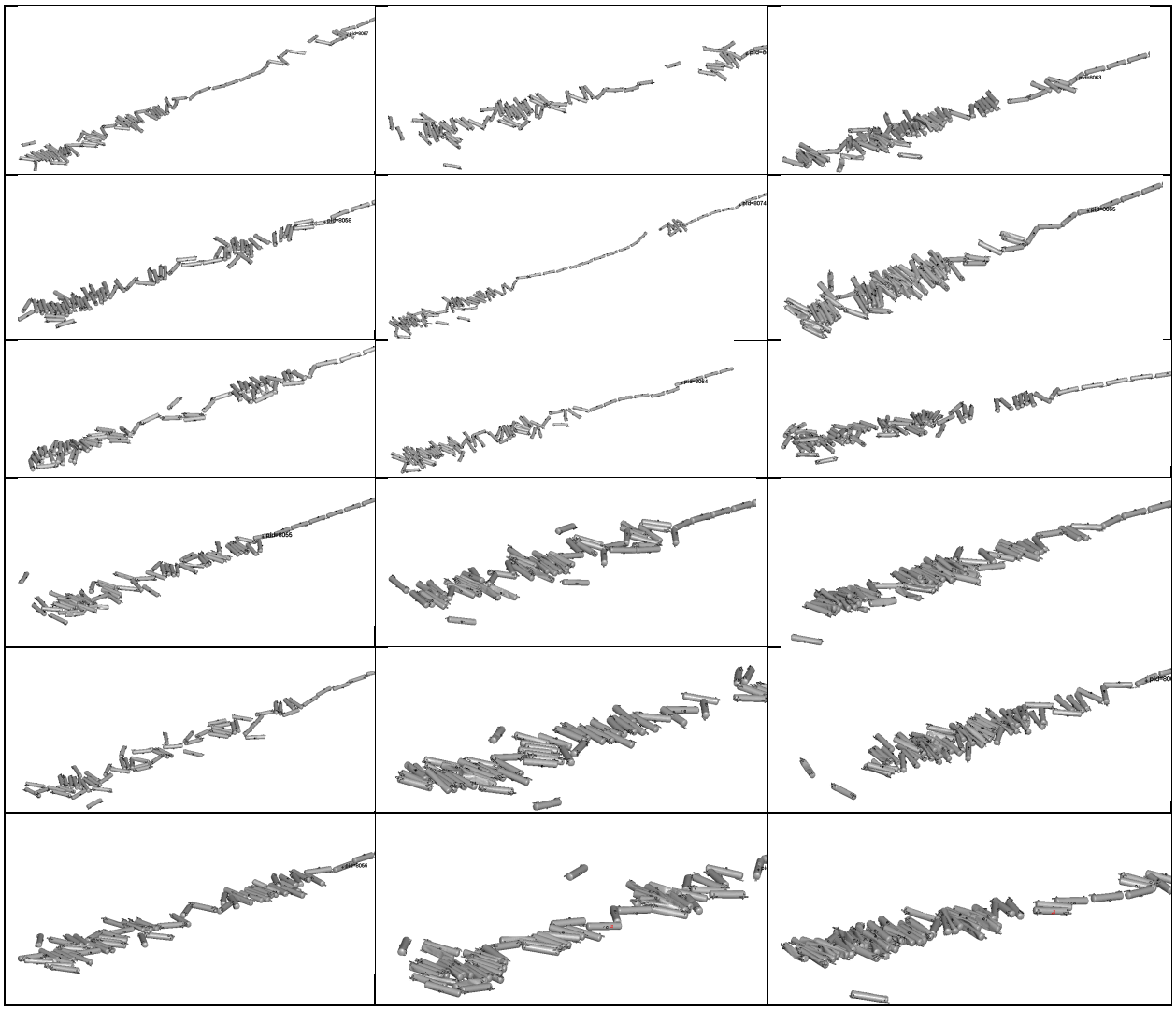

**Figure A9. Final pile-up, simulated derailment of 100-car train, 60mph**

## APPENDIX B - BAO-WIERZBICKI CRITERION FOR DAMAGE INITIATION

The equations used to define the Bao-Wierzbicki curve are included below. $C_1$=0.223 and $C_2$=0.868 for steel TC128B as referenced by Jeong et al [18].

$$\varepsilon_i^{pl} = \begin{cases} \infty & \eta \le -\frac{1}{3} \\ C_1/(1+3\eta) & -\frac{1}{3} < \eta \le 0 \\ C_1 + (C_2 - C_1)\,(\eta/\eta_0)^2 & 0 < \eta \le \frac{1}{3} \\ C_2\,\eta_0/\eta & \frac{1}{3} < \eta \end{cases}$$

During the analysis, a state variable $\omega_D$ is computed at each time increment and the damage initiation point is met when the accumulated $\omega_D$ reaches the limit value. By default, the damage limit value is 1.0.

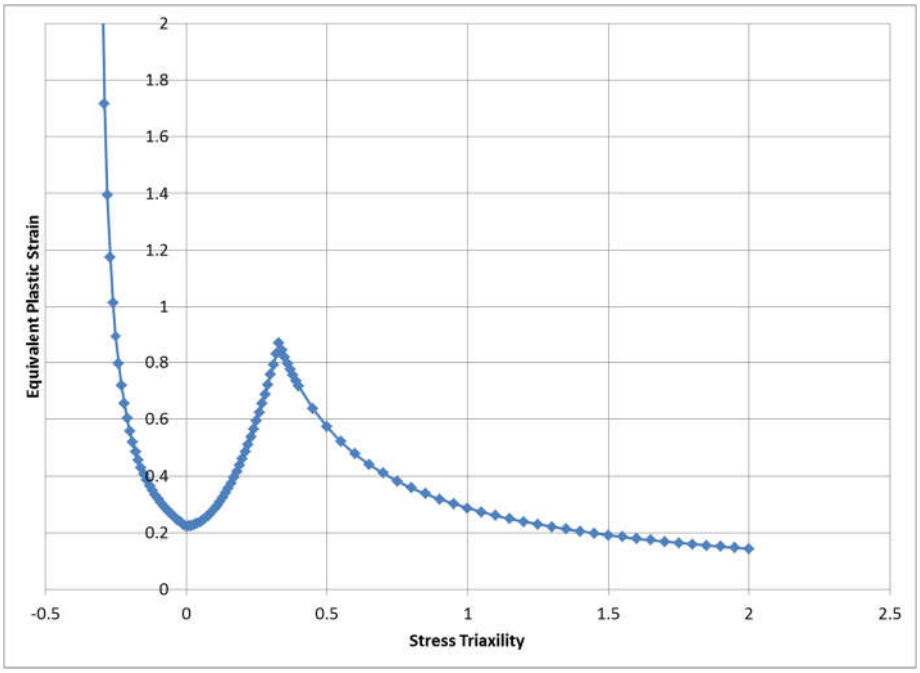


**Figure B1. Bao-Wierzbicki criterion**

Results from the FE modelling of the Charpy impact test were used to study the failure mode. One representative solid element, #438493, was selected from the top layer at the center notched area as shown in Figure B2. The stress-strain curves included in Figure B3 show the energy contribution differences among the FE models with varied $G_f$ values. Figure B4 evaluates the state status of stress triaxiality/equivalent plastic strain to the Bao-Wierzbicki curve. These responses matched well with the FE modelling expectations.

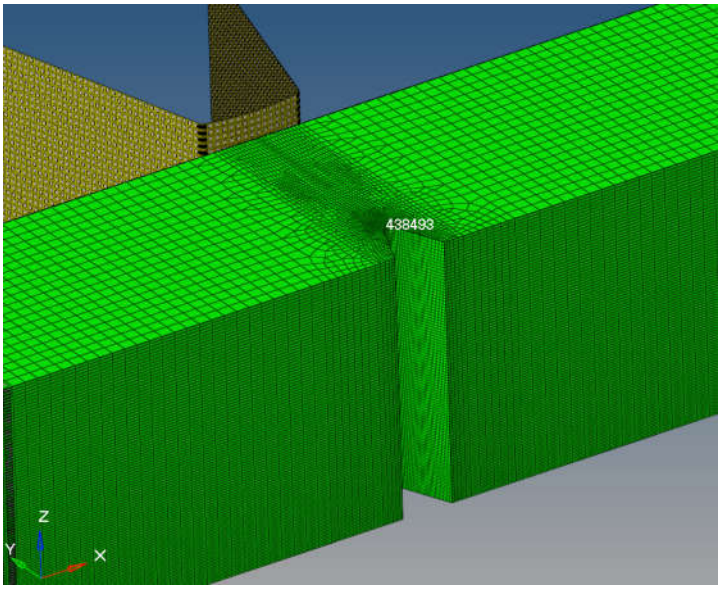


**Figure B2. Location of solid element #438493**

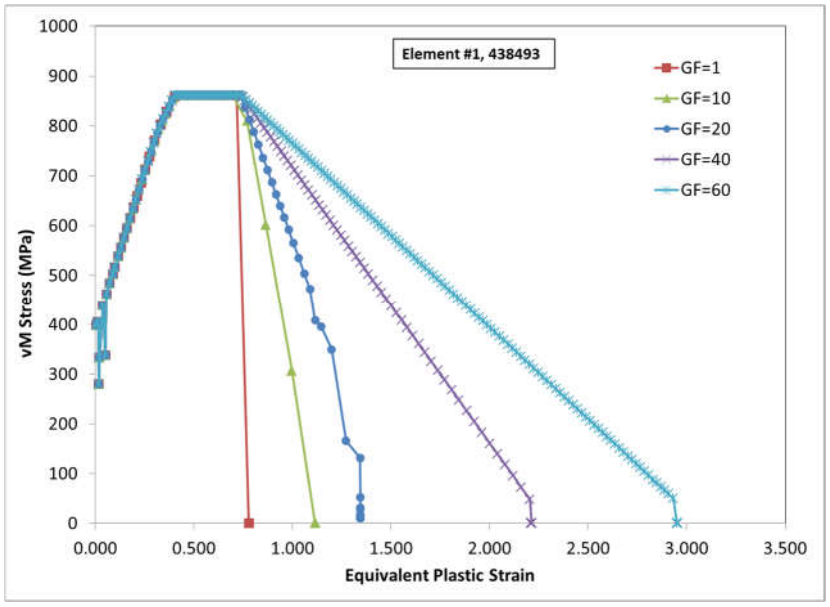


**Figure B3. Stress-strain responses of element #438493 in the FE Charpy simulations**

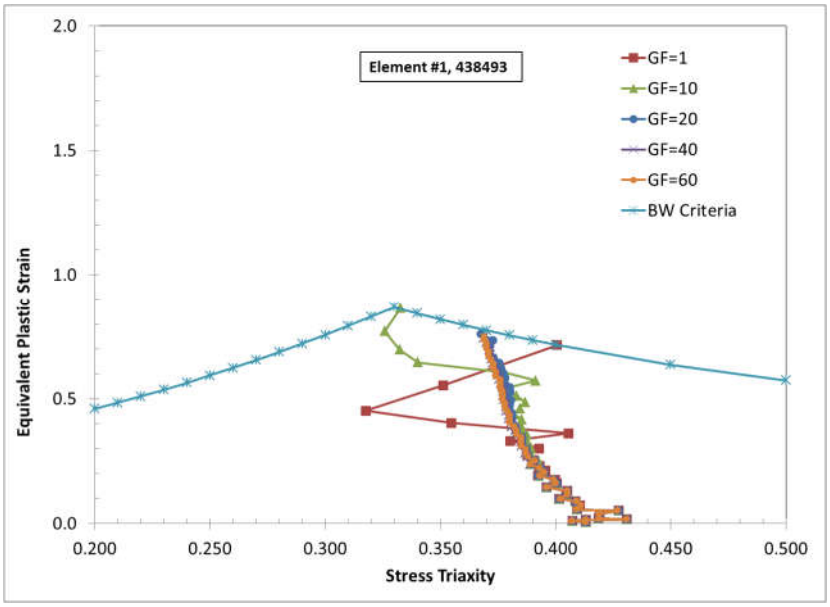


**Figure B4. Stress triaxiality maps of element #438493 in the FE Charpy simulations**

# STRUCTURAL PERFORMANCE OF 117J TANK CARS AND 117R VARIANTS UNDER DERAILMENT CONDITIONS

## MIXED TRAIN MODELLING AND RESULTS

SHARMA & ASSOCIATES, INC.



Submitted To:

TDG, Transport Canada

For Contract #: T8080-200562
TP 15544E

March 2023

**1. Background**

This current project has been evaluating the crashworthiness performance of TC-117 tank car variants from both puncture resistance and fittings protection perspectives; the effort has been focused on tank cars in 100-car unit trains, and this has raised some questions about whether the relative risk predictions from the unit train models could also be extrapolated to the performance of these TC-117 tank car designs in mixed consist service.

As there are many car types that may be seen in a mixed consist train, such as box cars, hopper cars, gondolas, intermodal cars, etc., as well as a potentially infinite number of combinations by which such cars could be assembled into a train, the team had to select a combination of cars and consists that could be used for a mixed consist evaluation.

After discussions internally and with TC, the team selected the box car as a key candidate for car type, because the car's geometry offers several edges and vertices that could maximize the number of possible interactions between tank cars and rigid planes/vertices of the box cars. The next decision was the train consist that these cars should be built into. The team decided to develop a 100-car model in which there were tank cars and box cars in alternate locations. While such a consist would not be realistic, it again offers an opportunity to maximize the number of interactions between the tank cars and the box cars. Therefore, choosing a box car and opting to use it in alternate positions would create a very severe derailment scenario and allow us to bookend the performance expected from the tank cars.

**2. Box Car Model – Dimensional Details**

While box cars are available in multiple sizes, the team picked one that was reasonably common. Initially, a CAD model of the design representing key geometry was developed, including overall dimensions, key structural members such as the center sill, side sill, and end sills, as well as key elements in the floor, roof, and sides. The CAD model is shown in Figure 1.

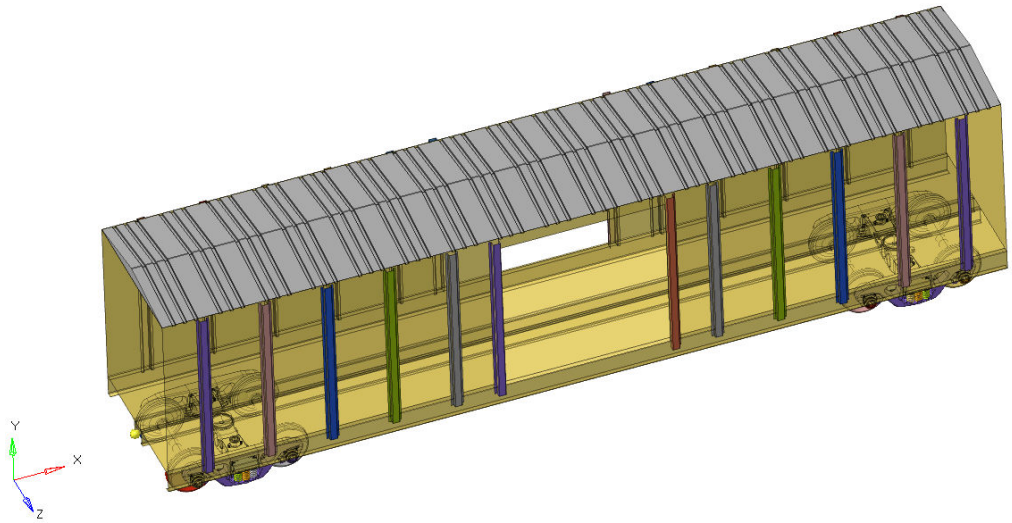


**Figure 1. CAD model of the box car**

The next step was to extract the mid-surfaces from the CAD model and to convert the key, representative structural elements into a Finite Element (FE) mesh. This was done using the HyperMesh meshing tool. A part of the side wall of the box car is used as an example to show the mid-surfaces, Figure 2.

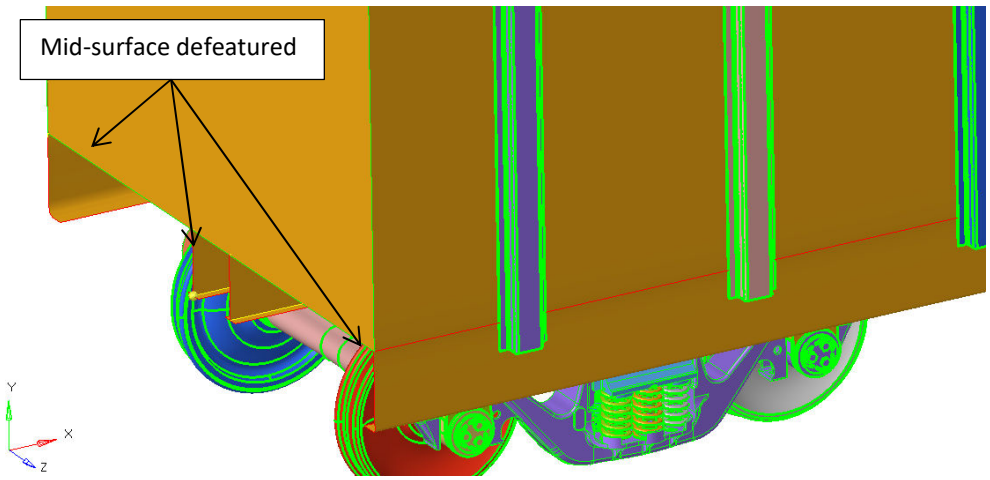


**Figure 2. Mid-surface of the box car and side sill**

Note that the intent of the modeling is to represent the stiffness of the box car so that the potential contact forces between the box cars and the tank cars can be developed correctly, not to assess damage to the box cars themselves. With this in mind, secondary elements of the model such as ribs were represented using equivalent thickness sections in the FE model, using standard de-featuring techniques. As seen in subsequent images, the FE model represents the stiffnesses of all the edges and vertices using increased thickness elements that correspond to the structural elements that are used in these locations. Note that the sliding door of the box car is not considered a structural element, as it is on rollers and generally not thought to contribute to the structural behavior of the car; the door frame around the opening is structurally reinforced on all four sides and this is represented in the FE model. The weight of the doors is included in the total weight of the car.

Key dimensions of the box car model are shown in Figures 3 and 4, and the overall mesh is shown in Figure 5.

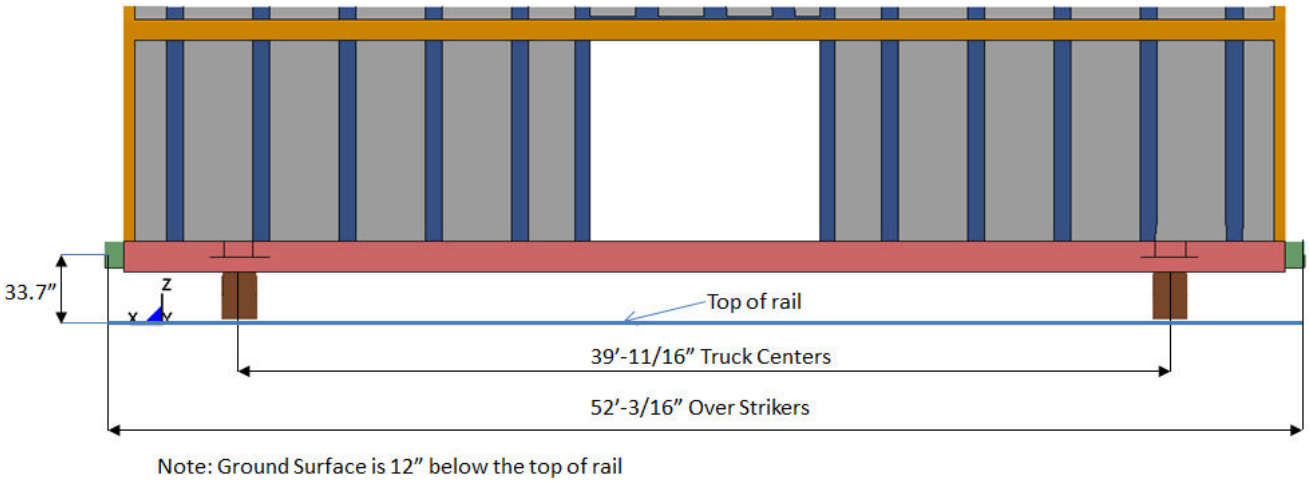


**Figure 3. Box car model for train derailment simulations (Side View)**

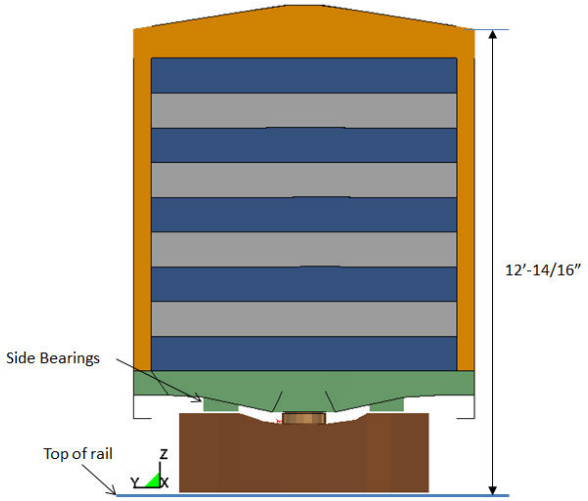


**Figure 4. Box car model for train derailment simulations (Front View)**

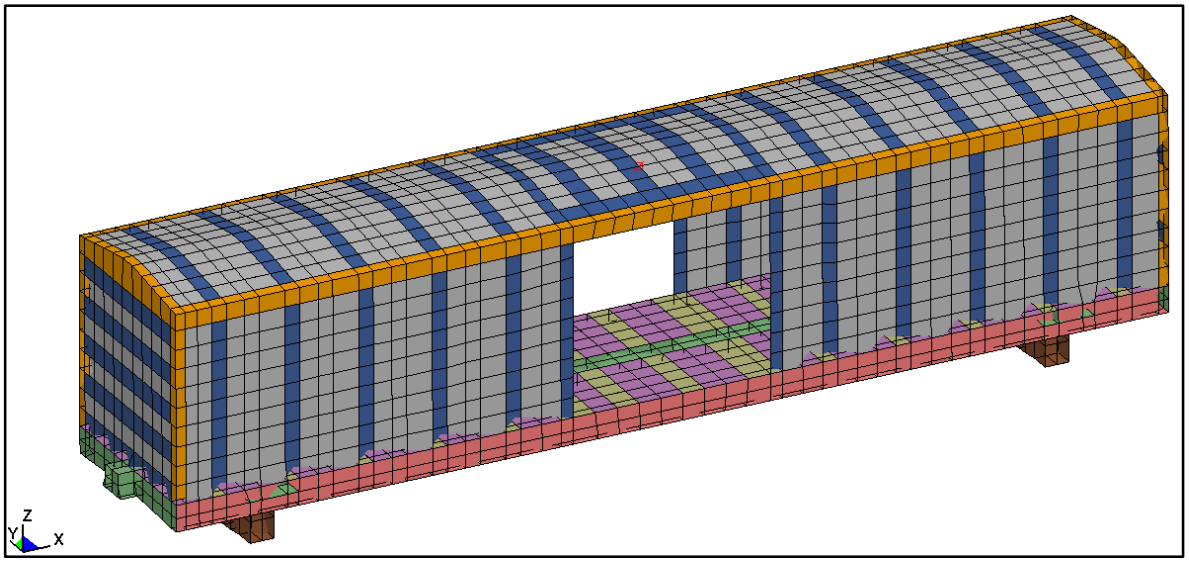


**Figure 5. Mesh of the box car**

Key dimensions of the box car are listed in Table 1 and primary structural features are identified in figures 6 & 7.

**Table 1. Box Car Characteristics**

| Item | Data |
|---|---|
| Length Over Strikers | 52 feet 3/16 inches (15.85m) |
| Length Over Truck Centers | 39 feet 11/16 inches (11.90m) |
| Maximum Height | 12 feet 14/16 inches (3.68m) |
| Door Opening, Width | 10 feet (3.05m) |
| Gross Rail Load (Full) | 263,000 pounds (119,295kg) |
| Truck Weight (Each) | 9,360 pounds (4,246kg) |

To represent the gross rail load, 80% of the load was distributed over the floor by increasing the density of the components shown in Figure 6. The other 20% of the load was distributed over the side wall and roof components of the box-car.

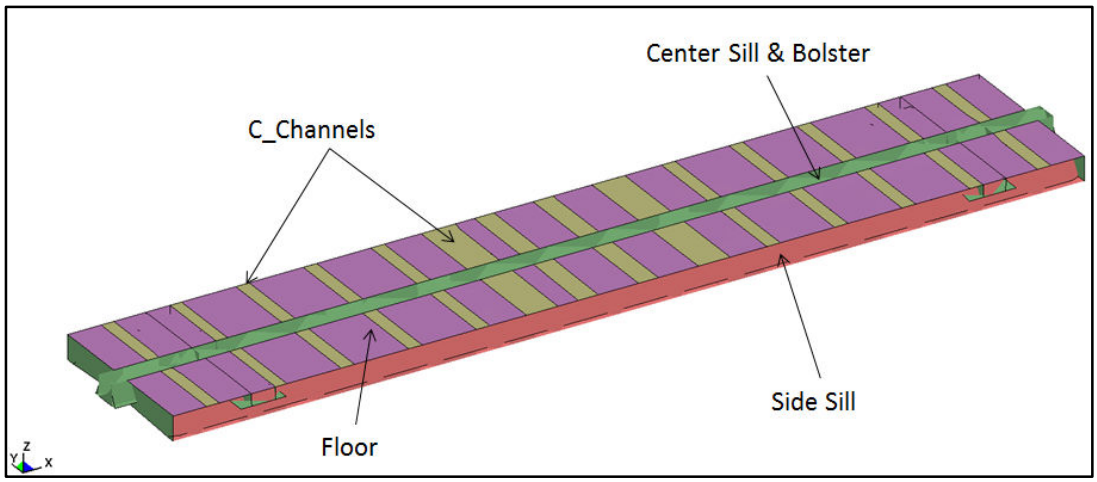


**Figure 6. Box car floor component representations**

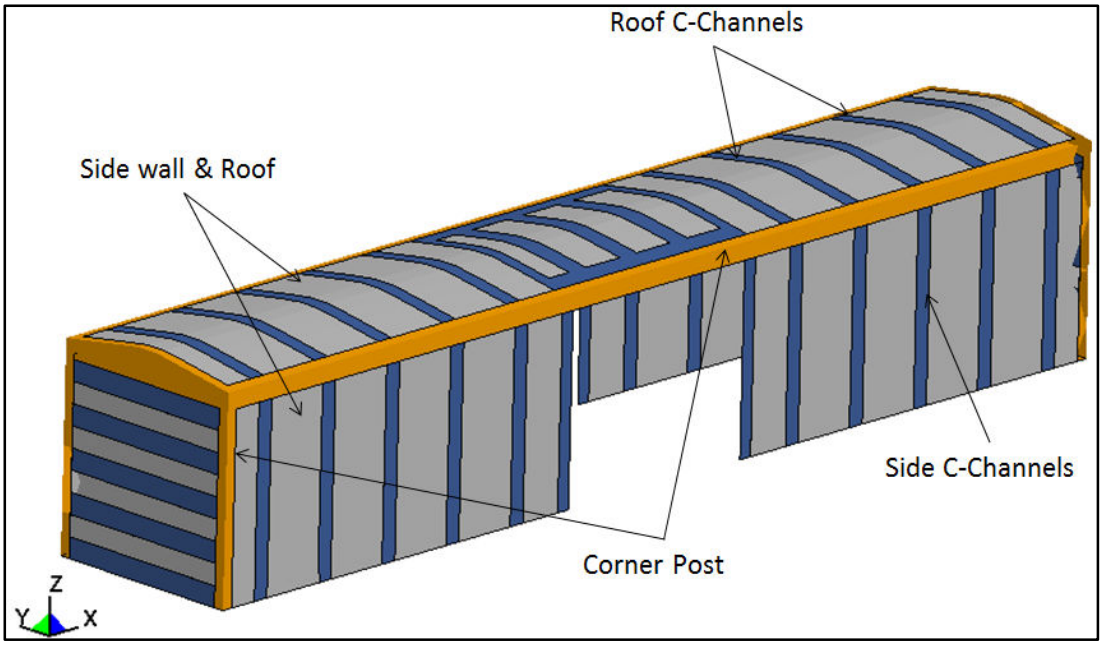


**Figure 7. Box car side wall & roof component representations**

### 3. Other Modeling Details

Once the meshing was complete, the model was transferred from HyperMesh to LS-Dyna3D for use in dynamic simulations. Appropriate part thicknesses, material properties, element formulations, and contact definitions were also assigned. As in the case of the tank car model (see the main body of TP15544E for more information), the box car model was created using shell elements. Shell elements best represent parts that are relatively thin compared to their overall surface area and typically have a uniform thickness. For this model, the shell elements use a Belytschko-Tsay formulation, which was also used on the tank cars.

The box car structure is assumed to be fabricated using carbon-steel material type, ASTM A572-Grade 50. Table 2 lists corresponding mechanical properties for this material type.

**Table 2. Material Summary for the FE Box car Model**

| **Property** | **ASTM A572 – Grade 50** |
|---|---|
| Young's Modulus (ksi) | 29,000 |
| Yield Strength (ksi) | 50 |
| Tensile Strength (ksi) | 65 |
| Elongation (%) | 18 |
| Poisson's Ratio | 0.30 |

The trucks and coupler arrangements used for the tank car model were also used for the box car model. Once the initial model of the box car was prepared, several checks and simple analyses were conducted to ensure that the car behavior was as expected, updating the model as needed to address issues.

**4. Assembling the Train**

The box car model was then replicated and inserted into alternate locations in the tank car train, to make up the mixed consist train. The tank cars and box cars are then connected to each other using the beam/link coupling elements in sequence.

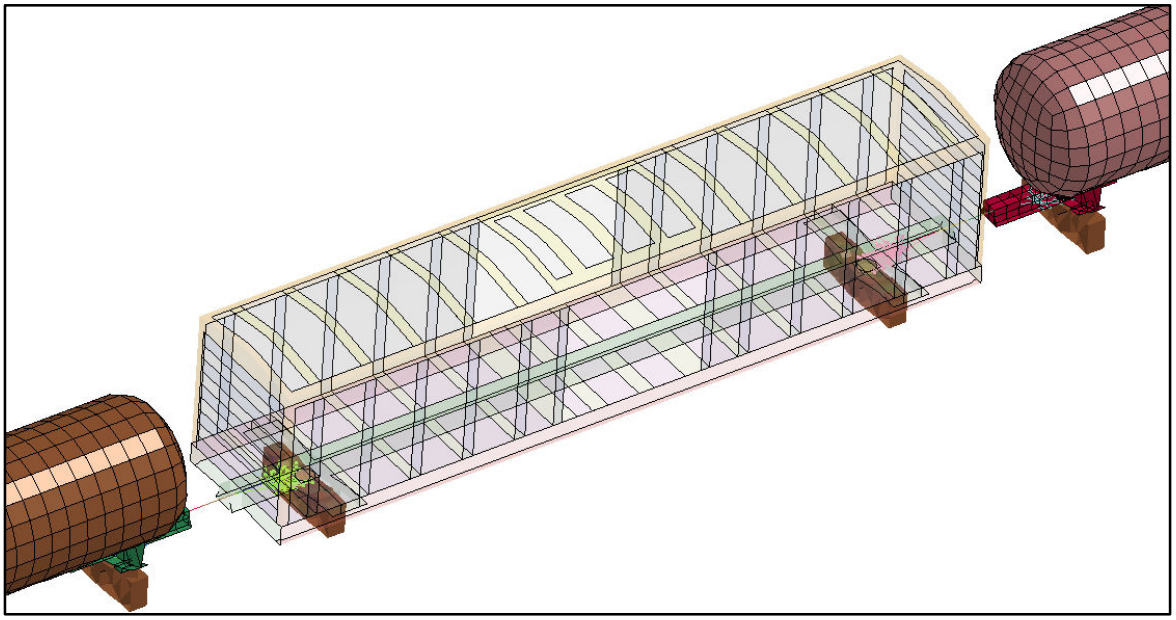

**Figure 8. Box car to tank car and truck connections**

Initially a five-car train was prepared to verify functionality and help with troubleshooting. Subsequently, the train was extended to 100 cars, with tank cars and box cars in alternating locations, starting with a tank car in position 1. Figures 9 and 10 present images of the mixed consist train.

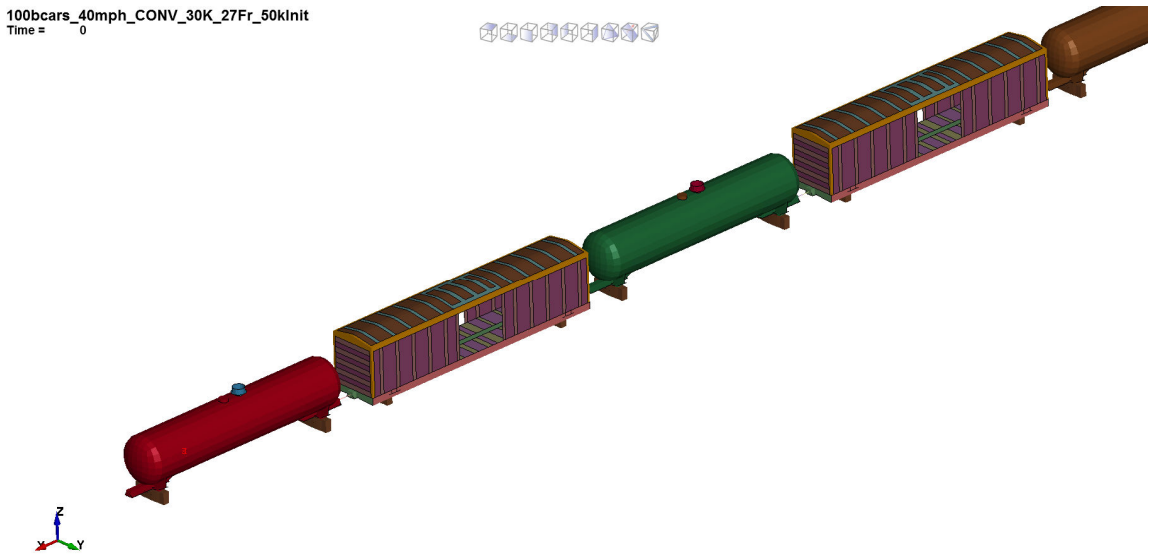


**Figure 9. Zoomed-in view of mixed consist train**

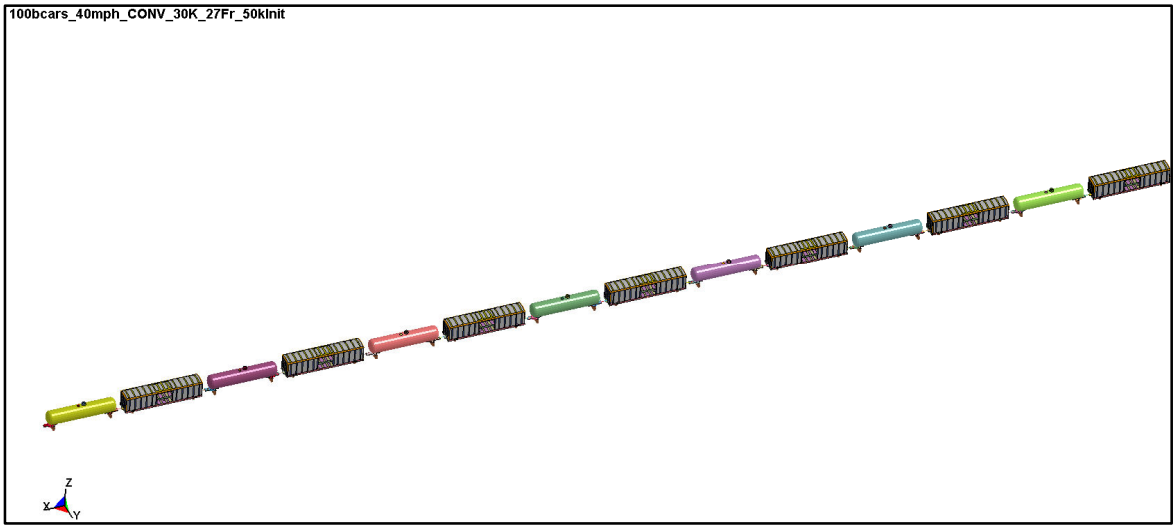


**Figure 10. Segment of mixed consist train**

The only modification made to the mixed consist train was the addition of the box cars. Other modelling details beside the addition of the box cars are similar to what was used on the unit train tank car model, including representation of the track and ground height, the coupler connections, as well as simplified truck representations to better capture the initial height of the cars as they roll off. The difference between the top of the rail and ground surface is assumed to be 12 inches. The ground surface is modeled as a finite rigid-wall; the truck representation is defined to move along the centerline of the track through a lateral spring connection between the truck representation and the ground, with the spring stiffness representing a measure of the lateral track stiffness; when the displacement of this spring exceeded a nominal 1”, the truck was considered to have derailed and the car was subsequently free to move laterally.

**5. Analysis Methodology and Simulation Parameters**

The methodology for the derailment performance evaluation is the same as that adopted for the unit train analysis (see the main body of TP15544E for a full discussion of the modelling and analysis methodology), and is as follows:

- Characterize the load environment associated with derailments through multiple derailment simulations of trains to derive a histogram of 'nominal' impact forces
- Quantify the puncture resistance of given tank car designs for a nominal range of impactor sizes and impact forces, based on prior research
- Combine the load environment histograms, the puncture resistance curves, and nominal impactor size distributions, to evaluate the safety performance or probability of puncture for a set of designs and operating speeds

The derailments were simulated at speeds of 30 mph, 40 mph, and 50 mph. These are the speeds of the train when the derailment was initiated. To initiate the derailment, the leading truck of the first car was subjected to a brief lateral force. Three values of lateral forces were used to initiate derailment: 50, 70, and 90 kips. Two values of lateral track stiffness were used to represent variations in track quality: 30 and 40 kips/in. Three values of coefficient of friction between the cars and the ground were used: 0.27, 0.3, and 0.5. The above combinations result in 18 simulations per derailment speed, as summarized in Table 3.

**Table 3. Derailment scenarios for each speed**

| Run # | Track Stiffness (kips/in) | Friction Coefficient | Initiating Force (kips) |
|---|---|---|---|
| 1 | 30 | 0.27 | 50 |
| 2 | 30 | 0.30 | 50 |
| 3 | 30 | 0.50 | 50 |
| 4 | 30 | 0.27 | 70 |
| 5 | 30 | 0.30 | 70 |
| 6 | 30 | 0.50 | 70 |
| 7 | 30 | 0.27 | 90 |
| 8 | 30 | 0.30 | 90 |
| 9 | 30 | 0.50 | 90 |
| 10 | 40 | 0.27 | 50 |
| 11 | 40 | 0.30 | 50 |
| 12 | 40 | 0.50 | 50 |
| 13 | 40 | 0.27 | 70 |
| 14 | 40 | 0.30 | 70 |
| 15 | 40 | 0.50 | 70 |
| 16 | 40 | 0.27 | 90 |
| 17 | 40 | 0.30 | 90 |
| 18 | 40 | 0.50 | 90 |

**6. Derailment Simulations**

Final pile-up images for each of the speeds used in this study are provided below.

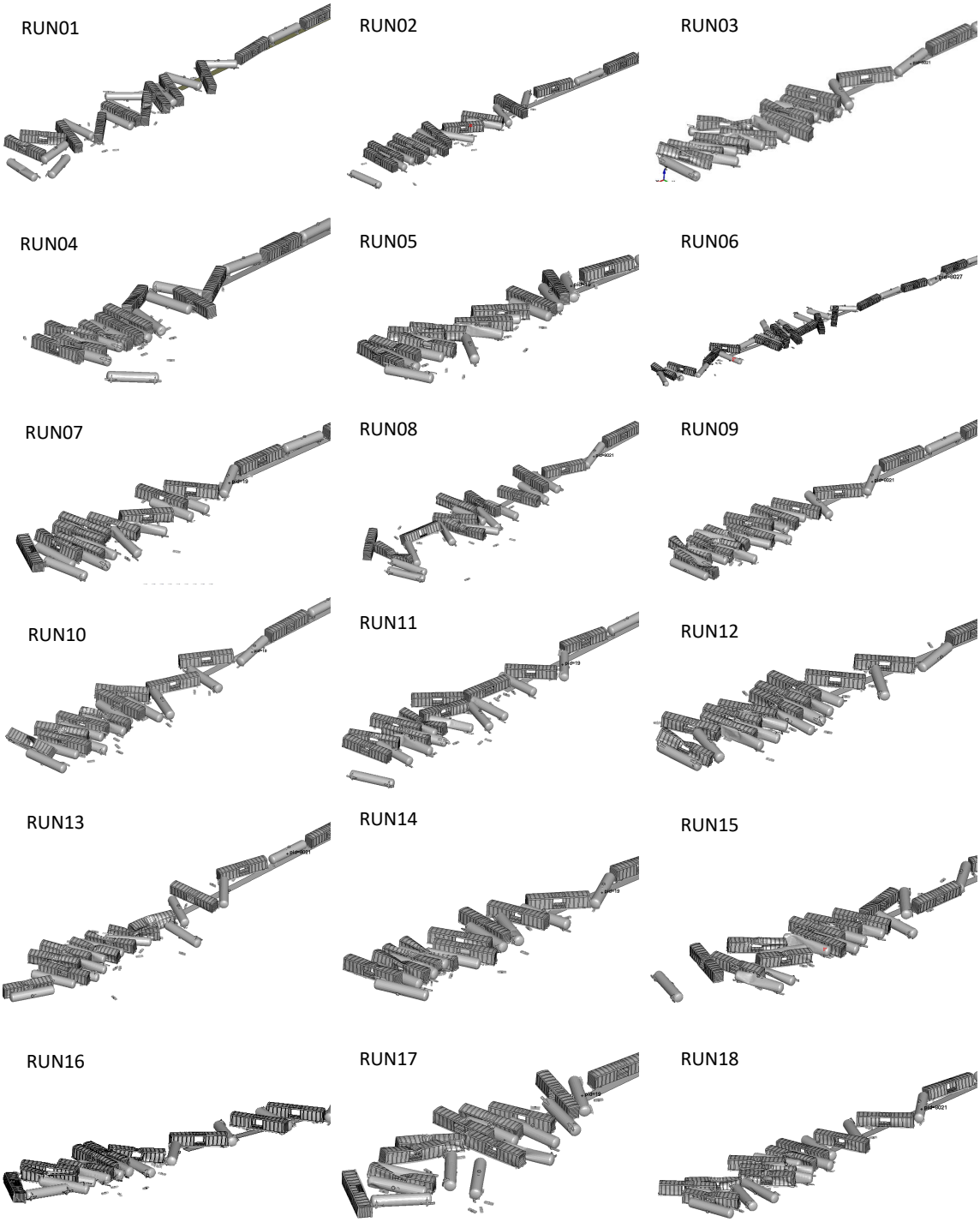


**Figure 11. Final pile-up, simulated derailment of 100-car train, 30mph**

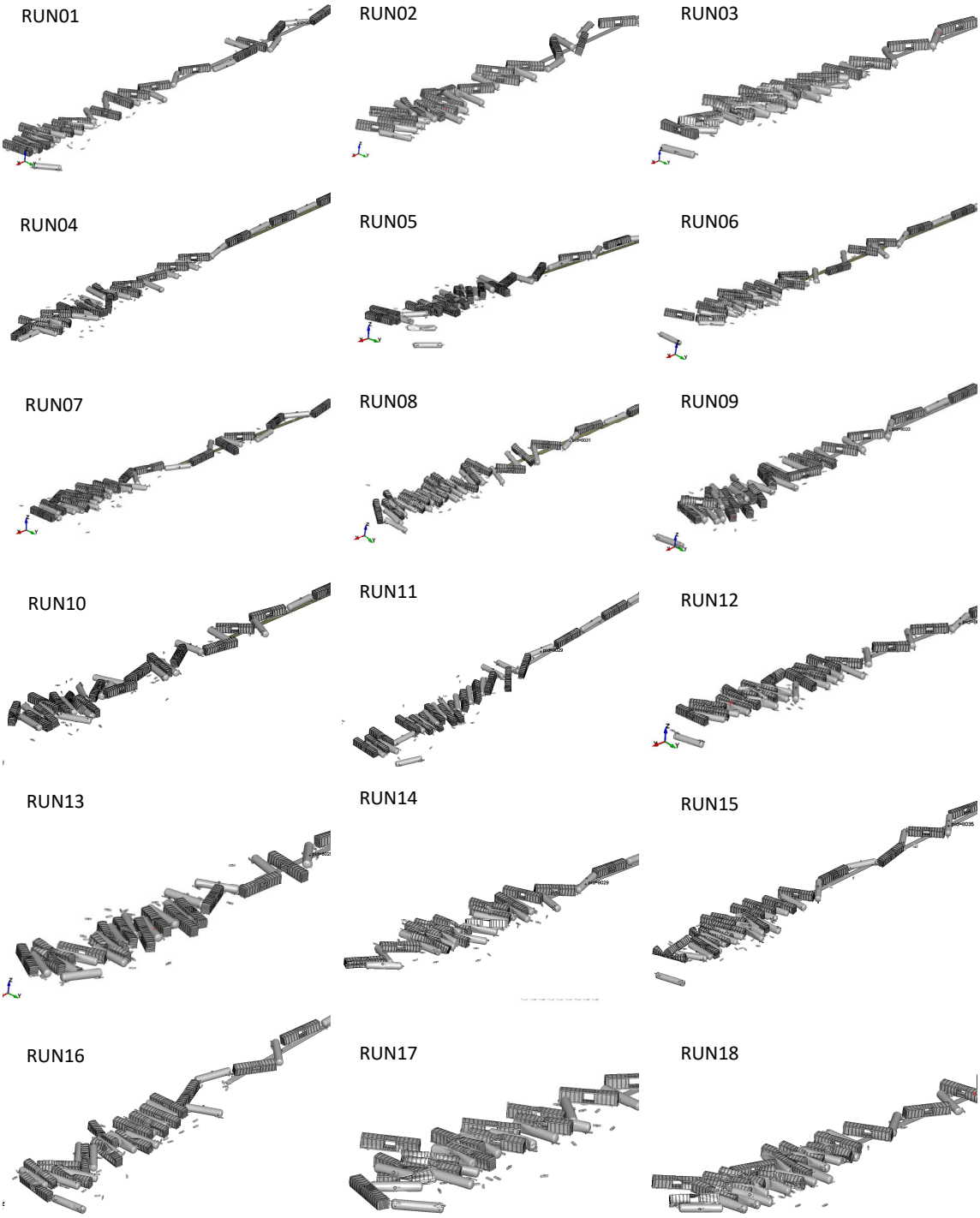


**Figure 12. Final pile-up, simulated derailment of 100-car train, 40mph**

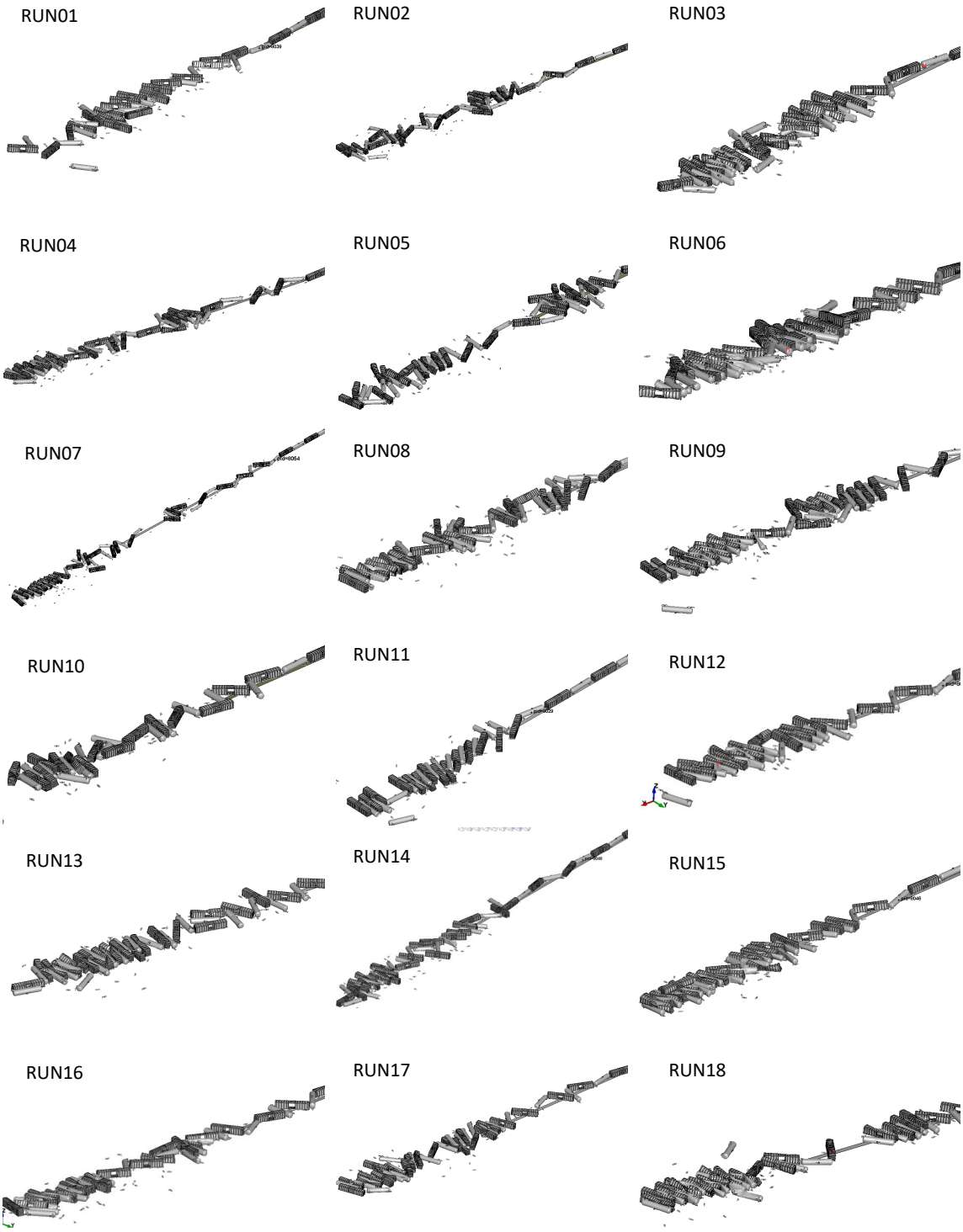


**Figure 12. Final pile-up, simulated derailment of 100-car train, 50mph**

Each simulation results in multiple car-to-car impacts between the involved cars. Table 4 lists the average number of impacts to only the tank cars in the consist for each speed. The number of cars derailed includes tank cars and box cars.

**Table 4. Derailment scenarios for each speed**

| Derailment speed (mph) | Number of impacts on tank cars (Averaged over 18 runs) | Numbers of cars derailed (Averaged over 18 runs) |
|---|---|---|
| 30 | 21 | 20 |
| 40 | 29 | 33 |
| 50 | 36 | 48 |

The histogram from all simulations were gathered and then cumulated over the 18 simulations at a given speed to generate a histogram of impact forces at each speed. Figure 13 below shows the results for all three speeds.

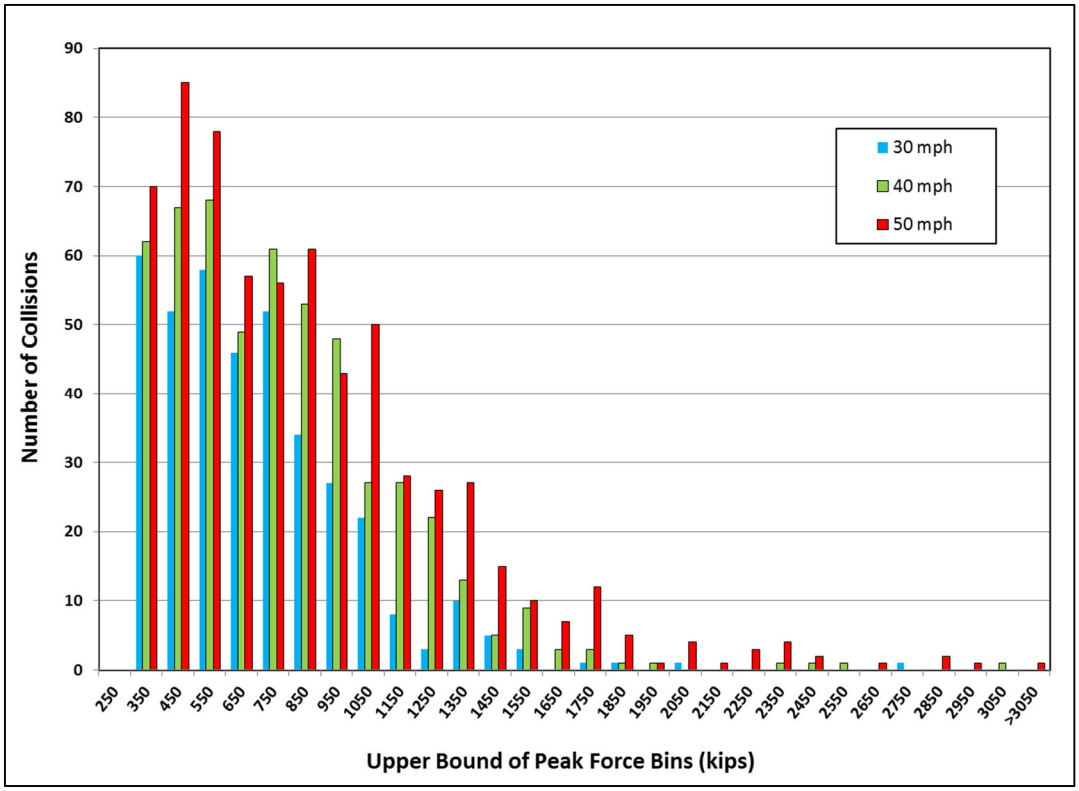


**Figure 13. Cumulative histogram of impact loads resulting from derailments**

As shown in Section 3.2 of the main report, impact velocities were extracted from the derailment simulations results by examining the vertical displacements of nodes on the upper periphery of each car's top fittings protection (bonnet). For this study, only impacts between the bonnet and the ground were included because other types of interactions are considered to be less likely. The impact velocities were analyzed and sorted to generate a histogram of velocities associated with each of the simulated

derailments. The histograms from individual derailments are further cumulated and averaged to develop a composite velocity histogram of the impact velocities experienced.

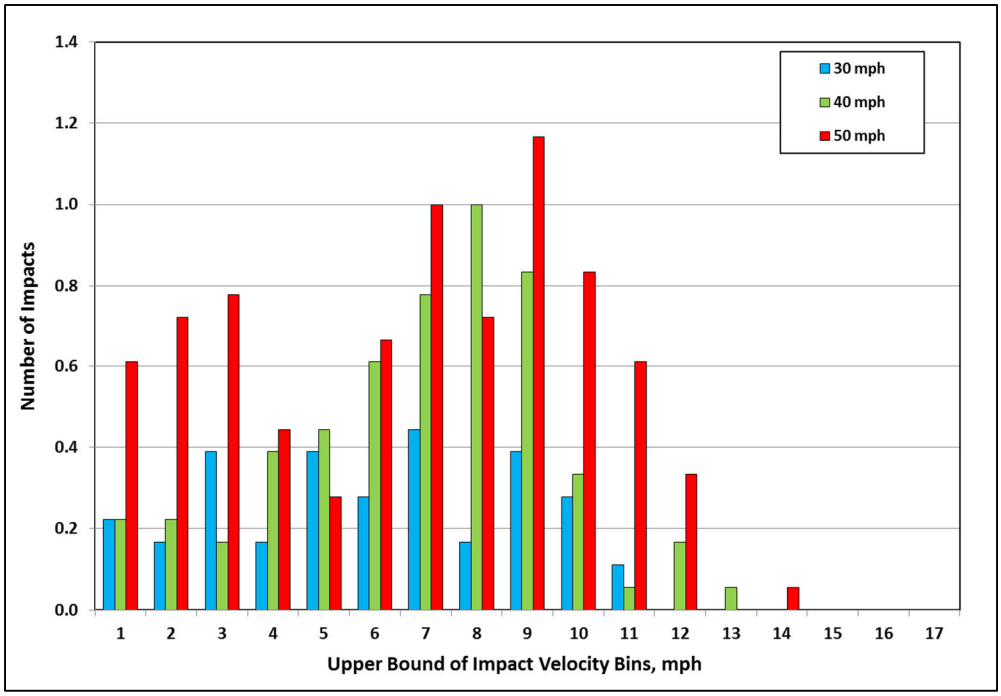


**Figure 14. Histogram of bonnet impact velocities for different speeds**

Previous work on the survivability of top fittings was used to estimate the number of failures for a protective fitting bonnet thickness of ½". Results were calculated for impact with soft soil, medium stiffness soil and concrete. Table 5 shows the results averaged over these ground conditions.

**Table 5. Predicted fittings failures**

| Derailment Speed (mph) | Top Fittings Failures |
|---|---|
| 30 | 1.6 |
| 40 | 3.5 |
| 50 | 4.9 |

The impact force histogram discussed in Section 3 of the previous report was used to predict the number of punctures for a TC-117J tank car design and two TC-117R (TC-F and TC-K) tank car designs. These tank car designs were chosen because TC-117J was the best performing model from the main body of the main report, TC-117K because was the worst performing one, and TC-117F because it uses non-normalized steel at a lower thickness so is more vulnerable to impacts and punctures. Table 6[1] below shows the predicted number of tank car punctures in a 100-car mixed train for derailment speeds 30, 40 and 50mph, and the four different temperatures. More common and representative operational speeds were chosen, with lower speeds being skipped as they resulted in fewer punctures.

[1] Table 7 presents results from the unit train simulations for reference.

**Table 6. Puncture Performance of TC-117 Designs in an Alternating Tank Car-Box Car Mixed Consist Train**

| | | | | Number of punctures for Mixed Consist Train - 50 tank cars | | | | | | | | | | | |
|---|---|---|---|---|---|---|---|---|---|---|---|---|---|---|---|
| Model Code | Tank car type | Steel Material | Shell Thickness | (20 °C) | | | (-15 °C) | | | (-25 °C) | | | (-40 °C) | | |
| | | | | 30 mph | 40 mph | 50 mph | 30 mph | 40 mph | 50 mph | 30 mph | 40 mph | 50 mph | 30 mph | 40 mph | 50 mph |
| TC-A | **TC-117J** | TC128B normalized | 9/16” | 3.11 | 4.99 | 6.96 | 3.19 | 5.11 | 7.10 | 3.25 | 5.19 | 7.20 | 3.39 | 5.39 | 7.43 |
| TC-F | **TC-117R** | TC128B non-normalized | 7/16” | 4.10 | 6.37 | 8.57 | 4.19 | 6.49 | 8.71 | 4.25 | 6.58 | 8.80 | 4.40 | 6.70 | 9.04 |
| TC-K | **TC-117R** | A516-70, normalized | 1/2” | 4.20 | 6.50 | 8.70 | 4.29 | 6.62 | 8.84 | 4.36 | 6.70 | 8.94 | 4.52 | 6.92 | 9.19 |

**Table 7. Puncture Performance of TC-117 Designs in a Tank Car Unit Consist Train**

| | | | | Number of punctures for Unit Consist Train - 100 tank cars | | | | | | | | | | | |
|---|---|---|---|---|---|---|---|---|---|---|---|---|---|---|---|
| Model Code | Tank car type | Steel Material | Shell Thickness | (20 °C) | | | (-15 °C) | | | (-25 °C) | | | (-40 °C) | | |
| | | | | 30 mph | 40 mph | 50 mph | 30 mph | 40 mph | 50 mph | 30 mph | 40 mph | 50 mph | 30 mph | 40 mph | 50 mph |
| TC-A | **TC-117J** | TC128B normalized | 9/16” | 3.30 | 6.94 | 9.97 | 3.43 | 7.12 | 10.20 | 3.50 | 7.24 | 10.43 | 3.68 | 7.56 | 10.93 |
| TC-F | **TC-117R** | TC128B non-normalized | 7/16” | 4.61 | 9.15 | 13.44 | 4.73 | 9.42 | 13.77 | 4.81 | 9.55 | 13.98 | 5.02 | 9.84 | 14.54 |
| TC-K | **TC-117R** | A516-70, normalized | 1/2” | 4.80 | 9.40 | 13.87 | 4.91 | 9.60 | 14.20 | 4.99 | 9.74 | 14.43 | 5.23 | 10.11 | 15.02 |

**7. Discussion of Results**

To perform a soundness check on the new mixed train modelling approach, we reviewed the total number of cars derailed (averaged over 18 runs) between the unit train and the mixed train simulations (see Table 8), and observed that the results are largely similar. This was expected, as it was not anticipated that the type of car modeled would fundamentally change the likelihood that a car may or may not derail. The minor increase in the number of cars derailed for the mixed car consist at 50 mph, is reasonably within the variance seen among the simulations.

**Table 8. Comparison Cars Derailed between Unit and Mixed Train**

| Derailment speed (mph) | Numbers of cars derailed averaged over 18 runs **(Unit Train)** | Numbers of cars derailed averaged over 18 runs **(Mixed Train)** |
|---|---|---|
| 30 | 20 | 20 |
| 40 | 33 | 33 |
| 50 | 46 | 48 |

Table 9 presents sample puncture results from unit and mixed trains for two different tank car designs (TC-117J and TC-117R-K, the worst performing design) at two operating speeds (40 and 50 mph). It may be observed from these results that:

1. While the mixed car train has only half the number of tank cars, it still experiences a substantial number of punctures. This is expected, as the modelling approach was intended to maximize the number of edge and vertex contacts between the cars to make a more severe derailment environment, and this increase in exposure is seen in the results.
2. The number of punctures can not be directly compared between the unit and mixed consist trains, because even though the total number of cars derailed is the same, the number of tank cars derailed is different. The increased number of punctures in the mixed train is a direct result of the alternating box car consist, and simply doubling the number of punctures to put both values on a “per 100 tank car” basis is an oversimplification as it neglects the interplay of train length, cars derailed, and tank car type.
3. When the performance across designs is compared, it is observed that irrespective of whether the more robust car (117J, in this example) is in a unit train or a mixed train, it offers improved performance over the less robust designs simulated (TC-117R-K), in the case shown).
4. Similarly, when the derailment speeds are reduced, the number of punctures reduces in both unit and mixed consist trains.

**Table 9. Puncture Performance of TC-117 Variants in Unit (100 Tank Cars) and Mixed (50 Tank Cars) Train Consists at 20°C**

| | | | Most Likely Number of Punctures | | # of Fewer Punctures Compared to TC-117R_K | | # of Fewer Punctures Due to Speed Reduction | % Improvement Compared to TC-117R_K | | % Improvement Due to Speed Reduction |
|---|---|---|---|---|---|---|---|---|---|---|
| | Tankcar Type | Tankcar Details | 40 mph | 50 mph | 40 mph | 50 mph | 50 mph to 40 mph | 40 mph | 50 mph | 50 mph to 40 mph |
| Unit Train | TC-117J | 9/16" TC128B<br>11 Gauge Jacket<br>1/2" Head Shield | 6.9 | 10.0 | 2.5 | 3.9 | 3.1 | 27% | 28% | 31% |
| | TC-117R_K | 1/2" A516-70<br>11 Gauge Jacket<br>1/2" Head Shield | 9.4 | 13.9 | | | 4.5 | ~ | ~ | 32% |
| Mixed Train | TC-117J | 9/16" TC128B<br>11 Gauge Jacket<br>1/2" Head Shield | 5.0 | 7.0 | 1.5 | 1.7 | 2.0 | 23% | 20% | 29% |
| | TC-117R_K | 1/2" A516-70<br>11 Gauge Jacket<br>1/2" Head Shield | 6.5 | 8.7 | | | 2.2 | ~ | ~ | 25% |

## 8. Summary

A finite element model of a box car, suitable for derailment simulations has been prepared and integrated into a mixed consist train model, consisting of 50 tank cars and 50 box cars in alternating locations. Eighteen derailment simulations were conducted for each of the three derailment initiation speeds of 30, 40, and 50 mph, similar to the approach followed for the unit tank trains.

Predicted impact forces and velocities were used to calculate the number of punctures and top fittings failures for TC-117J tank cars and two variants of TC-117R tank cars.

Given that the intent of the modeling was to maximize the exposure to the sharp edges and vertices of a box car and in general represent a more severe derailment environment, the results showed that structural damage observed on tank cars in the mixed consist scenarios was significant (especially considering that there are fewer tank cars in the consist). As seen in the unit train cases, the number of cars derailed, the number of punctures, and the number of fittings failures increase with speed. The results also confirm that the more robust tank cars continue to offer better performance even in mixed traffic service.

Temperature continued to have a slight effect on the number of punctures. The predicted number of punctures increases by 5-10% when temperature drops from 20 to -40°C in all modelled cases.

The results confirm that the more robust TC-117J tank car design continues to offer better performance even in more severe scenarios. Additionally, the difference in punctures between the two modelled TC-117R variants (i.e. TC-F and TC-K) was small.

When we compare differences in designs, it appears that performance improvement may be slightly lower in more severe derailment scenarios. For example, a 28% improvement in performance between a TC-117J and a TC 117R-K at 50 mph is observed in the unit train simulations compared to a 20% improvement in the same scenario in the mixed consist simulations, but there is still a significant improvement in performance when using a TC-117J tank car design.

This work does not support using train configuration as a consideration for reducing punctures, because an unrealistic mixed consist was modelled and the study did not take into account factors such as the effect of train marshalling on the likelihood of derailment.